MOTION-MODE ENERGY METHOD AND ITS IMPLEMENTATION BASED ON ACTIVE HYDRAULICALLY INTERCONNECTED SUSPENSION

by

Lifu Wang

Submitted in fulfillment of the requirements for the degree of

Doctor of Philosophy

Faculty of Engineering and Information Technology

University of Technology, Sydney

October 2013

CERTIFICATE OF ORIGINAL AUTHORSHIP

I certify that the work in this thesis has not previously been submitted for a degree nor has it been submitted as part of requirements for a degree except as fully acknowledged within the text.

I also certify that the thesis has been written by me. Any help that I have received in my research work and the preparation of the thesis itself has been acknowledged. In addition, I certify that all information sources and literature used are indicated in the thesis.

Signed:

_____

Lifu Wang

Acknowledgements

I would like to take the opportunity to thank a number of people for their assistance, encouragement and support throughout my candidature.

First and foremost, I extend my gratitude to my supervisor, Professor Nong Zhang for his outstanding guidance, encouragement and caring support throughout the duration of this project. Over the years, Nong's personal brand of professional and intellectual excellence became a source of inspiration and role model for my professional and personal development. I also sincerely thank my co-supervisor, Dr Haiping Du, for his first-class and unfailing assistance, guidance and support over the past few years. His extensive experience and dedication have been much appreciated throughout my research.

Chris Chapman's help at the initial stage of this project is gratefully appreciated. Dr Holger Roser's expertise in the lab was a tremendous asset to the project, and I greatly appreciated his help in the test rig design, construction and testing. I would like to thank Dr Paul Walker and Dr Nga Hoang for all of their help and insightful input. My appreciation is also extended to Robert Hill for his help in the field test and for proofreading my papers. Building the test rigs and conducting the field tests required a lot of work, and I would like to thank all the Capstone students that worked with me on this project: Benjamin West, Zhuojie Liang, Stefano Sansone, Yunfei Gao, Michael Lee, Scott Russell, Adam Martinez, William Wait, and Matthias Wong, and also thank two other Ph.D students: Sangzhi Zhu and Guangzhong Xu. Without their dedicated work and help, I could not have conducted such a large scale project. The financial support of this work by the Australian Research Council (ARC DP0988429) and the University of Technology, Sydney, is gratefully acknowledged.

I would like to thank my parents, for their love and support over the years, my grandparents for their encouragement and for serving as such fine role models in my life, and my wife Yupu to whom I owe so much for her continuing love and support. Lastly, I wish to acknowledge the birth of my beautiful daughter Maggie who has made my Ph.D candidature more enjoyable than it would have been without her! I can't wait to see her reading my thesis one day!

Lifu Wang

Sydney, October 2013

List of publications based on this research

Journal articles

[1]. Zhu, S., **Wang, L.**, Zhang, N., and Du, H., "H∞ Control of a Novel Low-cost Roll-plane Active Hydraulically Interconnected Suspension: an Experimental Investigation of Roll Control under Ground Excitation," *SAE International Journal of Passenger Cars- Mechanical Systems*, vol. 6 (2), pp. 882-893, 2013.

[2]. **Wang, L.**, Zhang, N., and Du, H., "Experimental Investigation of a Hydraulically Interconnected Suspension in Vehicle Dynamics and Stability Control," *SAE International Journal of Passenger Cars- Mechanical Systems,* vol. 5 (2), pp. 759-768, 2012.

[3]. Zhang, N., **Wang, L.**, and Du, H., "Motion-Mode Energy Method for Vehicle Dynamics Analysis and Control," accepted by *Vehicle System Dynamics,* September 2013.

[4]. **Wang, L.**, Zhang, N., and Du, H., "Full-Car Application and Field Test of a Roll-Plane Hydraulically Interconnected Suspension," *submitted to Vehicle System Dynamics,* 2013.

[5]. **Wang, L.**, Zhang, N., and Du, H., "Real-time Identification of Vehicle Motion-Modes Using Neural Networks," *submitted to Mechanical Systems and Signal Processing,* 2012.

[6]. Du, H., Zhang, N., and **Wang, L.**, "Switched Control of Vehicle Suspension Based on Motion-Mode Detection," *submitted to Vehicle System Dynamics,* 2013.

Conference papers

[7]. **Wang, L.**, Xu, G., Zhang, N., and Roser, H., "Empirical Analysis of a Roll –plane Hydraulically Interconnected Suspension in Comparison with Anti-roll Bars on a Sport Utility Vehicle: Articulation (Warp) mode," SAE Technical paper 2013-01-0710, Detroit, US, 2013.

[8]. Zheng, M., **Wang, L.**, Zhou, Q., and Zhang, N., "Drop-test based parameter estimation of a two-axis commercial vehicle," the 23rd International Association for Vehicle System Dynamics (IAVSD), Qingdao, China, 19-23 August 2013.

[9]. Xu, G., Zhang, N., Roser, H., and **Wang, L.**, "Simulation study of roll-plane hydraulically interconnected suspension compared with anti-roll bar in articulation mode," the 23rd International Symposium on Dynamics of Vehicles on Roads, IAVSD, Qingdao, China, 19-23 August 2013.

[10]. Xu, G., Roser, H., and **Wang, L.**, "Experimental study of a roll-plane hydraulically interconnected suspension system under vehicle articulation mode," under reviwer of ASME 2013 International Mechanical Engineering Congress and Exposition (IMECE), San Diego, CA, USA, 2013.

[11]. Shao, X., Du, H., Zhang, N., and **Wang, L.**, "Fuzzy Control of Hydraulically Interconnected Suspension with Configuration Switching," under reviwer of the IEEE International Conference on Vehicular Electronics and Safety (ICVES'13), Dongguan, China, 2013.

[12]. Lam, Q. V. C., **Wang, L.**, and Zhang, N., "Experimental implementation of a Fuzzy controller for an active hydraulically interconnected suspension on a sport utility vehicle," the 2013 IEEE Intelligent Vehicles Symposium, Gold Coast, Australia, 23-26 June 2013.

[13]. Hong, H., **Wang, L.**, and Zhang, N., "Investigation of a roll-plane hydraulically interconnected suspension with motion-mode energy method," the 23rd International Symposium on Dynamics of Vehicles on Roads and Tracks, Qingdao, China, 19-23 August 2013.

[14]. Zhang, N., Smith, W., and **Wang, L.**, "Passive and active hydraulically interconnected suspensions and their applications," the 7th Australasian Congress on Applied Mechanics (ACAM 7), Adelaide, Australia, 9-12 December 2012.

[15]. **Wang, L.**, Zhang, N., and Du, H., "Modelling and parameter estimation of an active hydraulic suspension using experimental method," the 7th Australasian Congress on Applied Mechanics, Adelaide, Australia, 9-12 December 2012.

[16]. Roser, H., **Wang, L.**, and Zhang, N., "Empirical analysis of a roll-plane hydraulically interconnected suspension system under vehicle articulation mode," the 7th Australasian Congress on Applied Mechanics (ACAM), 9-12 December 2012.

[17]. Zhang, N., **Wang, L.**, and Hu, W., "Handling analyses of a Vehicle Fitted with a Roll-resistant Hydraulically Interconnected Suspension," IAVSD, Manchester, UK, 14-19 August 2011.

[18]. **Wang, L.**, Zhang, N., and Du, H., "Onboard Detection of Energy Distribution onto Vibration Modes of a Vehicular System," the 14th Asia Pacific Vibration Conference, Hong Kong, 5-8 December 2011.

[19]. Zhang, N., **Wang, L.**, Hu, W., and Ding, F., "Dynamic Characteristics of a Vehicle Fitted with a Roll-Resistant Hydraulically Interconnected Suspension," the First IFToMM Asian Conference on Mechanism and Machine Science, Taipei, Taiwan, 21-25 October 2010.

[20]. Zhang, N., Hu, W., and **Wang, L.**, "Modelling and Simulation of a Full Car Fitted with a Hydraulically Interconnected Suspension undergoing Extreme Manoeuvres," 1st International Conference on Vibration Utilization and Control (ICVUC), Shenyang, China, 19-21 August, 2010.

[21]. **Wang, L.**, Zhang, N., and Du, H., "Modelling, parameter estimation and testing of a vehicle with anti-roll systems," the 6th Australasian Congress on Applied Mechanics, Perth, Australia, 12-15 December 2010.

[22]. Zhang, N., **Wang, L.**, and Du, H., "Modeling of a New Active Suspension for Roll Control," the 13th Asia Pacific Vibration Conference, University of Canterbury, New Zealand, 22-25 November 2009.

[23]. **Wang, L.**, Zhang, N., and Du, H., "Design and Experimental Investigation of Demand Dependent Active Suspension for Vehicle Rollover Control," the 48th IEEE Conference on Decision and Control, Shanghai, P.R. China, pp. 5158-5163, 16-18 December 2009.

Table of Contents

Abstract

Vehicle motion and vibration control is a fundamental motivation for the development of advanced vehicle suspension system, and high performance active suspension with its forcefulness, flexibility and effectiveness is desired to fit the control role. However, the main constraint for the commercial application of these active suspensions is their high component cost and power consumption. The principal idea of this thesis is that by proposing an energy efficient control strategy and a novel active suspension system, the active suspension's initial cost can be reduced and its running power consumption can be minimised.

The new control strategy, designed to improve energy efficiency by prioritizing the dominating vehicle dynamic aspects, is based on a motion-mode energy method (MEM). It classifies vehicle body-wheel motions into several motion-modes according to their modal properties and quantifies the contribution of each motion-mode by its energy intensity in real time. The motion-mode energy and mode contribution ratio are used to determine the control priority on the control of the most dominating motion-mode. Neural networks are trained to implement the MEM in practice in an economical manner, and an MEM-based switched control is proposed to perform the multi-mode control.

The new suspension system developed to implement the MEM-based switched control strategy is called active hydraulically interconnected suspension (active HIS), which is equipped with only one servo valve to reduce the system's cost and energy consumption. In addition, by switching its hydraulic configuration into different modes, the vehicle primary dynamic response can be significantly improved with less power consumption.

Three test facilities have been designed and developed to study this novel suspension system, including a six-channel vehicle dynamic test rig, a multi-functional anti-roll

HIS test rig and a reconfigurable HIS test rig. Test results provided include vehicle parameter estimation, passive anti-roll HIS laboratory and field test, and active HIS anti-roll test. The active HIS is found to be an effective and feasible way of controlling a vehicle's motion. However, further investigation into this system, including the full-car MEM-based switched control and circuit reconfiguration test, is recommended for future studies.

Abbreviations

ABS	Anti-Lock Brake System
ASCA	Active suspension via control arm
BSR	Buzz, squeak and rattle
CG	Centre of gravity
DOF	Degree of freedom
ESC/ESP	Electronic Stability Control/Program
FFT	Fast Fourier transformation
HIS	Hydraulically interconnected suspension
KDSS	Kinetic dynamic suspension system
LQR	Linear quadratic regulator
LVDT	Linear variable differential transformer
MEM	Motion-mode energy method
MHIS	Multi-function hydraulically interconnected suspension
NI	National Instruments
NN	Neural network
RCF	Rollover critical factor
RHIS	Reconfigurable hydraulically interconnected suspension
RMS	Root mean square
SUV	Sport utility vehicle
SVM	State variable method
UTS	University of Technology, Sydney

List of Symbols

u	Longitudinal velocity of the sprung mass centre of gravity (CG)
v	Lateral velocity of the sprung mass CG
z_s	Vertical displacement of the sprung mass CG
z_{ui}	Vertical displacement of the unsprung masses (i =1, 2, 3, 4)
z_{ii}	Vertical displacement of sprung mass at four suspension mounting points, $ii = fl, fr, rl, rr$
z_{gi}	Road disturbance input for each tire (i =1, 2, 3, 4)
fl, fr, rl, rr	Front-left, Front-right, Rear-left, Rear-right
φ	Roll angle of the sprung mass around its x-axis
θ	Pitch angle of the sprung mass around its y-axis
ψ	Yaw angle of the vehicle
m_s	Vehicle sprung mass
m_{ui}	Vehicle unsprung mass (i =1, 2, 3, 4)
I_{xx}	Moment of inertia about the x-axis of the vehicle sprung mass
I_{yy}	Moment of inertia about the y-axis of the vehicle sprung mass
I_{zz}	Moment of inertia about the z-axis of the vehicle sprung mass
I_{xz}	Product of inertia about the x-z axes of the vehicle sprung mass
I_{zz_u}	Moment of inertia about the z-axis of the vehicle unsprung mass
l_f	Distance from the sprung mass CG to the front axle
l_r	Distance from the sprung mass CG to the rear axle
t_f	1/2 width of the front axle
t_r	1/2 width of the rear axle
h_s	Vertical distance from the sprung mass CG to the roll axis
k_{si}	Spring stiffness for each suspension (i =1, 2, 3, 4)
c_{si}	Damping coefficient for each suspension (i =1, 2, 3, 4)
k_t	Vertical tire stiffness

δ_f	Front tire steer angle
δ_r	Roll induced steer angle at rear
λ_i	System eigenvalues (i =1, 2,⋯7)
ϕ_i	System eigenvectors (i =1, 2,⋯7)
e_{ki}	The kinetic energy in the i^{th} motion-mode (i =1, 2,⋯7)
e_{pi}	The potential energy in the i^{th} motion-mode (i =1, 2,⋯7)
e_i	The total energy in the i^{th} motion-mode (i =1, 2,⋯7)
η_i	The i^{th} mode-ratio
E	The total energy of seven motion-modes
$w, \overline{w}$	Weighting matrices of neural network
w^*, $\overline{w}^*$	The updated weighting matrices during neural network training
τ	The learning constant of the neural network delta training rule
Λ	System eigenvalue matrix
Ψ	System eigenvector matrix
Γ	Modal transition matrix in motion-mode energy method
X	System state vector
$X_{M/H}$	Subsystem state vector, i.e, mechanical subsystem (M) and hydraulic subsystem (H)
p_j^i, q_j^i	Hydraulic pressure p or flow rate q, the subscripts j define the specific location, top/bottom chamber, j =*U/B*, other points, j =*A, C...S*, and the superscripts i denote the relevant hydraulic element: two letters represents a pipeline element; the letter *A1* and *A2* represent two accumulators
T_H, S_H	Coefficient matrices determining the hydraulic system dynamics
F_m	Road input and nonlinear components of the 9-DOF vehicle model
F_h	Coupling coefficient matrix, from mechanical system to hydraulic system
S_{H2M}	Coupling coefficient matrix, from hydraulic system to mechanical system

CHAPTER 1 INTRODUCTION

1.1 Overview of the project

Research on vehicle dynamics has been conducted for many decades [1-3]. It provides valuable insights to the dynamic behaviour of vehicles as well as laying foundation for advanced control design [4]. In particular, the study of the vehicle suspension systems, which form the coupling between the vehicle body and its wheels, is considered to be one of the most important areas in vehicle dynamics, and contributes considerably to the ride, handling and safety analysis of road vehicles [5].

Three kinds of suspensions, that is, passive, semi-active, and active suspensions, have been proposed so far [5-7]. Semi-active and active suspensions are controllable suspensions, and they represent the current mainstream in research for a few decades [8, 9] due to the rapid development in mechatronic systems. Active suspensions, in particular, which are known for their effectiveness and flexibility, are considered ideal in relation to achieving the best ride comfort, integrated vehicle handling and safety control. Active systems are also able to directly govern a vehicle's motions in bounce, roll, pitch, and articulation (warp), and can indirectly control a vehicle's planar dynamics through the tire/ground contacts.

However, despite the above advantages, the widespread application of active suspensions in ordinary passenger cars has not occurred owing to their high overall cost and control system power consumption. Typical active suspensions have four individually controlled linear motors or electro-hydraulic actuators, assigned with ambitious control objectives that cover a very wide frequency range. This makes the active suspensions costly to manufacture and run.

To overcome these problems, it is necessary to identify the primary control targets of active suspensions and refine their control strategy.

For a vehicle, which is a multi-mode system with complex dynamics, the design of multi-motion integral control would have multiple objectives (e.g., bounce, roll, pitch, and articulation properties). This requires a clearly defined framework which can cover these objectives. Moreover, to increase cost effectiveness and efficiency, optimization based on the prioritized objectives in real time is necessary because both the control energy and the physical control input channels, are limited (e.g., active suspensions, torque/braking control of wheels). Hence, a systematic method to perform the real-time assessment and comparison of vehicle dynamic modes needs to be developed.

Thus, the author proposes a motion-mode based active control and accordingly an active hydraulically interconnected suspension (HIS) system for its implementation. Both theoretical and experimental approaches are taken in this study. On the theoretical side, computer-based analysis based on linear/nonlinear multi-body system dynamics is used to derive the motion-mode energy method; neural networks are trained to simplify the implementation of this method in practice; and an architecture of integral control is proposed. On the experimental side: three test rigs have been built to investigate questions and issues associated with developing the active HIS system. Based on the vehicle parameter estimation and experimental studies of the passive HIS system, an active HIS has been further designed and tested.

1.2 Research objectives and contribution to knowledge

The specific objectives and contributions are as follows:

1. To review the literature relating to controlled suspensions and interconnected suspensions, highlighting the advantages of active suspensions, outlining the

current barriers in terms of adopting active suspensions, and introducing the active HIS system.

2. To develop a methodology to detect the dominating vehicle motion-mode with real-time capability; (1), study vehicle motions and vibrations from the modal analysis perspective and classify the relative motions between vehicle body and wheels into several body-wheel motion modes, (2), employ the vehicle state vector to calculate each motion-mode's energy and its contribution ratio, (3), use a trained neural network to provide a reasonably accurate motion-mode energy contribution ratio from measured suspension travel, (4), conceptually develop a motion-mode energy based switched control with H∞ optimization.

3. To develop a series of test facilities for the research: (1), a six-channel vehicle dynamic test rig, (2), a multi-functional HIS test rig, (3), a reconfigurable HIS test rig.

4. To conduct experiments: (1), develop a parameter estimation method of a vehicle and HIS systems, (2), perform field test of a vehicle fitted with passive HIS, under different types of manoeuvre and ground excitation according to the articulation mode, (3), develop and test the active HIS system with H∞ control.

1.3 Scope of thesis

1.3.1.Areas that are addressed

The following areas are within the scope of this thesis:

- the definition of motion-modes
- the derivation of the motion-mode energy method (MEM)

- the derivation of the neural network method for primary mode detection up to three modes
- the MEM-based switched control
- test facility development
- the vehicle parameter identification
- the laboratory and field tests of the passive HIS system
- the preliminary laboratory tests of the active HIS system

1.3.2.Areas that are not addressed

The following areas are beyond the scope of this thesis:

- the derivation of the used 10 degree-of-freedom (DOF) full car model
- transient analysis of the active HIS
- vehicle full state vector estimation

1.4 Outline of thesis

The thesis will consist of eight chapters, organised as follows:

Chapter 2: background information and a literature review on controlled suspension system and interconnected suspensions are provided in Chapter 2. A detailed literature survey reviews the past work in this field and summarises the gaps in the current knowledge.

Chapter 3: the MEM is introduced in detail in this chapter, including motion-modes definition and classification, MEM derivation, and several numerical examples of implementing the MEM in vehicle dynamics analysis and control.

Chapter 4: an alternative approach by employing neural networks (NNs) to identify vehicle primary motion-modes with acceptable accuracy is presented in this chapter, including structure design, training procedures, and numerical validations.

Chapter 5: a conceptual MEM-based switched control architecture for vehicle integrated motion control is presented in this chapter, including vehicle model identification and reduction, dominating mode identification, and H∞ optimization.

Chapter 6: development of a series of test facilities for the research is presented in this chapter, including: (1), a six-channel vehicle dynamic test rig, (2), a multi-functional anti-roll HIS test rig, (3), a reconfigurable HIS test rig.

Chapter 7: experimental investigation conducted in this research is presented in this chapter, including: (1) vehicle parameter estimation, (2), a passive HIS field test, (3), an active HIS laboratory test with an H∞ controller.

Chapter 8: discussion and further development recommendations are given and the contributions of this thesis are summarised.

CHAPTER 2 BACKGROUND AND LITERATURE REVIEW

2.1 Introduction and rationale

There has been a long history of the employment of suspension systems on vehicles and how they contribute to the myriad dynamic aspects of automobiles. Considering the vast body of literature related to various suspension systems in different types of vehicular systems, this chapter is only intended to serve as an introduction to active interconnected suspension systems on four-wheel vehicles. In this spirit, the author briefly reviews the area of passive suspensions, interconnected suspensions and controlled suspensions, and draw attention to the development of active interconnected suspension systems. It should also be noted that, to provide necessary background knowledge to variable methods that are proposed or employed in this study, some of the literature review contents have also been placed in other chapters of the thesis.

2.2 Passive suspensions

Automobiles have advanced a long way since the first road vehicle was propelled by a four-stroke gasoline engine in 1886 in Germany [10]. After the first assembly line was installed in 1913 in America, the automobile industry entered its massive-production era which has lasted till today. The appearances of suspension systems actually tracks back far earlier than the invention of automobiles, e.g., the leaf springs that were used on horse drawn vehicles. Although suspension systems have improved vastly from those early days, they nonetheless possess three fundamental elements: springing, damping, and location of the wheels [5].

As one of the most important systems in an automobile from the control perspective, there are many potential roles that a suspension system can play in vehicle dynamics, but the primary functions of a suspension system are [11]:

1) to isolate the chassis from road roughness and allow the wheels to follow the road;
2) to maintain required wheel orientation relative to the road, such as the steer and camber angles;
3) to transmit forces and moments produced by the tires on the vehicle;
4) to resist chassis roll;
5) and to maintain tire–road contact and minimise normal load variations.

At the early stage of vehicle dynamics studies, most research efforts focused on the role of suspension systems in providing ride performances to isolate the vehicle body from excitation sources [12, 13]. By the 1950s, with a growing emphasis on dynamic performance and safety, handling and stability became major topics of investigation [14, 15]. These two objectives set for a suspension system are at times conflicting and the design of conventional suspension systems has to be a compromise of ride and handling. Moreover, since their springing and damping parameters are fixed and non-controllable, passive suspension is not adaptive to changes in relation to vehicle parameters, e.g., loaded and unloaded, and has a very limited ability to compensate under extreme conditions, e.g., rough terrain, sharp cornering, etc.

For a two-axle vehicle, its relative motions between the body and wheels can be decoupled into seven body-wheel motion-modes. Four of them contribute most to vehicle ride comfort and handling and are generally referred to in the literature [16-19], namely, body-dominated bounce motion-mode, body-dominated roll motion-mode, body-dominated pitch motion-mode, and wheel-dominated articulation motion-mode.

For simplicity, they are referred to as bounce, roll, pitch, and articulation (warp) in this section.

Bounce, roll and pitch are body-dominated motion-modes, which can be excited by steering, accelerating/braking, and ground disturbance. Articulation, also known as warp, is a motion in which only diagonally-opposed wheels move in phase relative to the vehicle body [5]. This constitutes a non-planar mode, allowing the vehicle to travel on spatial surfaces, which is important to maintaining proper road surface contact [20]. In the existing literature, articulation is generally reported to be associated with road holding, braking/traction, roll and yaw stability.

These four motion-modes generally have conflicting requirements for suspension stiffness and damping, For example, a soft bounce motion-mode is desired for ride comfort; a reasonably soft articulation motion-mode can enhance a vehicle's road-holding performance; whilst stiff roll and pitch motion-modes are beneficial for inhibiting a vehicle's attitude fluctuation during steering, braking, and acceleration. Therefore, suspension design is also a compromising process between these modes.

2.3 Controlled suspension

More recently in the last few decades [8, 21, 22], to overcome the inevitable compromises encountered in passive suspensions, advanced controlled suspension systems have been intensively researched and developed in industrial and academic sectors. A controlled suspension can be differentiated from passive ones because of its control input to a vehicle, which makes the vehicle more adaptive in variable situations. Vehicle manufacturers wish to employ them to improve the performance and quality of their products to be more competitive, and researchers believe that based on the rapid developments in actuators, sensors and low-cost electronics, the automatic control of

vehicle suspensions will be the next logical progression of modern suspension [23]. Therefore, controlled suspensions have been widely studied for a few decades. A recent review work on controlled suspension design can be found in [5], and the optimal control theories in controlled suspension are thoroughly reviewed in [4].

Controlled suspensions can be further classified into two types: semi-active and active suspensions. Semi-active systems have control over some suspension parameters, e.g., damping, stiffness or both. They remove energy but are unable to add energy. Active suspensions require actuators and consume external power sources. They can either add or subtract energy from the system.

2.3.1.Semi-active suspension

Karnopp and Crosby first introduced the semi-active suspension concept in the early 1970s [8, 21]. Since then, variable semi-active systems, mostly semi-active dampers, have been explored and are available on a large number of high-end luxury passenger vehicles. The general survey of semi-active suspension can be found in [6, 24-27]. In semi-active suspensions, the passive dampers are replaced with dampers capable of changing their damping characteristics, such as dampers with a controllable orifice, or dampers with controllable fluids [28, 29]. Please see Figure 2.1, a magnetorheological damper [30]. The general referred advantages of being semi-active are cost effectiveness, energy efficiently and structure simplicity.

Figure 2.1. Photo of a magnetorheological damper [30].

Semi-active suspensions with adjustable dampers are less expensive than the available active options. However, semi-active dampers have an inherent limitation: they are not able to provide the control force that aligns with the velocity across the damper. Semi-actives can neither provide external energy to directionally control the vehicle motions, nor restore the vehicle body's position, such as tilting the vehicle body back to the neutral position from a motion.

2.3.2.Active suspension

Active suspensions, which have more control over suspension parameters, have a longer implementing history than the semi-actives. The first recorded attempt at active suspension technology development was in 1955 by Citroen 2CV [31]. Over the past four decades, the subject of active suspension design has been intensively reviewed by

Hedrick and Wormley [9], Goodall and Kortum [32], Sharp and Crolla [25], and Nagai[33]. Hrovat [6] presented an extensive survey covering the area of active suspension developments, including the most effort and results in this area. Other relevant reviews include [4, 34-37].

Active systems with four independent actuators (photo in Figure 2.2) ideally remove optimization constraints for comfort and handling performance at the same time, and accordingly, they have been studied the most in the existing literature. Earlier surveys in the late 1990s on these active suspensions can be found in [6, 36, 37]. Theoretical analysis indicates that active suspensions have incompatible performance with idealized actuators and optimal controllers. Sharp and Peng for instance, recently reviewed the optimal control theories that have been applied in active suspensions [4]. The actuators of these systems should have fast response and their independent structure offers the ideal control solution to a vehicle, adapting to various driving situations (braking, accelerating, and cornering), and continuously compensating for road roughness [23, 38].

Figure 2.2. Photo of a typical active suspension using linear electromagnetic motors [39].

Ideal ride and handling performance can be achieved in simulation with these idealised actuators and advanced optimal controllers, but with respect to practicality, there are some issues with realising these actuator systems. As stated in [4], with the current technology, such an independently controlled actuator would have to be a servo-valve driven, precision-made, super-clean, energy-hungry hydraulic strut, which would cost too much to make and maintain. This is also the reason behind why the active suspensions are not as available as semi-actives on the market, despite their longer history and better performance.

Efforts attempting to overcome the limitation of active suspension have been observed over the past decade. In order to make them more affordable, most designs narrow down the control objectives of active suspensions by using cheaper, less performing actuators with less ambitious, more focused control strategies. Based on the different principles, these cost effective designs can be classified into three catalogues: 1) frequency-based system; 2) single-mode-based system; and 3) mode-switchable system.

Frequency-based active suspensions are generally referred to as limited-bandwidth or low-bandwidth active systems in literature [40-43]. By leaving the high-frequency vibrations to passive components, low-bandwidth active systems focus on the primary motions of vehicle body to narrow down control objectives. The reported peak power consumption of a limited-bandwidth system can be reduced to 4 kW [5], and the actuator bandwidth is around 5 Hz. Overall, the frequency-based active suspension recognised and preserved the main advantage of an active suspension over a passive one with a tolerable energy consumption. As a result, this form of suspension is commercially available across several major vehicle manufacturers [4].

Single-mode-based active suspensions employ a single actuating device with interconnected suspension configuration to perform in a particular mode (roll, pitch, etc.). Thus they are more focused and energy efficient. One of the production systems is active anti-roll bars. The Active anti-roll bar is a mechanically interconnected suspension in roll-plane. D. Cebon from Cambridge University Transportation Research Group has developed active anti-roll bar systems for large trucks [44-48], and a photo of an electromechanical active anti-roll bar [49] is shown in Figure 2.3. By employing hydraulically interconnected configuration, similar active hydraulic anti-roll systems have also been developed in [50, 51]. Apart from roll-mode suspensions, similarly, active systems can also be design in pitch-mode to prevent pitching of a vehicle, and these pitch-mode focused active suspensions can be found in [52, 53]. Overall, the features of the single-mode-based active system can be summarised as follows: it is effective in control in one particular mode; its energy consumption is even lower than the frequency-based active suspensions, and its cost is much lower than the full-mode control system since it only requires one actuating device rather than four. Limitation is that they are not able to control other vehicle modes.

Figure 2.3. Photo of an electromechanical active anti-roll bar [49].

Mode-switchable active suspension take the advantage of the single-mode-based system, and further add in a mode-switching unit, to switch the control from one mode to another, based on the detected primary mode in real time. This design maintains the merit of having only one actuating device, but extends its application to multi-modes by re-configuring the interconnection between each wheels. At one time, the active system only controls the primary vehicle mode as the single-mode-based system does (e.g., roll mode), but switches to control other modes once they become more predominant (e.g., pitch mode). The proposed active hydraulically interconnected suspension falls into this catalogue, and is equipped with only one servo-valve as actuating device, and a set of directional valves as mode-switching unit. Servo-valves are considered as the main cost of a high-end electrohydraulic system, and by removing three of them, the system cost can be significantly reduced. Developing this type of suspension is the focus of this thesis and a survey of active interconnected suspension is provided next.

2.3.3.Active interconnected suspension

Interconnected suspensions have been proposed in passive forms since the 1920s [54] and have achieved commercial success, but have not received equal attention in the research community. Very recently, attention has been focused on interconnected suspensions. A survey of passive interconnected suspension has been done in [55]. A comprehensive survey on recent suspension development is presented with a focus on interconnected suspension in [5].

A passive interconnected suspension system is one in which the motion (displacement, velocity) at one wheel station can produce forces at other wheel stations, which is generally realised through either mechanical or fluidical means. From the kinematics point of view, suspensions of four-wheel vehicles have four important modes that are

generally referred to in literature: bounce, roll, pitch, and articulation (warp) [16-19]. Interconnected suspensions in a full-car level theoretically have the potential to uncouple these four modes [16, 19]. The vertical ride generally requires a soft bounce mode, while stiff roll and pitch modes are beneficial for inhibiting vehicle attitude during steering, braking, and acceleration. It has also been well accepted that the suspension warp mode should be as soft as possible for road-holding performance. These four fundamental modes are strongly coupled and are therefore difficult for a conventional passive suspension system to deal with. For example, the use of passive anti-roll bars increases the roll stiffness but at the same time yields a stiffer suspension warp mode which is undesirable.

Interconnections can be realised through different means. The mechanical interconnections among the suspension units in a full-vehicle model have been developed and investigated for many years [18]. The full-vehicle mechanically interconnected suspensions could decouple different suspension modes, in order to provide a more favourable compromise between ride and handling requirements, but their design is complex and their weight is considerable. In addition, they are also difficult to be tuned to adapt to various road and operating conditions. Unlike passive mechanical interconnected suspensions, fluidic suspension systems are lighter in weight and can offer viable options in improving mode properties. Their interconnection can be realised through hydraulic fluids, pneumatic fluids, or a combination of the two. The first and third types of media are most common in the literature, and they are called hydraulically interconnected suspensions and hydro-pneumatic suspensions. Full-vehicle fluidically coupled suspension systems have been investigated on the topics of pneumatically interconnected suspensions [56], hydraulically interconnected suspension, [20, 55, 57-59], hydro-pneumatic suspensions [17, 60-63], and interconnection configuration [16, 64].

One successful example of hydraulically interconnected suspension is the Kinetic H2 suspension; developed by the Australian company Kinetic Pty Ltd. Kinetic H2 suspensions typically contain four double-acting hydraulic cylinders to replace the original shock absorbers. The cylinders are mounted on the car body and the piston rods are fixed on the wheel assemblies. The chambers in the cylinders are interconnected by hydraulic circuits, arranged to counter vehicle roll motion. Each circuit comprises elements such as damper valves, hydraulic accumulators, pipelines, fittings and flexible hoses. The Kinetic Dynamic Suspension System (KDSS) is a successful commercial application of this kind of technology, and different versions are available in many applications, e.g., the Lexus GX 470 and the 200 Series Toyota Land Cruiser. The performance is reported in [59, 65].

Both semi-active and active features can be applied to interconnected suspensions, and are reviewed below. In 2004, Lovins and Cramer proposed a concept of a semi-active pneumatically interconnected suspension with adjustable pressure [56]. It consisted of four pneumatic actuators and electromagnetic dampers, a pneumatic pump and an air reservoir. The primary features were firstly that the vehicle roll stiffness could vary by changing the pressure in the pneumatic cylinder, and secondly, that the electromagnetic dampers could respond in less than a millionth of a second. Lovins and Cramer also claimed that this single-mode-based suspension, could vary the vehicle height during driving. However, the proposal was purely conceptual and detailed mechanisms to realise the proposed functions were not presented.

Since the Kinetic was taken over by Tenneco Automotive, the H2 system has been further developed with semi-active damping control, shown in Figure 2.4. The semi-control is realised through dampers and a pressure unit, referred to as CES (continuously controlled electronic suspension) valves and APMU (automatic pressure maintenance unit) in the figure. Each cylinder performs the normal wheel/car body

damping functions using the most recent damping technology incorporated within the cylinders, and modifies the damper characteristic via the semi-active setting of the CES valves. The drivers can also adjust the roll stiffness to their driving needs. Some modelling and simulation results are presented in a recent paper [66]. Nissan Patrol is reported to have Hydraulic Body Motion Control Suspension (HBMC), which is a further development of the Kinetic hydraulic suspension [67].

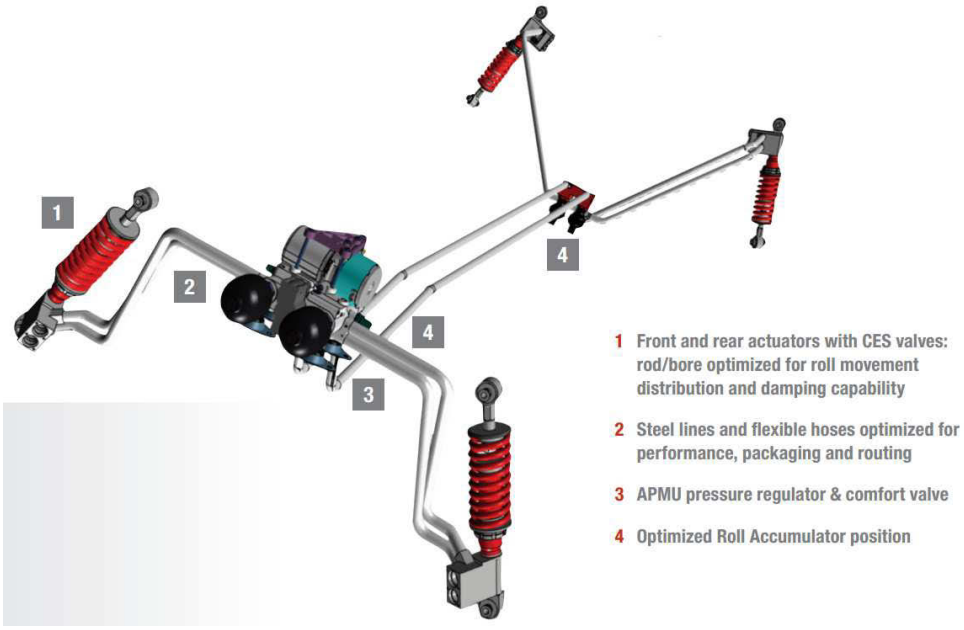

Figure 2.4. Kinetic H2 CES [68].

In the late 1990s, Rosam and Darling [69] presented the development and simulation of a sealed low bandwidth active roll control suspension based on the existing interconnected Hydragas system. The results show that the active interconnected suspension has superior performance to the passive one [70-72], but it also brought up concerns such as slow response which is owing to the high compressibility nature of pneumatic fluids in the system. In contrast, hydraulic fluids are less compressible and hydraulic active systems are faster and more forceful. For example, a diagonally interconnected active hydraulic suspension with fast responses has been employed on a racing car [73]. This system, called Dynamic Ride Control suspension, uses a pump to

provide additional pressure in the diagonally linked shock absorbers during cornering, to counteract rolling and pitching.

The above reviewed controlled interconnected suspensions directly evolve from their passive counterparts by adding pressure control features. In all of these systems, their inherent interconnecting configuration remains unchanged. Recently, Zhang proposed an interconnection reconfigurable active suspension [74], the schematic diagram of which is presented in Figure 2.5. Based on this concept, the author developed a prototype of this novel active suspension and proposed a motion-mode-based switchable control strategy.

The reconfigurable active HIS is a mode-switchable active system. It is equipped with only one servo valve to reduce the system's cost and energy consumption. The reconfigurable hydraulic interconnections is realised through a set of directional valves to reset its fluid circuits into a corresponding mode to counteract the identified primary motion-mode. The details of this system will be presented in the following chapters.

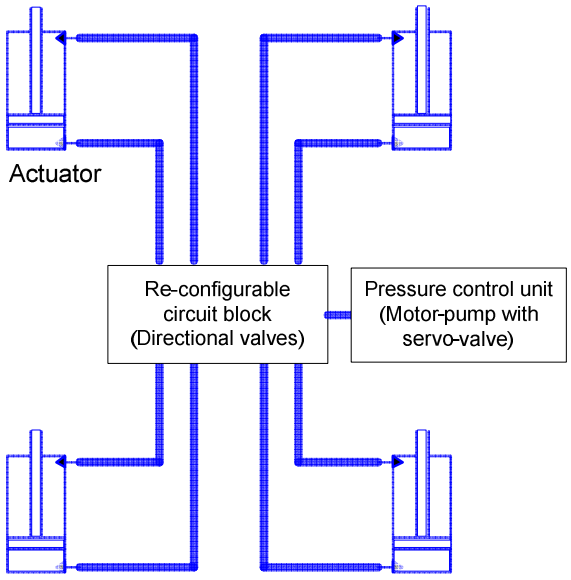

Figure 2.5. Schematic diagram of a reconfigurable hydraulically interconnected suspension.

CHAPTER 3 MOTION-MODE ENERGY METHOD FOR VEHICLE DYNAMICS ANALYSIS AND CONTROL

3.1 Introduction and rationale

The motions of a vehicular system can be classified into *body-wheel motions* and *integral multi-body motions*. *Body-wheel motions* refer to the relative motions between the vehicle body and wheels, and *integral multi-body motions* refer to rigid-vehicle-model motions, in which the vehicle's sprung and unsprung masses move together and can be treated as one object, such as lateral sliding, longitudinal travel, and yaw. These two types of motions are coupled to some extent through the tire/ground contact forces [75].

Vehicle suspension, which forms the coupling between vehicle body and wheels, has an important role to play in both types of motion. Due to the rapid development in mechatronic systems, control applications through controllable suspension systems have been in the mainstream of research for several decades [6, 7]. Controllable suspension systems are able to directly govern a vehicle's *body-wheel motions*, such as bounce, roll, pitch, and articulation (warp), and are also able to indirectly control a vehicle's *integral multi-body motions* (planar dynamics) through the control of its body-wheel motions. For example, a Crosswind Assistant System to control yaw motion by an active suspension system was reported in the literature [38]. It is a good demonstration of the indirect control of vehicle planar dynamics through the controlled articulation mode, where the active suspension pushes a diagonal wheel-pair to the ground to vary the tires' dynamic load, resulting in a yaw moment applied to the vehicle.

Vehicle *body-wheel motions* can be classified into several modes, according to the classic approach of modal analysis [76]. To date, however, no clear description of each modal mode and its contribution to the physical motions of the vehicle, have yet been detailed, investigated and presented. Therefore, the study of vehicle body-wheel motions from the modal perspective is necessary and could reveal the properties of unclear modes, such as warp and wheel-hop modes.

The potential exists to design active suspensions that are more affordable and energy-conservative by employing a switchable controller to detect and control the dominating vehicle mode. An example of such a switchable controller can be found in [77], and is designed to separately control the bounce, pitch and roll motions of a vehicle through active/semi-active actuators. This raises the fundamental question of how to detect the dominating mode of a vehicle in real time. A method therefore needs to be developed to assess and compare different modes with real-time capacity.

Motivated by the above-mentioned concerns, the author proposes a motion-mode energy method (MEM) to identify predominating modes for vehicle dynamics analysis and control.

3.2 Vibrations and motions

A vehicle is an integrated system of multiple bodies, some of which are connected elastically with each other, which changes its physical location in the course of operation, while its sub-bodies experience vibration. Conventionally, the terms *vibration* and *motion* are used alternately in a vague manner in describing a vehicle's dynamic behaviours [78], but for rigid bodies, the energy levels of motion and vibration can be very different. Based on energy intensity, vehicle vibrations and motions can possibly be unified and controlled under the same framework.

Vibration refers to the oscillation of a mechanical or structural system around its point of equilibrium. After the removal of external excitations, a system will eventually return to a state of equilibrium as long as damping exists. Modal analysis techniques can be applied to linear systems to study their modal properties as described by system natural frequency, mode shape and damping ratio. In vehicle dynamics, vibration is conventionally considered to have a minor influence on vehicle handling and stability. It is mainly associated with ride comfort and is thus treated along with noise issues and so forth.

Motion is the process of continual change in the physical position of a body relative to a reference frame. Generally, the removal of applied external forces will not lead to the body returning to its original position. In studies on vehicle dynamics, wheel motion is usually neglected when the vehicle body's motion plays a dominant role, and the vehicle system is treated as a single body having one motion. For example, during severe cornering, vehicle "*roll motion*" is conventionally used to highlight the main dynamic issue.

The author therefore propose to unite the concepts of vehicle vibrations and motions, and re-classify them into "*vibration*", "*vib-motion*", and "*ext-motion*", based on energy intensity as illustrated in Table 3.1.

Vib-motions refer to vehicular system motions that originate from system vibration modes but are beyond the level conventionally referred to as "vibration". They can be described as vibration-mode-based motions, or *vib-motions* in short. In the case of *vib-motions*, a system should eventually return to its equilibrium state or position following the removal of external excitations. When the energy intensity of motions increases further, a point will be reached where the balance of the system will be

breached, resulting in a new position for the system. These motions are defined as extreme motions, written as *ext-motions*.

Table 3.1. Classification of relative body-wheel vibrations and motions.

		Relative body-wheel vibrations and motions		
		Vibrations	*Vib-motions*	*Ext-motions*
Example		Roll vibration	Roll motion	Rollover
Energy level (J)		$0 \sim \alpha^*$	$\alpha^* \sim \beta^*$	$> \beta^*$
Continuous gradation		Vibration → Motion		
Excitation Sources		Engine, change gear, etc	Braking, turning, uneven ground input, etc	Impact, extreme manoeuvre, etc
Excitation energy		Minor	Medium	Extreme
Affect area	*Ride*	√	√	√
	Handling		√	√
	Safety			√
Control strategy		Absorb energy	Absorb energy/Active counteraction	Active counteraction
Implementation system		Passive/Semi-active	Semi-active/Active	Active

* Determination of the energy levels α and β should consider both theoretical study and practical experience

Take vehicle body roll as an example to illustrate the continual evolution from *vibration* to *vib-motion* and eventually to *ext-motion*. In high-speed cornering, a vehicle's dynamic condition can be described as *roll vibration*, *roll motion* or even *rollover*, depending on whether the amplitude of the steering input is small, moderate, or severe. These terms are used to distinguish gradual dynamic stages with increased kinetic energy.

Different control strategies can be applied at different stages of vibration and motion, as listed in Table 3.1. For *vibration*, the absorption of its dynamic energy using semi-active suspension is considered to be most efficient and effective. For *vib-motions*, either semi-active or even active measures can be taken to prevent *ext-motions* from happening. For *ext-motions*, active suspension is the most capable system. To effectively control vehicle vibrations and motions and also be energy

efficient, the combination of semi-active and active systems is a good option. Successful combination requires a method to quantify the energy intensity of different stages to enable the integration of the semi-active and active controls.

3.3 Vehicle motion-modes

Vehicle *body-wheel motions* are classified into v*ibrations*, *vib-motions and ext-motions* based on energy intensity, but they also follow modal space principle and are the superposition of its modal modes. According to modal analysis theory, the *body-wheel motions* of a vehicle can be decomposed into several modal modes. To emphasize the physical meaning rather than the mathematical meaning of these modes, they will be referred to as *motion-modes* in the following sections.

One of the most important properties of motion-modes is their orthogonality. The physical meaning of orthogonality is that the energy contained in one motion-mode does not transfer to other motion-modes. Given that a vehicle's body-wheel motions are propelled by the energy contained in its motion-modes, tracking motion-mode energy can provide us with a clear image of the dominant energy source responsible for the physical motion of the vehicle. Therefore, motion-mode energy is considered to be more stable, accurate, and comprehensive in monitoring dynamic states of a vehicle than a small number of isolated measurements.

There are seven body-wheel motion-modes for a two-axle four-wheel vehicle [79]. Based on the leading moving-element in their mode shapes, motion-modes can be further classified into two groups: body-dominated and wheel-dominated motion-modes.

The three body-dominated motion-modes are well known and are usually referred to as vehicle bounce, roll and pitch in the literature. Their frequencies generally range between 1 and 3 Hz, and in their mode shapes, the vehicle body has a much larger displacement than the wheels'. Vehicle body-dominated motions contribute most to vehicle ride and handling, and thus naturally attract more attention from researchers. The research on vehicle dynamics is mostly dedicated to the study and control of these three motion-modes.

The four wheel-dominated motion-modes are not as well known as the aforementioned body-dominated motion-modes. Their frequencies generally range between 10 and 15 Hz, and in their mode shapes, the vehicle wheels have much larger displacements compared to that of the vehicle body. In the literature, they are not distinguished and are generally referred to as wheel 'hop' modes, regardless of the relative phases of the wheels. Here these wheel 'hop' modes are named individually after their mode shape characteristics as vehicle wheel-dominated bounce, roll, pitch and articulation motion-modes. Definitions of these motion-modes are as follows: wheel-dominated bounce mode is when, relative to vehicle body, the four wheels move up and down in phase; wheel-dominated roll mode is when the left and right wheels move out of phase while the front and rear wheels move in phase; wheel-dominated pitch mode is when the front and rear wheels move out of phase while the left and right wheels move in phase; and articulation mode is when the diagonal wheels move in phase and the adjacent wheels move out of phase.

For convenience, body-dominated motion-modes and wheel-dominated motion-modes will henceforth be referred to as 'body mode' and 'wheel mode' respectively, except where ambiguity might occur.

3.4 Vehicle dynamic modelling

Two vehicle models are used in this study: a simplified 7-DOF linear full-car model is used to derive the proposed motion-mode energy method, and a 10-DOF nonlinear full-car model is employed to assess the realistic functionality of the method. The 10-DOF model is presented in this section and the 7-DOF model is presented in the subsequent section.

The 10-DOF nonlinear full-car model employed in this study has evolved from a 9-DOF model in [80] with the addition of one DOF in the longitudinal direction of the car. The 10 DOFs of the vehicle model are: sprung mass longitudinal, lateral and vertical center-of-mass motions, roll and pitch rotations for the sprung mass, yaw rotation for the total vehicle, and four center-of-mass vertical motions of the unsprung masses. The vehicle model considered here consists of a rigid sprung mass supported by four independent suspensions, which include wheel assemblies as four unsprung masses. Anti-roll bars are not used in this study and are not included in the model. Due to the constraints between the bodies, the unsprung masses cannot translate laterally with respect to the sprung mass, which means that the unsprung masses have no independent lateral degree-of-freedom. In yaw motion, the unsprung masses move with the sprung mass relative to the earth-fixed inertial reference; however, the roll and pitch rotations are restricted only to the sprung mass. The MF tire model [81], considered as state-of-the-art for modelling tire-road interaction forces and moments in vehicle dynamics studies, is employed in the modelling.

Under the assumption of the above constraints, the DOF number of the vehicle model is set to ten: sprung mass longitudinal, lateral and vertical rigid body motions, roll and pitch rotations for the sprung mass, yaw motion for the total vehicle, and four vertical motions of the unsprung masses.

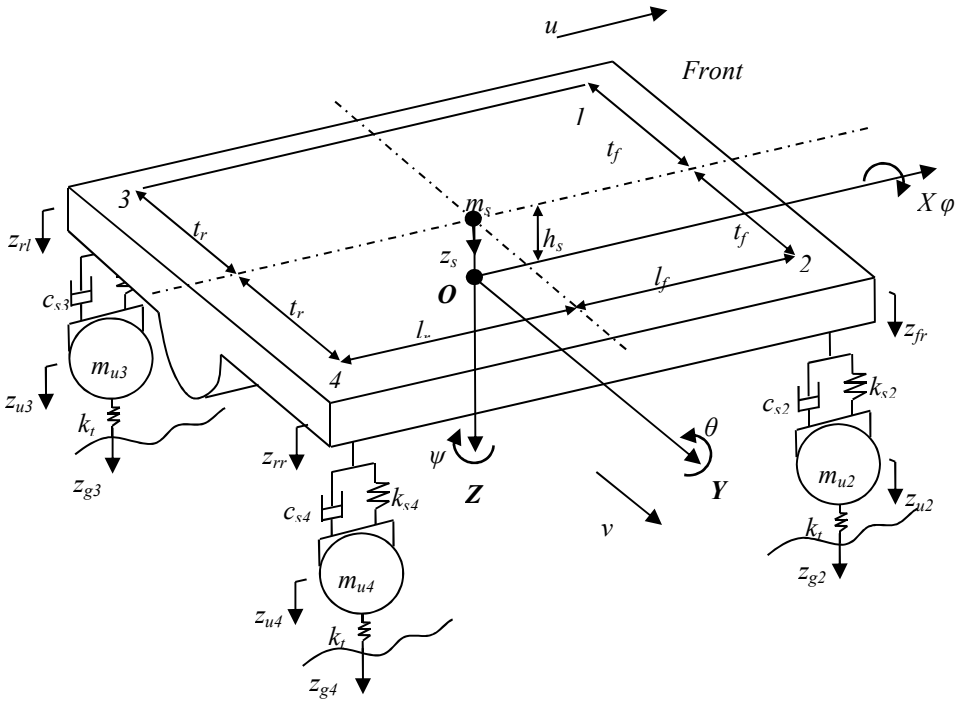

Figure 3.1. Schematic of 10-DOF vehicle model.

In Figure 3.1, z_s is the vertical displacement at the centre of gravity; θ, φ and ψ are the pitch, roll and yaw angles of the sprung mass; m_s and m_u denote the sprung and unsprung masses. The front and rear displacements of the sprung mass on the left and right sides are denoted by z_{fl}, z_{rl}, z_{fr}, and z_{rr}. The front and rear displacements of the unsprung masses on the left and right sides are denoted by z_{u1}, z_{u2}, z_{u3}, and z_{u4}. The disturbances, which are caused by road irregularities, are denoted by z_{g1}, z_{g2}, z_{g3}, and z_{g4}. The suspension stiffness and damping coefficients are denoted by k_{s1}, k_{s2}, k_{s3}, k_{s4} and c_{s1}, c_{s2}, c_{s3}, c_{s4} respectively, and tire stiffness is denoted by k_t. The parameter values used for this study are presented in Table 3.2. These parameters are obtained from a Ford SUV through experimental testing and the estimation method is provided in Section 7.

Table 3.2. Parameters and their values of the 10-DOF vehicle dynamic model.

Symbol	Value	Units	Description
m_s, m_{ui}	1800/40	kg	Sprung / unsprung mass (i =1, 2, 3, 4)
I_{xx}	780	kg·m^2	Sprung mass moment of inertia about the x-axis
I_{yy}	3800	kg·m^2	Sprung mass moment of inertia about the y-axis
I_{zz}	4050	kg·m^2	Sprung mass moment of inertia about the z-axis
I_{xz}	99	kg·m^2	Sprung mass moment of inertia about the x-z axis
I_{zz_u}	1	kg·m^2	Unsprung mass moment of inertia about the z-axis
l_f	1.36	m	Distance from sprung mass CG to the front axle
l_r	1.43	m	Distance from sprung mass CG to the rear axle
t_f, t_r	0.575	m	Half width of the front/ rear axle
h_s	0.33	m	Height of sprung mass CG above the roll axis
k_{si}	40	kN·m^{-1}	Suspension spring stiffness (i =1, 2)
k_{si}	46.5	kN·m^{-1}	Suspension spring stiffness (i =3, 4)
k_t	270	kN·m^{-1}	Tire spring stiffness
c_{si}	2500	Ns·m^{-1}	Suspension damping coefficient (i =1, 2, 3, 4)

For simplicity, only modifications to the model of [16] are presented in the chapter: the added-in/modified equations of motions for longitudinal and yaw are presented as follows, for the rest of the equations please refer to [80].

Longitudinal equation for the entire vehicle mass

$$\sum F_{tl} = \left(m_s + \sum_{i=1}^{4} m_{ui} \right) a_x \tag{3.1}$$

where a_x is the longitudinal acceleration of sprung and unsprung masses, and $\sum F_{tl}$ is the total longitudinal force between the tires and the ground:

$$\begin{aligned}\sum F_{tl} =&\left(F_{x1}+F_{x2}\right)\cdot\cos\delta_f+\left(F_{x3}+F_{x4}\right)\cdot\cos\delta_r\\&-\left(F_{y1}+F_{y2}\right)\cdot\sin\delta_f-\left(F_{y3}+F_{y4}\right)\cdot\sin\delta_r\end{aligned}\tag{3.2}$$

F_{xi} and F_{yi}, $i=1, 2, 3, 4$, are the ground contact forces for each wheel, where the subscript x indicates the tire force component in the direction of wheel head (different from the direction of vehicle travel) and the subscript y indicates the force component perpendicular to the wheel head direction. δ_f is the front tire steer angle and δ_r is the roll induced steer angle at rear. Note, the MF tire model uses the ISO axis system for calculating translating and rotational velocities, and it is different from the SAE sign convention.

Yaw equation for the entire vehicle mass

$$\begin{aligned}\sum M_z=\dot{H}_z=&\left[\left(F_{x1}+F_{x2}\right)\cdot\sin\delta_f+\left(F_{y1}+F_{y2}\right)\cdot\cos\delta_f\right]\cdot l_f\\&-\left[\left(F_{x3}+F_{x4}\right)\cdot\sin\delta_r+\left(F_{y3}+F_{y4}\right)\cdot\cos\delta_r\right]\cdot l_r\\&+\left[\left(F_{x1}-F_{x2}\right)\cdot\cos\delta_f-\left(F_{y1}-F_{y2}\right)\cdot\sin\delta_f\right]\cdot t_f\\&+\left[\left(F_{x3}-F_{x4}\right)\cdot\cos\delta_r-\left(F_{y3}-F_{y4}\right)\cdot\sin\delta_r\right]\cdot t_r\\&+M_{z1}+M_{z2}+M_{z3}+M_{z4}\end{aligned}\tag{3.3}$$

where M_{zi} (i =1, 2, 3, 4) is the tire self-aligning moment, which is the moment that a tire creates as it rolls along, which tends to steer it, i.e. rotate it around its vertical axis. The magnitude of this torque can be calculated as the product of the lateral force generated at the contact patch and the distance behind the wheel centre at which that force acts.

3.5 Motion-mode energy method (MEM)

The motion-mode energy method (MEM) analyses vehicle body-wheel relative dynamics based on the linear modal analysis theory; therefore, its derivation requires a linearized vehicle model in the vehicle-fix coordination system. The 10-DOF nonlinear

vehicle model is further simplified down to a 7-DOF linear model, which consists of 3 DOF for the sprung mass (bounce, pitch, roll) and a single DOF for each unsprung mass in vertical direction. Assuming that the pitch angle θ and the roll angle φ are small enough, the following linear approximations are applied

$$\begin{aligned} z_{fl} &= z_s + l_f\theta + t_f\varphi \\ z_{fr} &= z_s + l_f\theta - t_f\varphi \\ z_{rl} &= z_s - l_r\theta + t_r\varphi \\ z_{rr} &= z_s - l_r\theta - t_r\varphi \end{aligned} \tag{3.4}$$

where z_{fl}, z_{fr}, z_{rl}, z_{rr} represent the vertical displacement of the sprung mass at four suspension contact points, namely, front left (*fl*), front right (*fr*), rear left (*rl*) and rear right (*rr*). Equation (3.4) can be summarized as

$$x_s = L^T \mathrm{x}_\mathrm{m} \tag{3.5}$$

where $x_m = [z_s\ \theta\ \varphi]^\mathrm{T}$, $x_s = [z_{fl}\ z_{rl}\ z_{fr}\ z_{rr}]^\mathrm{T}$, and

$$L = \begin{bmatrix} 1 & 1 & 1 & 1 \\ l_f & l_f & -l_r & l_r \\ t_f & -t_f & t_r & -t_r \end{bmatrix}$$

The unsprung mass state vector is $x_u = [z_{u1}\ z_{u2}\ z_{u3}\ z_{u4}]^\mathrm{T}$, ground input vector is $x_g = [z_{g1}\ z_{g2}\ z_{g3}\ z_{g4}]^\mathrm{T}$. By defining the following vehicle system's physical parameter matrices

$$M_s = \begin{bmatrix} m_s & 0 & 0 \\ 0 & I_\theta & 0 \\ 0 & 0 & I_\varphi \end{bmatrix},\quad M_u = \begin{bmatrix} m_{u1} & 0 & 0 & 0 \\ 0 & m_{u2} & 0 & 0 \\ 0 & 0 & m_{u3} & 0 \\ 0 & 0 & 0 & m_{u4} \end{bmatrix},\quad K_s = \begin{bmatrix} k_{s1} & 0 & 0 & 0 \\ 0 & k_{s2} & 0 & 0 \\ 0 & 0 & k_{s3} & 0 \\ 0 & 0 & 0 & k_{s4} \end{bmatrix},$$

$$K_t = \begin{bmatrix} k_t & 0 & 0 & 0 \\ 0 & k_t & 0 & 0 \\ 0 & 0 & k_t & 0 \\ 0 & 0 & 0 & k_t \end{bmatrix},\quad C_s = \begin{bmatrix} c_{s1} & 0 & 0 & 0 \\ 0 & c_{s2} & 0 & 0 \\ 0 & 0 & c_{s3} & 0 \\ 0 & 0 & 0 & c_{s4} \end{bmatrix},$$

the motion equations of the 7-DOF model can be formalized in the form of second order differential equations as

$$\begin{bmatrix} M_s & 0 \\ 0 & M_u \end{bmatrix}\begin{bmatrix} \ddot{x}_m \\ \ddot{x}_u \end{bmatrix}+\begin{bmatrix} LC_sL^T & -LC_s \\ -C_sL^T & C_s \end{bmatrix}\begin{bmatrix} \dot{x}_m \\ \dot{x}_u \end{bmatrix}+\begin{bmatrix} LK_sL^T & -LK_s \\ -K_sL^T & K_s+K_t \end{bmatrix}\begin{bmatrix} x_m \\ x_u \end{bmatrix}=\begin{bmatrix} 0 \\ K_t \end{bmatrix}x_g \quad (3.6)$$

which is further written as

$$M\ddot{Z}+C\dot{Z}+KZ=F \quad (3.7)$$

where

$$M=\begin{bmatrix} M_s & 0 \\ 0 & M_u \end{bmatrix},\ C=\begin{bmatrix} LC_sL^T & -LC_s \\ -C_sL^T & C_s \end{bmatrix},\ K=\begin{bmatrix} LK_sL^T & -LK_s \\ -K_sL^T & K_s+K_t \end{bmatrix},\ Z=\begin{bmatrix} x_m & x_u \end{bmatrix}^T,\ F=\begin{bmatrix} 0 \\ K_t \end{bmatrix}x_g.$$

By defining $X=\begin{bmatrix} Z & \dot{Z} \end{bmatrix}^T$, system Equation (3.7) can be further arranged into state-space form as $\dot{X}=AX+\overline{F}$ (3.8)

where

$$A=\begin{bmatrix} 0 & I \\ -M^{-1}K & -M^{-1}C \end{bmatrix},\ \overline{F}=\begin{bmatrix} 0 \\ M^{-1}F \end{bmatrix}.$$

The matrix A is the system characteristic matrix (with dimension of 14×14), and its eigendecomposition gives an eigenvalue matrix $\overline{\Omega}$ and an eigenvector matrix U [82]. $\overline{\Omega}$ contains seven pairs of complex conjugate eigenvalues and U has seven pairs of corresponding complex conjugate eigenvectors, expressed in the following form:

$$\overline{\Omega}=diag\begin{pmatrix} \Lambda & \Lambda^* \end{pmatrix},\ U=\begin{bmatrix} \Psi & \Psi^* \\ \Psi\Lambda & \Psi^*\Lambda^* \end{bmatrix}.$$

Note, $*$ represents the conjugated counterpart of a complex number, vector or matrix. Λ and ψ are system eigenvalue and eigenvector matrices respectively, given as following:

$$\Lambda=diag\begin{pmatrix} \lambda_1 & \lambda_2 & \cdots & \lambda_7 \end{pmatrix},\ \Psi=\begin{bmatrix} \phi_1 & \phi_2 & \cdots & \phi_7 \end{bmatrix}.$$

The modal parameters of the vehicle are then abstracted and presented in Table 3.3.

Table 3.3. Modal parameters of vehicle body-wheel motion-modes.

Motion-mode	mode 1	mode 2	mode 3	mode 4	mode 5	mode 6	mode 7
Description	Body-dominated Roll mode	Body-dominated Pitch mode	Body-dominated Bounce mode	Wheel-dominated Bounce mode	Wheel-dominated Roll mode	Wheel-dominated Pitch mode	Wheel-dominated Articulation mode
Frequency	1.28	1.37	1.51	13.78	13.88	13.93	14.1
Damping ratio	0.2	0.23	0.22	0.37	0.36	0.36	0.35
Mode shape							
Z	0	0.96	1.00	-0.02 + 0.03i	0	-0.014+0.025i	0
θ	0	1.00	-0.45-0.09i	-0.01 + 0.02i	0	0.012-0.019i	0
φ	1.00	0	0	0	-0.36+0.052i	0	0.01-0.02i
Z_{u1}	0.07 - 0.03i	0.29 - 0.12i	0.04 - 0.04i	1	1.00	-0.07-0.03i	0.53+0.12i
Z_{u2}	-0.07 + 0.03i	0.29 - 0.12i	0.04 - 0.04i	1	-1.00	-0.07-0.03i	-0.53-0.12i
Z_{u3}	0.08 - 0.03i	-0.06+ 0.05i	0.24- 0.09i	0.07+0.03i	0.53+0.12i	1.00	-1.00
Z_{u4}	-0.08 + 0.03i	-0.06+ 0.05i	0.24- 0.09i	0.07+0.03i	-0.53-0.12i	1.00	1.00

It can be seen from Table 3.3 that the sprung mass in modes 1~3 has a larger movement than unsprung masses. Therefore, modes 1~3 are called body-dominated motion-modes, within the frequency range of 1.28 to 1.51 Hz. Similarly, modes 4~7 are called wheel-dominated motion-modes, within the frequency range of 13.78 to 14.1 Hz.

To be implemented in the study of vehicle dynamics and control, the motion-modes should have the same unit for comparison and also be measureable in real time. The dynamic energy contained in motion-modes, considered as a stable scalar that can be easily compared through different modes, is employed to form a unified reference frame for comparing motion-modes. The method of calculating motion-mode energy with real-time capability is called the motion-mode energy method, or MEM.

The MEM begins with a modal superposition of the vehicle state vector using the obtained system modal parameters. In this process, the physical motions in the three-dimensional physical coordinate frame are transferred into a vector of seven modal amplitudes in a seven-dimensional modal coordinate frame. A corresponding

state vector component can then be derived as the contribution of each motion-mode to the vehicle's motions, and used to calculate its motion-mode energy. A flow chart in Figure 3.2 illustrates the two-step coordinate transformation.

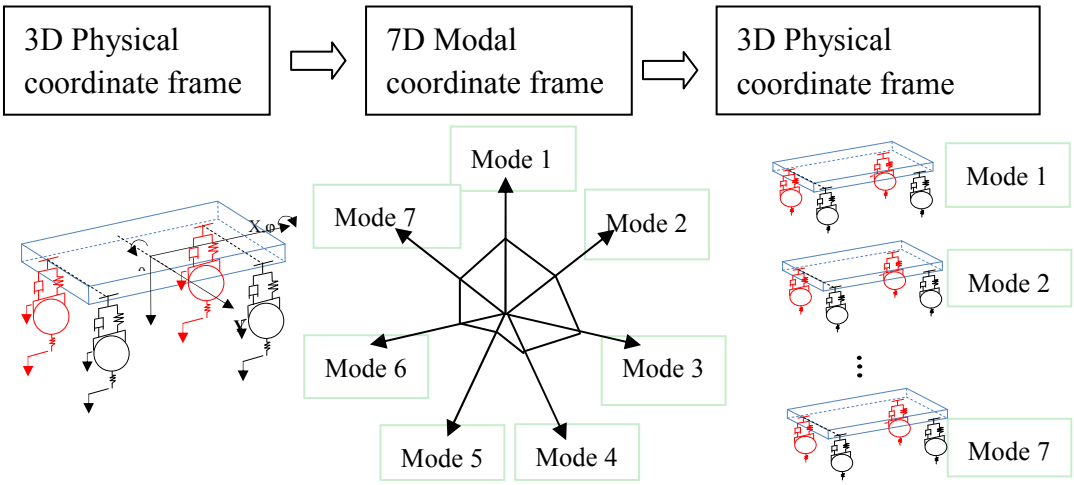

Figure 3.2. A flow chart of the MEM.

In a motion-mode, the kinetic energy of the masses and potential energy in the springs are calculated separately with the given physical properties (mass, mass moment of inertia, stiffness) of the vehicle. The sum of kinetic and potential energy in the motion-mode is defined as the mode energy, which indicates the energy intensity of this motion-mode. The normalization of all motion-mode energy gives the motion-mode energy contribution ratio, written as mode-ratio.

The following equations explain this function mathematically. From the modal analysis, the eigenvalue matrix Ψ and eigenvector matrix Λ are used to form a 14×7 modal transition matrix Γ, which is specified as

$$\Gamma = \begin{bmatrix} \Psi & \Psi\Lambda \end{bmatrix}^T$$

The vehicle 14×1 dimensional system state vector X then can be written as

$$X = \Gamma q \tag{3.9}$$

where $q = [q_1 \quad q_2 \quad \cdots \quad q_i]^T$ is the modal amplitude vector (i =1, 2,⋯7). Note that the modal amplitude q_i is a complex number; it contains the scalar quantity and the phase information of this mode for this time instant. Rewrite the Equation (3.9)

$$q = pinv\ (\Gamma)\, X \tag{3.10}$$

Where *pinv(Γ)* returns the Moore-Pensrose pseudoinverse of *Γ*. As indicated in Figure 3.2, the second coordinate transformation in the flow chart of the MEM requires the projection of the modal amplitude onto the physical coordinate frame. The projection of q_i in the physical coordinate frame is written as $[Y_i \quad \dot{Y}_i]$, where $Y_i = [y_{mi} \quad y_{ui}]$, i =1, 2,⋯ 7, derived from the following equations

$$Y_i = real\ (q_i \phi_i)\ , \dot{Y}_i = real\ (q_i \phi_i \lambda_i) \tag{3.11}$$

$[Y_i \quad \dot{Y}_i]$ is the corresponding state vector component in the form of displacement and velocity, and represents the i^{th} motion-mode's contribution to vehicle's body-wheel motions. y_{mi} and y_{ui}, similar to x_{mi} and x_{ui} in Section 5, are used to distinguish the body motions and the wheels' motions.

Since a motion-mode can only exchange energy with the external environment but not with other motion-modes, each motion-mode can be considered as an insulated energy channel to each other. For a free vibration, in each motion-mode its energy continuously converts between potential energy and kinetic energy, and decays due to the damping effect. In this way, the 7-DOF vehicle model can be decoupled into seven motion-modes corresponding to seven energetically isolated channels, and their energy is calculated below.

The kinetic energy e_{ki} and potential energy e_{pi} stored in the i^{th} mode are derived in Equation (3.12) and Equation (3.13). Their sum is defined as the motion-mode energy e_i in Equation (3.14)

$$e_{ki} = \frac{1}{2} M \dot{Z}_i^2 \tag{3.12}$$

$$e_{pi} = \frac{1}{2} H \begin{bmatrix} L^T y_{mi} - y_{ui} \\ y_{ui} - y_{gi} \end{bmatrix}^2 \tag{3.13}$$

$$e_i = e_{ki} + e_{pi} \tag{3.14}$$

where i=1, 2,⋯ 7; L please refers to Equation (3.5); M and H are the mass matrix and stiffness matrix for energy calculation, specified as

$$M = \begin{bmatrix} M_s & 0 \\ 0 & M_u \end{bmatrix}, \quad H = \begin{bmatrix} K_s & 0 \\ 0 & K_t \end{bmatrix}.$$

Note y_{gi} is the projection of the road excitation input x_g in the i^{th} motion-mode. The derivation of y_{gi} follows the same superposition principle with the $[Y_i \quad \dot{Y}_i]$ so it is omitted here. The sum of the energy from all modes is then written as

$$E = \sum_{i=1}^{7} e_i \tag{3.15}$$

Finally the mode energy contribution ratio η_i can be obtained as

$$\eta_i = \frac{e_i}{E}, \quad (i = 1, 2, \cdots 7). \tag{3.16}$$

Note η_i the energy contribution ratio of the i^{th} mode, is a function of time and is calculated at every time instant.

The MEM presented is derived from modal analysis theory but extends the theory into real-time application for vehicle dynamics analysis and control. It can be seen from the MEM equations presented that the system damping coefficient matrix is only used in

mode shape preparation but is not required in the motion-mode energy calculation algorithm. This allows the MEM to have both accuracy and real-time capability, which distinguishes it from many other traditional modal analysis techniques.

Conventional modal analysis methods (mostly frequency domain-based methods) either ignore the damping or assume that the damping matrix is proportional to the mass and stiffness to allow their algorithms to be solved, due to the complicated nature of damping and the commonly asymmetric system damping coefficient matrix. Once these assumptions have been made, the resultant errors about damping are unavoidable. In addition processing algorithms that require a large amount of historical data takes significant computing effort. Because of these constraints, it is not practical to implement traditional modal analysis techniques in real time cases. The MEM detects the primary motion-mode of the vehicle by employing the motion-mode energy concept, which is calculated using the state and mode shapes of the vehicle. Since dampers do not contain a system's instantaneous energy at a time instant, the MEM does not require the system damping coefficients or historical data for its on-board calculation and is therefore real-time capable.

3.6 Numerical examples

This section applies the MEM to the full-car model and demonstrates its effectiveness in assessing road vehicle dynamics under excitations arising from vehicle-road interactions, directional manoeuvres, and braking. In several realistic driving scenarios based on the 10-DOF full-car model, the MEM analyses the contribution of seven motion-modes, interpreting vehicle dynamics from the motion-mode perspective. The detected dominant motion-mode with respect to time could be used to prioritise the control objectives.

3.6.1.Road bump and pothole

First consider an isolated irregularity [83], further referred to as a bump or pothole, of the form

$$r(x)=\begin{cases}\frac{1}{2}a[1-\cos\frac{2\pi x}{b}], & 0\le x\le b\\ 0, & x<0,\ x>b\end{cases} \tag{3.17}$$

where a=100 *mm*, b=200 *mm* are the bump "height" and "width", respectively; and a negative value of a corresponding to a pothole.

3.6.2.Speed bump

This test involves driving a vehicle over a speed bump at a speed of 20 km/h, 30 km/h and 50 km/h, respectively. The vehicle's motion-mode energy and mode-ratio are presented in Figure 3.3-Figure 3.5. Figure 3.3(a) shows the speed bump impacting the vehicle at the front and rear wheels separately. Each impact has two energy peaks, and in total there are four energy peaks. For each impact, the first peak is dominated by a body mode, and the second peak is dominated by a wheel mode, as illustrated in Figure 3.3(b). For these four energy peaks, there are four corresponding motion-modes sequentially dominating the vehicle's body-wheel dynamics: body-pitch mode, wheel-bounce mode, body-bounce mode and wheel-pitch mode.

At different vehicle speeds, the sequence of the dominating mode is rather the same, as shown in Figure 3.3(b), Figure 3.4(b) and Figure 3.5(b), but for each impact, the energy distribution between its two peaks changes. It can be seen through the comparison of Figure 3.3(a), Figure 3.4(a) and Figure 3.5(a). Take the front wheel impact as an example; the comparison indicates that as the vehicle speed increases, more energy concentrates into its first peak which is dominated by the body-pitch mode. The first energy peak gradually increases with the vehicle speed: 2076 J at 20

km/h, 2411 J at 30 km/h and 2600 J at 50 km/h, while the second peak (dominated by the wheel-bounce mode) decreases with vehicle speed: 2688 J at 20 km/h, 1522 J at 30 km/h, and 600 J at 50 km/h. The rear wheel impact follows the same pattern.

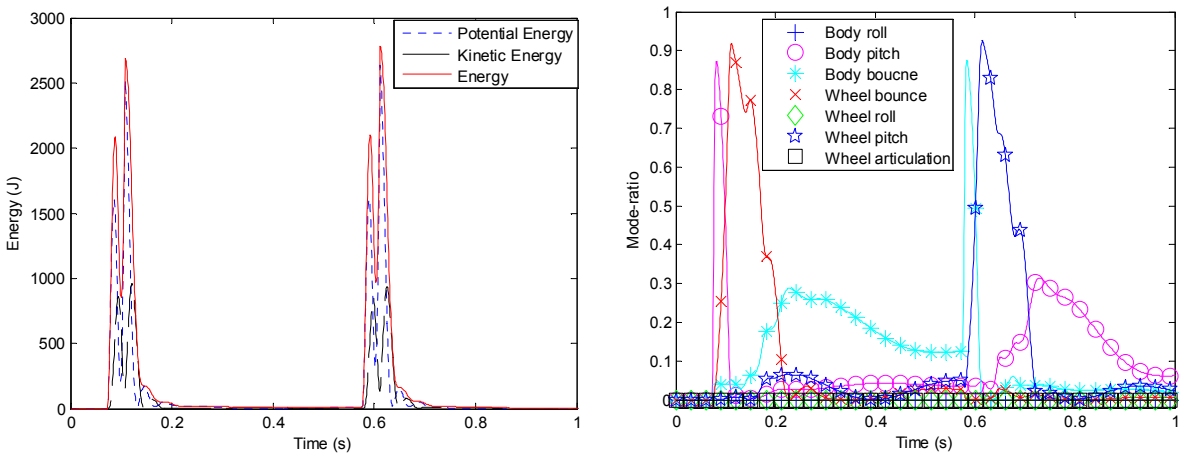

(a) (b)

Figure 3.3. Motion-mode study of a vehicle's passage over a speed bump at 20 km/h: (a) *motion-mode energy*; and (b) *mode-ratio*.

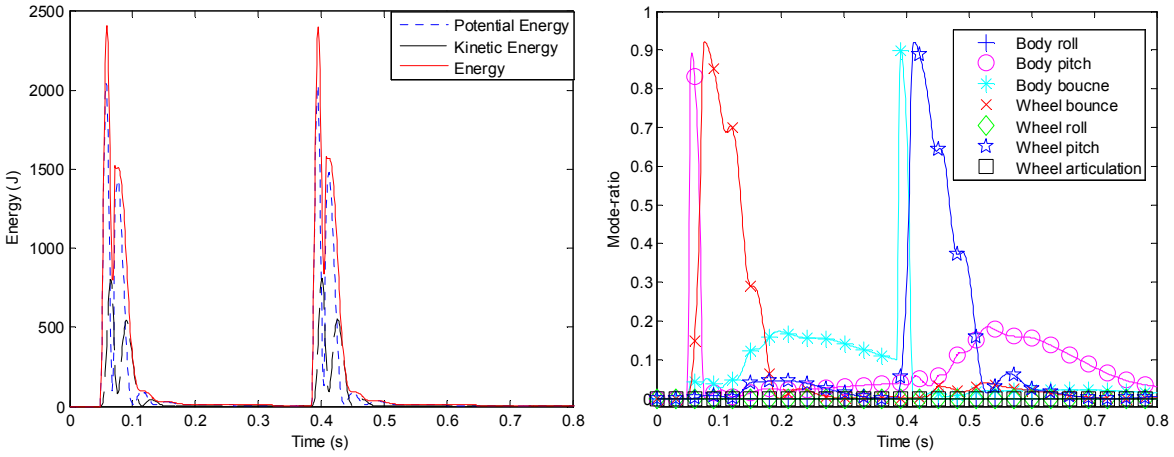

(a) (b)

Figure 3.4. Motion-mode study of a vehicle's passage over a speed bump at 30 km/h: (a) *motion-mode energy*; and (b) *mode-ratio*.

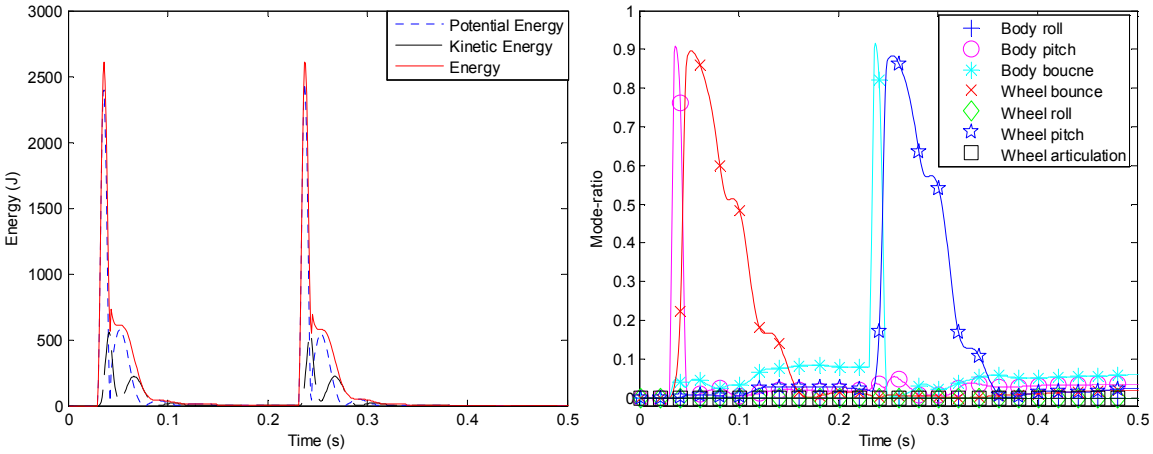

(a) (b)

Figure 3.5. Motion-mode study of a vehicle's passage over a speed bump at 50 km/h: (a) *motion-mode energy*; (b) *mode-ratio*.

This suggests, in the speed bump cases, the control focus should shift from wheel-dominated motion-modes to body-dominated motion-modes as the vehicle speed increases to maximise the control performance.

3.6.3.Road pothole

In this test, two sets of potholes are used as excitation along the left track, with a vehicle speed of 100 km/h. Pothole 1 represents a shallow bowl-shaped hole, where a = -50mm and b = 800mm are the depth and length, respectively. In Figure 3.6(a), the motion-mode energy graph is similar to the bump test at 30 km/h in Figure 3.4(a), but with a much smaller amplitude. Since in this test the input is not left-right symmetric, unlike the bump tests, the roll and articulation motion-modes are excited as well. It can be seen that Figure 3.6(b) shows the existence of the roll modes during the impact of front wheels and the articulation mode during the impact of rear wheels.

Pothole 2, where a=-80mm, b=200mm, represents a deeper but smaller hole. In Figure 3.7(b), the sequence of the primary modes appears in a similar manner to that in Figure

3.6(b). However for each impact, its second energy peak is notably absent in Figure 3.7(a). This indicates that the wheel modes are barely excited in this case and the control strategy can be made accordingly.

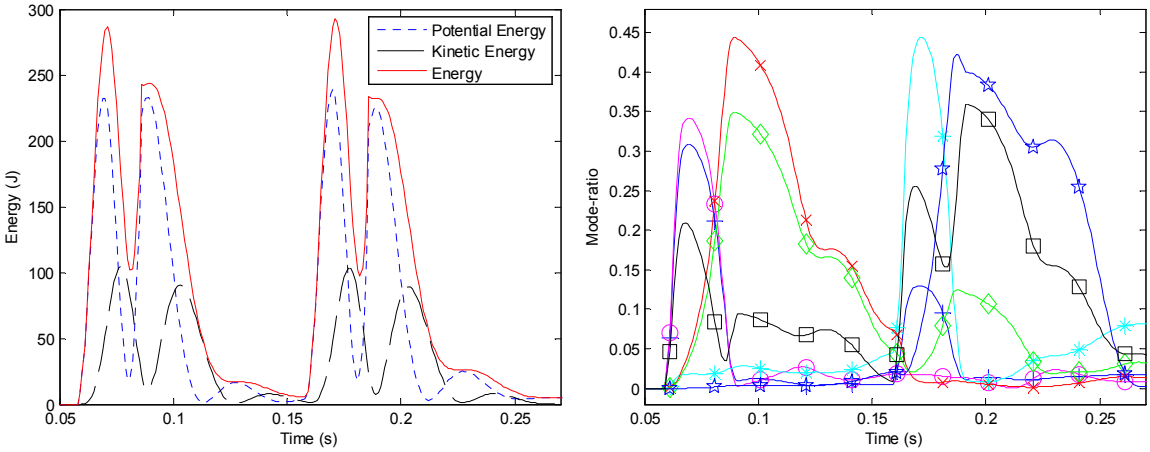

(a) (b)

Figure 3.6. Motion-mode study of a vehicle's passage over a road pothole of $a = -50mm,\ b = 800mm$: (a) *motion-mode energy*; (b) *mode-ratio*.

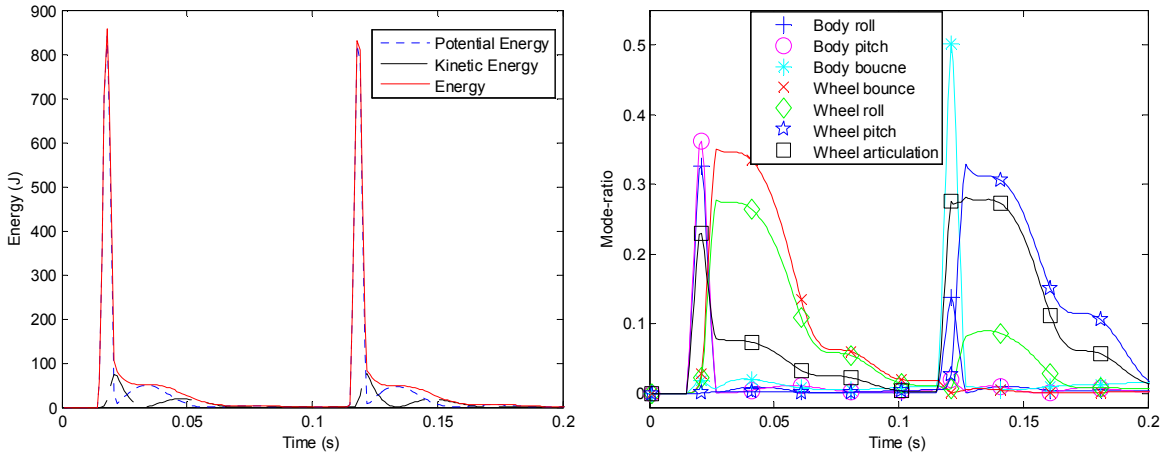

(a) (b)

Figure 3.7. Motion-mode study of a vehicle's passage over a road pothole of $a = -80m,\ b = 200mm$: (a) *motion-mode energy*; (b) *mode-ratio*.

3.6.4. Steering and braking

This example studies the combined operation of the steering and braking of a vehicle when exiting a highway. The test involves driving the vehicle on a smooth road at an initial speed of 120 km/h, applying a four-second brake (corresponding to a longitudinal acceleration of 0.4 g), and then applying a step steering wheel input during the last 2 seconds of the braking operation.

The vehicle speed, pitch angle, roll angle and CG vertical displacement are presented in Figure 3.8. The motion-mode energy and mode-ratio are presented in Figure 3.9. Although the vehicle state variables presented in Figure 8 illustrate the underlying dynamics of the vehicle, the different vehicle dynamic aspects can hardly be unified and compared in the same reference frame. By contrast, the MEM is able to bring different vehicle dynamic aspects together and compare them in the same manner. In this example, both vehicle pitching and rolling are stimulated in the overlap period (2~4 s), and vehicle roll and pitch dynamic aspects are compared with motion-mode energy in Figure 3.9(b).

Figure 3.9(b) shows that in the first two seconds of braking, the body-pitch mode is the dominating mode; the body-bounce and wheel-pitch modes are the secondary mode; and the wheel-bounce mode plays a minor role. However, after the steering starts at 2s, the vehicle body-roll mode quickly takes over as the dominant mode, while the wheel-roll mode and the body-pitch mode become secondary. In the overlapped overlap period of the two operations, the MEM suggests prioritizing the roll dynamics in the control in this case.

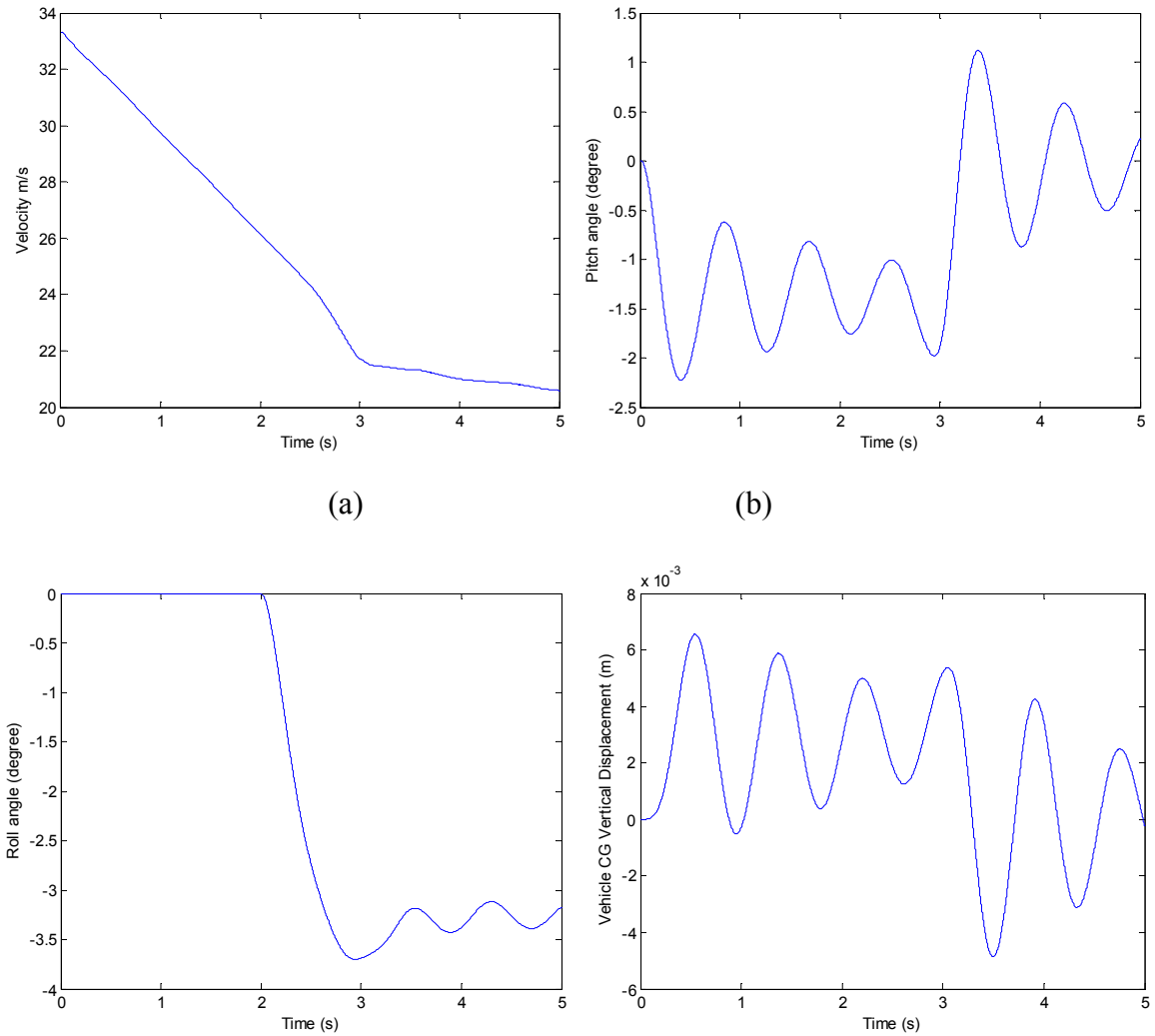

Figure 3.8. Dynamic responses of a vehicle in a combined dynamic event of braking and steering: (a) *vehicle speed*; (b) *sprung mass pitch angle*; (c) *sprung mass roll angle*; and (d) *CG vertical displacement*.

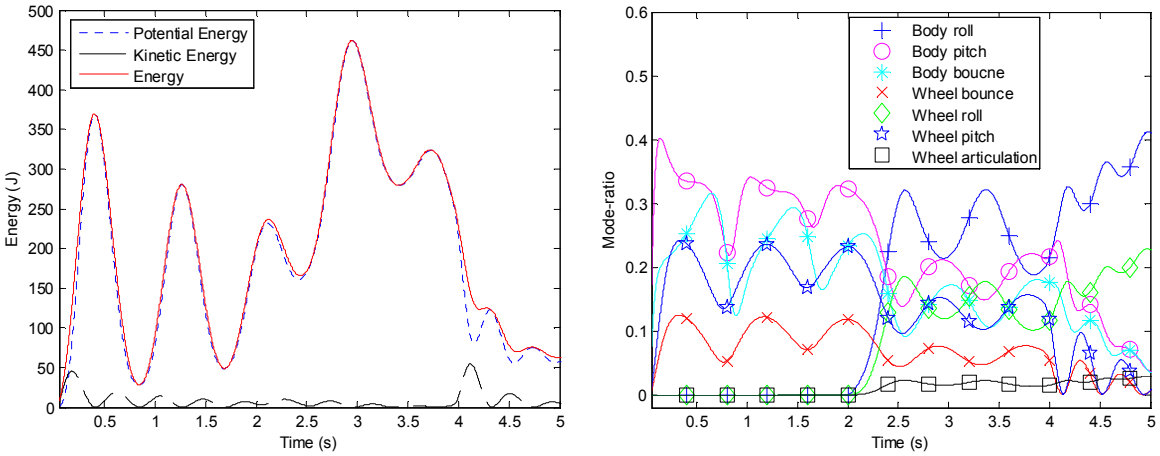

(a) (b)

Figure 3.9. Motion-mode study of a vehicle in a combined dynamic event of braking and steering: (a) *motion-mode energy*; (b) *mode-ratio*.

3.6.5.Fishhook manoeuvre with road excitation

Vehicle-road interactions provide excitations to the vehicle through its wheels, and the wheels' motions are predominantly determined by the wheel-dominated motion-modes. In the literature, it has been reported that ground excitation has an influence on vehicle handling behaviour through the variation of tire normal loads [75], and in particular the coherence of the excitations along the left and right tracks has a considerable effect on roll-plane vehicle dynamics [84]. The following example presents a study of the influence of ground excitation on vehicle handling from the motion-modes perspective.

The vehicle state vector can be processed as a superposition of seven motion-modes, and in a similar manner, the ground excitation to four wheels can also be considered as a superposition of seven modes. Different wheel-excitation modes stimulate corresponding vehicle motion-modes, resulting in different effects on vehicle ride, handling and even safety.

Roll mode is taken as an example here to elaborate on the effects of wheel-excitation on vehicle handling. The test is conducted in the following way: performing a fishhook manoeuvre at a speed of 75 km/h under three conditions: 1) no road excitation; 2) body-roll-mode excitation; and 3) wheel-roll-mode excitation. The body-roll-mode excitation consists of two out-of-phase 10 mm sinusoidal waves to the left and right wheels at a specified frequency (1.28 Hz) to stimulate the body-roll motion-mode. The wheel-roll-mode excitation is defined in a similar way but at a different frequency of 13.88 Hz in order to stimulate the wheel's mode. The steering wheel angle input of the fishhook manoeuvre is presented in Figure 3.10 and the obtained results are compared through the three cases in Figure 3.11-13.

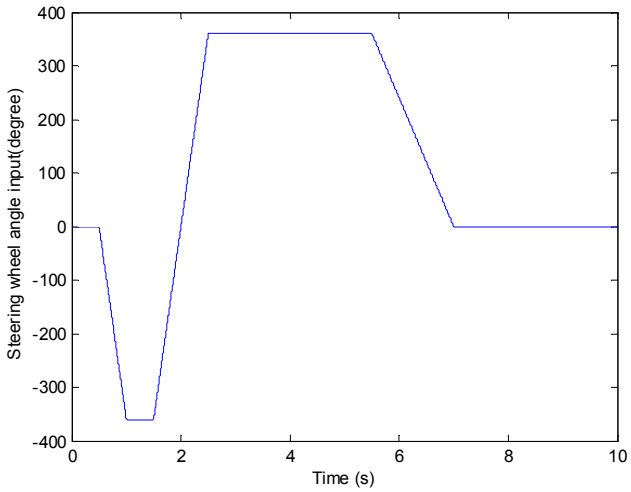

Figure 3.10. Steering wheel angle input of the fishhook manoeuvre.

By comparing Figure 3.11(a), Figure 3.12(a) and Figure 3.13(a), it can be seen that the ground excitation stimulates vehicle motion-mode energy: the vehicle's total motion-mode energy increases 84% with the body-roll-mode excitation and increases 62% with the wheel-roll-mode excitation. Furthermore, the mode-ratio graphs in Figure 3.11(b), Figure 3.12(b) and Figure 3.13(b) suggest that the body-roll-mode

ground excitation stimulates the corresponding body-dominated roll motion-mode and increases its proportion.

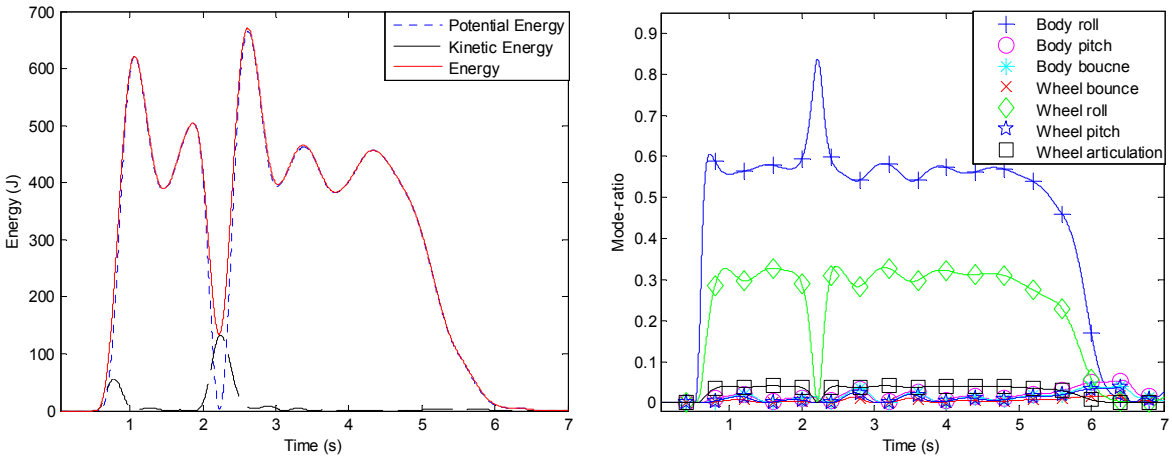

(a) (b)

Figure 3.11. Motion-mode study of a vehicle in the dynamic event of a fishhook manoeuvre with no road excitation: (a) *motion-mode energy*; and (b) *mode-ratio*.

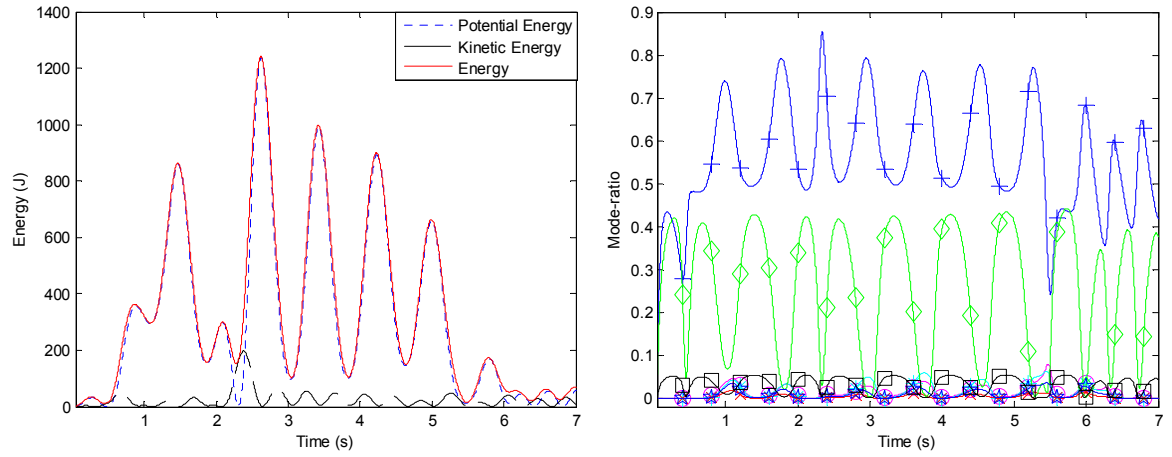

(a) (b)

Figure 3.12. Motion-mode study of a vehicle in the dynamic event of a fishhook manoeuvre with body-roll-mode road excitation: (a) *motion-mode energy*; and (b) *mode-ratio*. For the legend please refer to Figure 11(b).

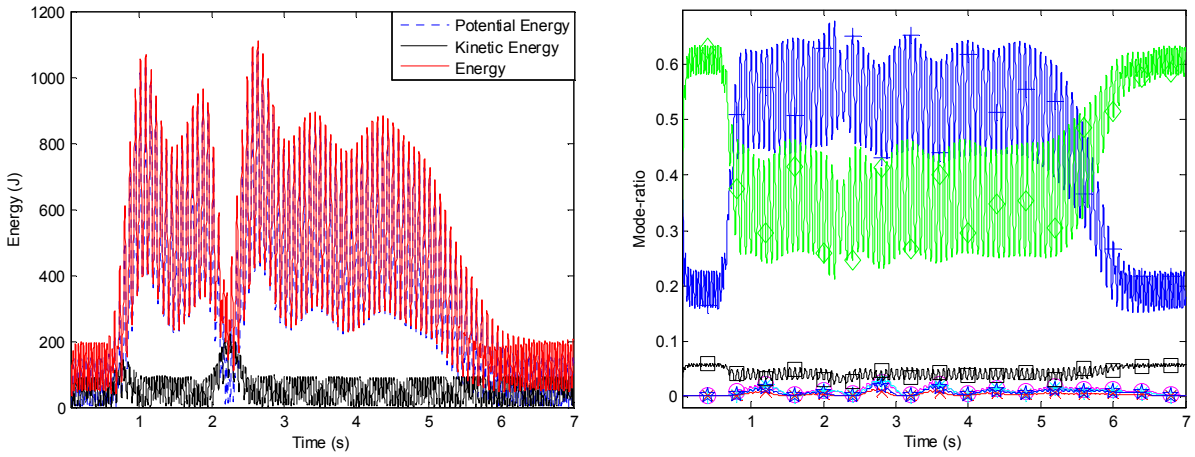

(a) (b)

Figure 3.13. Motion-mode study of a vehicle in the dynamic event of a fishhook manoeuvre with wheel-roll-mode road excitation: (a) *motion-mode energy*; and (b) *mode- ratio*, for the legend please refer to Figure 11(b).

The influences of the two types of ground excitations on vehicle handling are compared in Figure 3.14-15, in terms of vehicle speed, roll dynamics, vehicle slip angle, yaw rate, rollover critical factor (RCF) [80], lateral acceleration and tire/ground contact force. The body-roll-mode excitation has a detrimental effect on vehicle roll angle, roll rate, side slip angle and yaw rate, while the wheel-roll excitation's effects on these aspects are not notable, as shown in Figure 3.14(b~e). However, the hazardousness of wheel-roll-excitation is captured by RCF in Figure 3.14(f). A reduction in RCF represents an increased risk of rollover and a negative RCF value indicates the vehicle is in a dangerous state of potential rollover. The comparison of RCF through these three cases clearly shows that the vehicle under the wheel-roll-excitation has the worst dynamic roll stability and is in danger of rollover. Furthermore, wheel-roll-excitation causes large oscillations in the vehicle body lateral acceleration as shown in Figure 3.15(a).

The comparison indicates that the wheel-related mode is more dangerous than the body-related mode for a vehicle making a critical manoeuvre. The reason is that the wheel modes have a strong influence over tire/ground contact forces which is particularly significant for a vehicle under cornering. Figure 3.15(b) shows the extreme fluctuations of the tire's normal dynamic load in this study of the manoeuvre. This is because the wheel-dominant mode of vehicle is energized from the ground excitation, and the excessive motion of the wheels causes the fluctuations of tires' dynamic load.

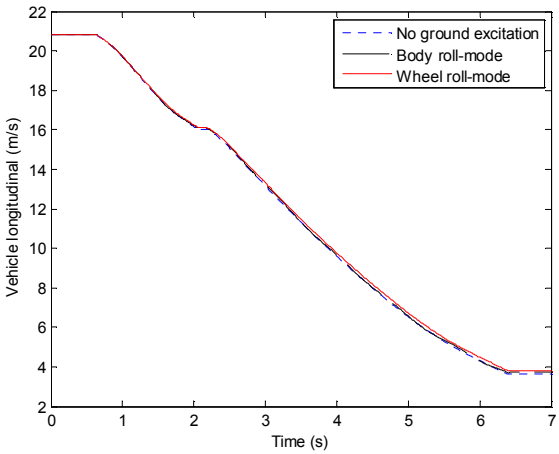

(a)

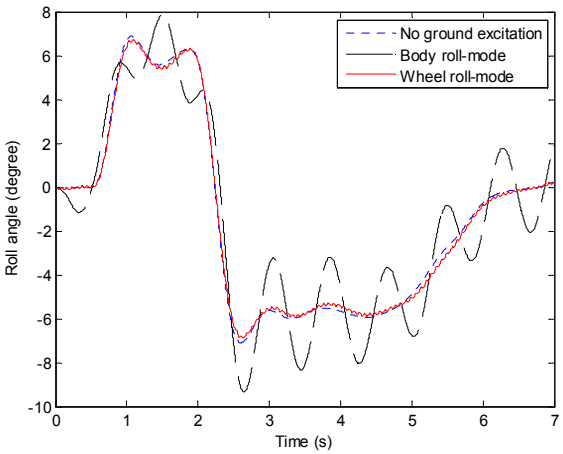

(b)

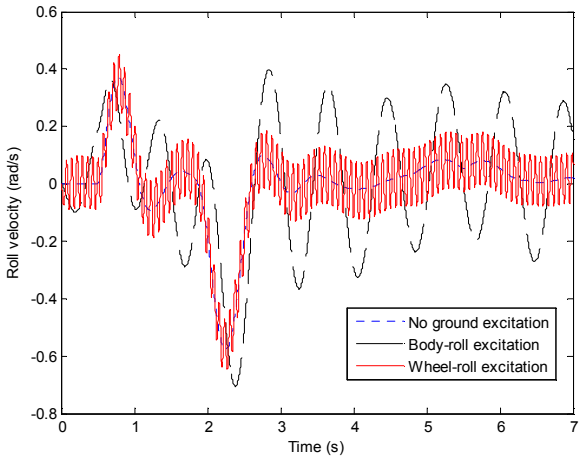

(c)

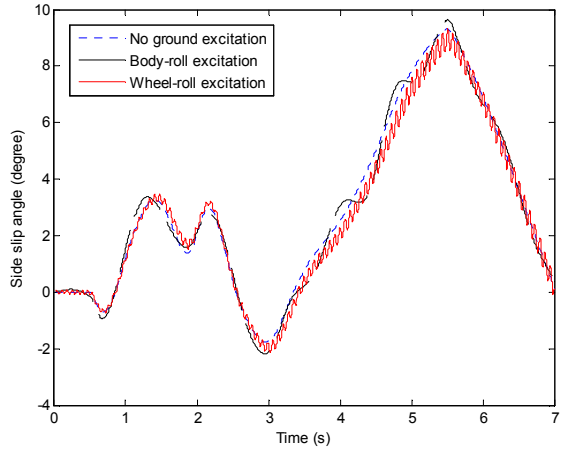

(d)

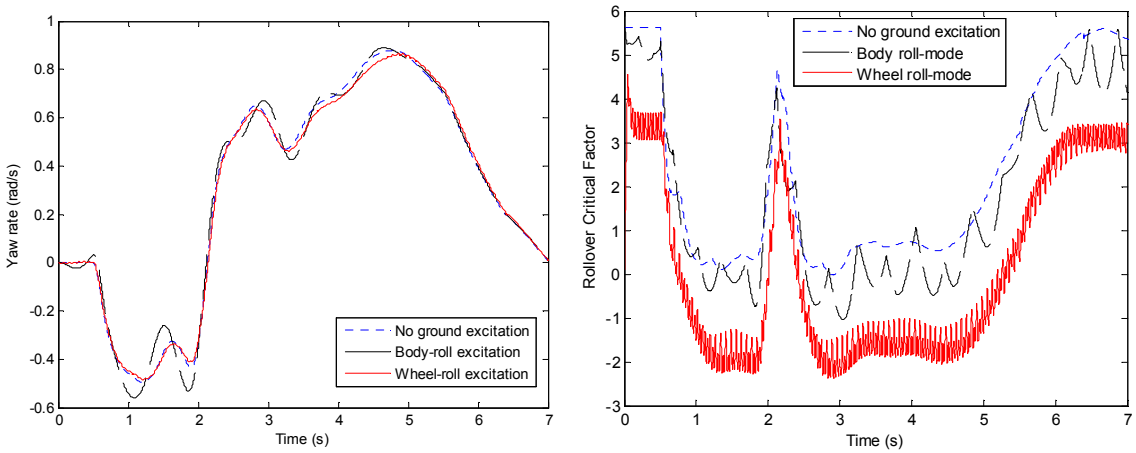

(e) (f)

Figure 3.14. Comparison of dynamic responses and indicators under different ground excitations: (a) *vehicle speed*; (b) *sprung mass roll angle*; (c) *sprung mass roll velocity*; (d) *vehicle side slip angle*; (e) *yaw rate*; and (f) *rollover critical factor*.

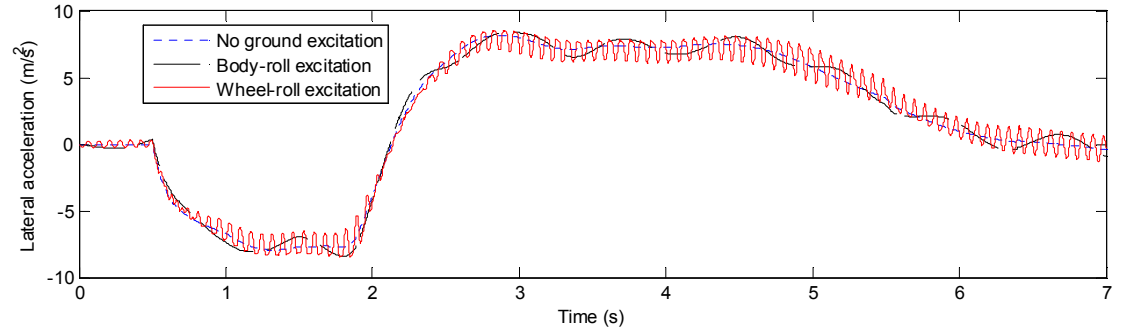

(a)

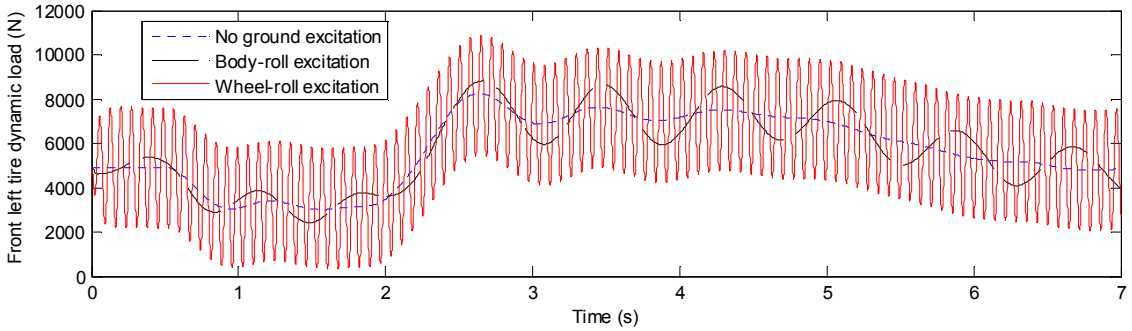

(b)

Figure 3.15. Comparison of vehicle lateral acceleration and tire dynamic load variation under different ground excitations: (a) *lateral acceleration*; and (b) *front left tire dynamic load*.

This example explores the importance of the wheel-roll mode in vehicle handling during critical manoeuvring. The wheel-roll mode should be carefully considered in the future development of roll control strategies. Moreover, the four wheel-dominated motion-modes, linking road excitation to vehicle handling through the tyre dynamics, play an important role in vehicle dynamics. A comprehensive detailed investigation of these four wheel-modes is recommended for future work because it will improve our understanding of the fundamentals of road-vehicle interactions and may, with the application of the proposed MEM, lead to the development of new control concepts.

3.6.6.Road excitation with random noise

Of the seven motion-modes discussed, the articulation mode is a motion-mode that can only be excited by road-vehicle interaction and is therefore particularly sensitive to road excitation noises. Thus, the articulation mode is selected for the noise resistance study of the proposed MEM. The ground excitations with random noise to the four wheels are described in the following equations with respect to time

$$z_{gi}(t) = Amp_i \sin(2\pi ft) + white\_noise_i(t) \tag{3.18}$$

where $Amp_1 = -Amp_2 = -0.55Amp_3 = 0.55Amp_4 = 0.02$m; $f = 5\ Hz$. A time section sample of the ground excitations to the four wheels and the resulting articulation mode-ratio are presented in Figure 3.16. As shown in Figure 3.16(b), the random ground excitations have two effects on the articulation mode-ratio detection: 1) they bring noise into the mode-ratio reading; and 2) they result in a lower average mode-ratio. The reason for the first effect is straightforward and the reason for the second effect is that the random ground excitations convey energy into other motion-modes and disperse the energy in the articulation mode.

The test is repeated at f = 1~30 *Hz* with the same random white noise, and the root-mean-square (RMS) value of the noise level in the mode-ratio reading is presented in Figure 3.17 with respect to the ground excitation frequency. The result obtained shows that the maximum noise contamination (RMS= 0.033) happens at 1 Hz excitation, and the lowest RMS valve of 0.004 is reached at 15 Hz, which is around the natural frequency of the articulation mode.

This indicates that the MEM is particularly robust when the ground excitation is close to the natural frequencies of motion-modes. The reason is that once a motion-mode is fully excited, its mode energy overwhelms other noise modes.

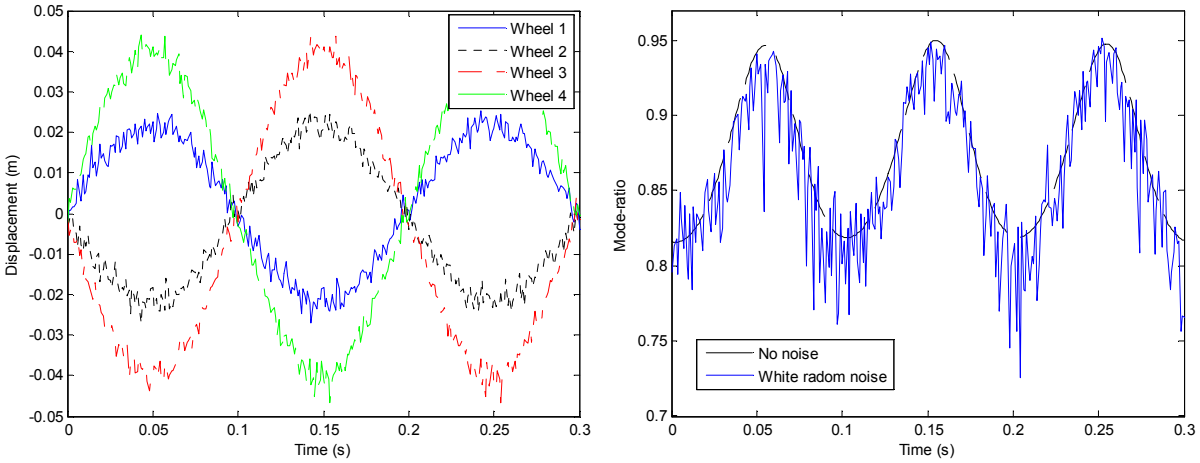

(a) (b)

Figure 3.16. 5 Hz road excitation in articulation mode with white random noise: (a) a time section of wheels' excitations corresponding to articulation mode; and (b) mode-ratio of articulation mode.

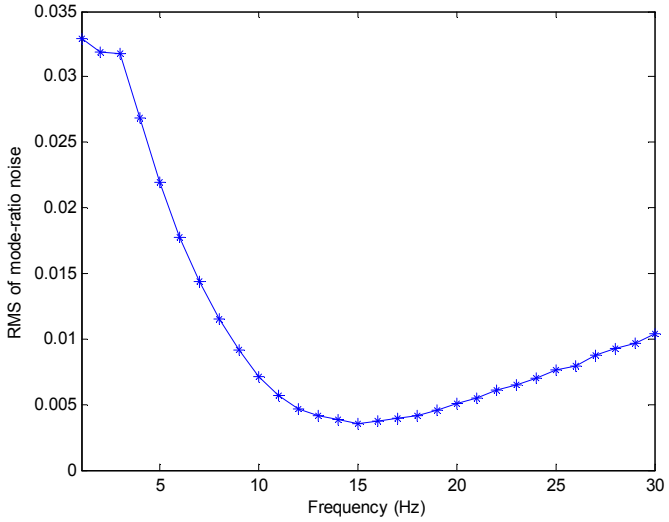

Figure 3.17. Root-mean-square (RMS) of the mode-ratio noise at different ground excitation frequency.

3.7 Discussion

The MEM is derived from linear modal analysis but is applicable to nonlinear systems, such as the 10-DOF nonlinear vehicle model used in the study. A nonlinear system can be decomposed into several motion-modes according to the MEM, but due to its nonlinearity these motion-modes are not completely "energetically isolated". This means that energy leakage exists between these motion-modes. This is an inherent limitation of the application of the MEM to nonlinear systems, and there is a clear need in future studies to track this energy leakage and investigate its effect on primary mode selection. Moreover, a more realistic vehicle model or actual road testing data could be used to address this issue and assess the realistic functionality of the MEM.

3.7.1.Mode-based switchable control strategy

The MEM provides a feasible way to integrate the individually developed controllers to form a new control framework; for example, the sky-hook and ground-hook control can be combined together under this method. It is known that the sky-hook control can reduce the vehicle body's motion to improve ride comfort, and the ground-hook control limits the wheel's motion and thus reduces the tire dynamic load in order to improve handling [85]. However, because these two different controllers have to be implemented through the same suspension system, at any time instant, judgment in the control of the motion-mode is vital. With the assistance of the MEM, the detected mode-ratio can be used as an indicator for the switch between these two controllers to form a systematic control. Furthermore, semi-active and active control can also be integrated based on the energy level detected by the MEM. For instance, it is more efficient to use semi-active systems to absorb the vibrations when the detected energy level is low, and to use active systems to effectively control the vehicle when the energy level is high.

In addition, an integrated control framework based on the MEM could be developed to cover the seven body-wheel motion-modes of two-axle vehicles. In developing this integrated control strategy, it would be wise not to take the mode-ratio as the sole basis, but also to consider the significance of different motion-modes to vehicle dynamics. For example, the roll motion-mode raises more concerns in vehicle handling and safety, and should be weighted more in making a control decision. This will be further discussed in Chapter 5.

3.7.2.Error reduction and implementation issues

To minimise the errors during the state vector superposition and errors from other sources, e.g., sensor noise, state estimation error, it is necessary to employ algorithms to optimise the superposition process. One of the possible algorithms is discussed here as an example.

The measured or estimated vehicle system state vector X, 14×1, can be represented as a superposition of its motion-modes plus error vector ε, 14×1, and then Equation (3.9) can be rewritten as

$$X = \Gamma q + \varepsilon \tag{3.19}$$

Assuming the error weighting coefficients are given, a weighting matrix W can be defined to minimise the error ε by taking advantage of the least square method. The estimated state vector $\hat{q}$ is shown in the following equation

$$\hat{q} = (\Gamma^T W \Gamma)^{-1} \Gamma^T W X . \tag{3.20}$$

Moreover, a sensitivity study can also be carried out in future to investigate the robustness of the proposed method to estimation and processing errors.

Apart from robustness analysis, practical approaches to implement the MEM, such as the algorithm to estimate vehicle state vector and tire deflection, need to be developed and tested. In practice, alternative artificial intelligent systems could be considered to assist the MEM to obtain approximate solutions in an economical manner, since the presented MEM requires the measurement of vehicle states and road inputs which are expensive to obtain in passenger vehicles. For example, the accurate solution obtained by the MEM can be used to train neural networks under different circumstances; the trained neural networks can then be employed with reasonable accuracy to provide a mode-ratio by measuring suspension relative motions only [86].

3.8 Summary

This chapter studied vehicle body-wheel motion from the perspective of energy intensity and modal modes, and proposed corresponding control strategies. Based on energy intensity, vehicle body-wheel motions could be classified into three categories, namely vibration, vib-motion and ext-motion; and based on modal properties they can also be classified into seven orthogonal motion-modes. The MEM with real-time capacity was proposed to quantify the energy intensity of each motion-mode and prioritise the control objectives for controllable suspensions.

The motion-mode energy method (MEM) was verified on the 10-DOF nonlinear full-car model using numerical examples. These included several realistic driving scenarios: road bump and pothole; braking and steering; and fishhook manoeuvre with road excitation. The results obtained show that the MEM is able to illustrate the presented dynamic events from the perspectives of motion-mode energy and mode-ratio, and to identify the primary contributing motion-mode. For example, for the 20 km/h speed bump test, the sequence of the dominating motion-mode was identified as body-pitch mode, wheel-bounce mode, body-bounce mode, and wheel-pitch mode. In the example of steering while braking, the MEM could quantitatively assess the different vehicle dynamic aspects and provide a unified reference for determining the dominating aspect as the prioritized control objective. In the fishhook manoeuvre test, the influence of ground excitation on vehicle handling was examined in motion-modes, and the results indicated that road excitation corresponding to wheel-roll motion-mode had a significant effect on a vehicle's rollover resistance capability. Furthermore, the MEM's resistance to noise was demonstrated in the articulation mode case study.

The MEM provided a feasible way to classify vehicle body-wheel motions into several modes and integrate the individually developed controllers to form a mode-based control strategy. Finally, some practical considerations of implementation and suggestions for future work were presented.

CHAPTER 4 REAL-TIME IDENTIFICATION OF VEHICLE MOTION-MODES USING NEURAL NETWORKS

4.1 Introduction and rationale

A four-wheel ground vehicle has three body-dominate motion-modes, that is, bounce, roll, and pitch motion-modes. Real-time identification of these motion-modes can make the vehicle suspensions, in particular, active suspensions, target the dominate motion-mode and apply appropriate control strategies to improve its performance with less power consumption. The motion-mode energy method (MEM) developed in Chapter 3 can identify the vehicle body motion-modes, but requires the measurement of full vehicle states and road inputs, which are not always available in practice. This chapter proposes an alternative approach to identify vehicle primary motion-modes with acceptable accuracy by employing neural networks (NNs). This method only requires the measurement of the coil-spring deflection of the suspension system and can determine the vehicle primary motion-modes in a real-time manner. The proposed NNs are feed-forward NNs with one hidden layer. To train the NNs, two 4 degree-of-freedom (DOF) half-car models in roll- and pitch- planes are used to generate the training data sets for the two NNs, respectively. The target outputs are the motion-mode energy contribution ratios calculated by the MEM. New feature extraction algorithm and interpretation method are also proposed to simplify the training process and increase the identification accuracy. The effectiveness of motion-mode identification of the trained NNs is verified on the 10-DOF full-car model (in Chapter 3) under various types of excitation inputs. The results confirm that

the proposed method is effective in determining vehicle primary motion-modes with comparable accuracy to the MEM.

4.2 Background

Although the MEM can provide the accurate solution of mode-ratio in real-time, it is obtained under the assumption that the system's state vector and ground road inputs are known. This, however, is impractical for most vehicles as the ground road inputs and some of the states are not measureable or can only be measured by sensors, which are too expensive for ordinary passenger cars. The estimation of ground road inputs and state vector is normally noise sensitive and can be computationally intensive. Therefore, an alternative method needs to be developed. This provides the motivation for the current chapter to present a Neural Networks based method for the recognition of motion-modes using the measured suspension deflections.

Neural networks have been proved effective and efficient in pattern recognition as well as control. For example, in automotive applications, neural networks have already been applied in driving pattern recognition [87], suspension dynamic control [88], and vehicle dynamic modelling [89]. In dynamic pattern recognition, NNs have been widely applied with different feature enhancement methods, such as, frequency domain methods [90], Principal Component Analysis (PCA) method [91] and Empirical Mode Decomposition (EMD) method [92, 93]. In this study, two feed-forward NNs are adopted. These two NNs will be trained by using the training data sets generated by two 4-DOF half-car models in roll- and pitch- planes, respectively. In the training data sets, the target outputs are the mode-ratios calculated by the MEM and the inputs are the corresponding suspension deflections. In order to effectively use NNs for recognising vehicle primary motion-modes, a new feature extraction algorithm will be proposed.

This algorithm is a model-based principal component decomposition method and it extracts the main features in relation to the motion-mode energy from the measured suspension deflections. In addition, to simplify the training process, the target outputs will be discretised into 11 sub-classes with equal intervals in the range of [0, 1]. The training inputs will also be appropriately generated to match these sub-classes. To interpret the results obtained from the NNs, which are the continuous values in the range of [0, 1], a probability mapping algorithm will be applied. Finally, the effectiveness of motion-mode recognition of the trained NNs is then verified on the 10-DOF full-car model under various types of excitation inputs. The obtained results confirm that the proposed method is effective in recognising vehicle primary motion-modes with comparable accuracy to the MEM.

The rest of the chapter is organised as follow. In Section 3, two simplified 4-DOF half-car models are introduced. These models will be used to generate the training data sets for the NNs. The configuration of the NNs along with the feature extraction, training, and result interpretation are presented in Section 4-6. The obtained results are validated in Section 7 for different cases, and the accuracy of the proposed method is discussed in Section 8. The conclusions are summarised in Section 9.

4.3 Vehicle dynamics modelling

To generate training data and train the proposed NNs for recognising vehicle motion-modes, two half-car models, that is, pitch- and roll-plane models, will be considered. The reason for employing two half-car models rather than a full-car model is that the training of NN to recognize energy mode-ratio in half-car model is more practical and implementable. Currently, training of NN on a full-car model is still under study. A 4-DOF half-car model is employed to represent the dynamics of a two-axle four-wheel vehicle in pitch- or roll-plane as shown in Figure 4.1. This

half-car model's sprung mass has freedoms in vertical and pitch/ roll directions, and each unsprung mass only has freedom in the vertical direction. In Figure 1, z_s is the vertical displacement at the centre of gravity, θ or φ *is* the pitch or roll angle of the sprung mass; m_s, m_{u1} *and* m_{u2}, denote the sprung and unsprung masses, respectively, and I_θ or I_φ is the pitch or roll moment of inertia. The front and rear (or right and left) displacements of the unsprung masses are denoted by z_{u1} and z_{u2}, respectively. The disturbances, which are caused by vehicle-road interaction from surface irregularities, are denoted by z_{g1} and z_{g2}. The suspension stiffness and damping coefficients are denoted by k_{s1}, k_{s2} and c_{s1}, c_{s2}, respectively, and tyre stiffness is k_t. The parameter values used in this study are presented in Table 4.1, which are consistent with the parameters in Table 3.2.

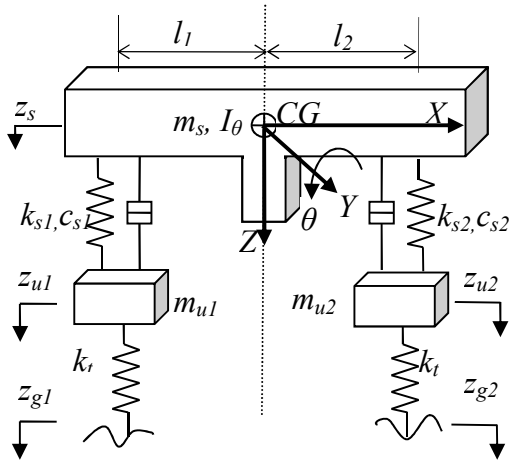

Figure 4.1. Pitch/roll-plane half-car model.

The motions of equations of the half-car model (take pitch-plane as an example) can be formed in Equation as

$$M\ddot{Z} + C\dot{Z} + KZ = F \tag{4.1}$$

where $Z = [\theta \quad z_s \quad z_{u1} \quad z_{u2}]^T$, F represents the ground excitations to wheels, and M, C, K matrices are specified as

$$M = \begin{bmatrix} I & 0 & 0 & 0 \\ 0 & m_s & 0 & 0 \\ 0 & 0 & m_{u1} & 0 \\ 0 & 0 & 0 & m_{u2} \end{bmatrix},$$

$$C = \begin{bmatrix} l_1^2 c_{s1} + l_2^2 c_{s2} & l_1 c_{s1} - l_2 c_{s2} & -l_l c_{s1} & l_2 c_{s2} \\ l_1 c_{s1} - l_2 c_{s2} & c_{s1} + c_{s2} & -c_{s1} & -c_{s2} \\ -l_1 c_{s1} & -c_{s1} & c_{s1} & 0 \\ l_2 c_{s2} & -c_{s2} & 0 & c_{s2} \end{bmatrix},$$

$$K = \begin{bmatrix} l_1^2 k_{s1} + l_2^2 k_{s2} & l_1 k_{s1} - l_2 k_{s2} & -l_l k_{s1} & l_2 k_{s2} \\ l_1 k_{s1} - l_2 k_{s2} & k_{s1} + k_{s2} & -k_{s1} & -k_{s2} \\ -l_1 k_{s1} & -k_{s1} & k_{s1} + k_t & 0 \\ l_2 k_{s2} & -k_{s2} & 0 & k_{s2} + k_t \end{bmatrix}.$$

Table 4.1. Parameter values of two 4-DOF half-car dynamic models.

Symbol	Roll-plane model	Pitch-plane model	Units	Description
m_s, m_{ui}	900,40	900,40	kg	Sprung/unsprung mass(i =1,2)
I	390	1900	kg·m^2	Sprung mass moment of inertia
l_1	0.575	1.37	m	Track distance for left/front wheel
l_2	0.575	1.48	m	Track distance for right/rear wheel
k_{si}	44	44	kN·m^{-1}	Suspension spring stiffness(i =1,2)
k_t	270	270	kN·m^{-1}	Tire spring stiffness
c_{si}	2500	2500	Ns·m^{-1}	Suspension damping coefficient(i =1,2)

4.4 Motion-modes identification by neural networks

The motion-mode energy method (MEM) proposed in Chapter 3 was used to identify the vehicle primary motion-modes [94]. It is noticed that the state vector and the ground road inputs need to be known when using the MEM to calculate the

motion-mode energy. However, in practice, not all the state variables are measurable and the ground road inputs are normally hard to be measured. To overcome this drawback, an alternative NNs based method, which only uses available suspension deflections as inputs, is developed in this section.

The schematic diagram of the NNs based method is illustrated in Figure 4.2. For the whole system, it has four suspension deflections as inputs, where FL is for front left suspension, FR for front right, RL for rear left, and RR for rear right, and three outputs, which are the mode-ratios for three primary motion-modes. To condense the size of the NNs and make the training time affordable, the four inputs are rearranged into two sets of inputs and sent to two NNs, which will be trained for the pitch and roll sub-systems, respectively. The output of each of the two NNs indicates the mode-ratio between pitch to bounce and roll to bounce, respectively. The final outputs of the NNs are the mode-ratios for bounce, pitch, and roll motions. The detailed explanation for each phase will be provided next.

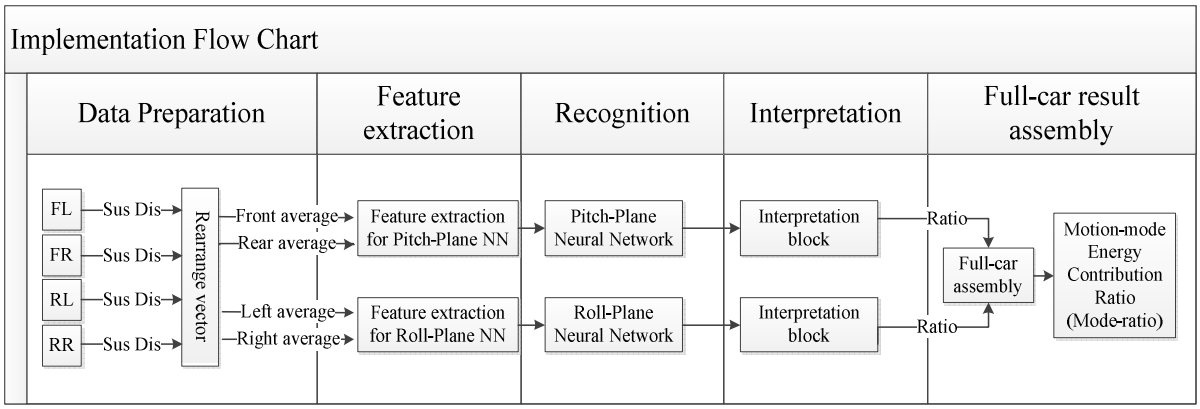

Figure 4.2. Schematic diagram of NNs based method.

4.4.1.Neural network architecture

A feedforward network, as shown in Figure 4.3, is chosen to detect the motion-modes in this chapter because feedforward networks with only one hidden layer have been proved to be sufficient and accurate in approximating a nonlinear function [95, 96].

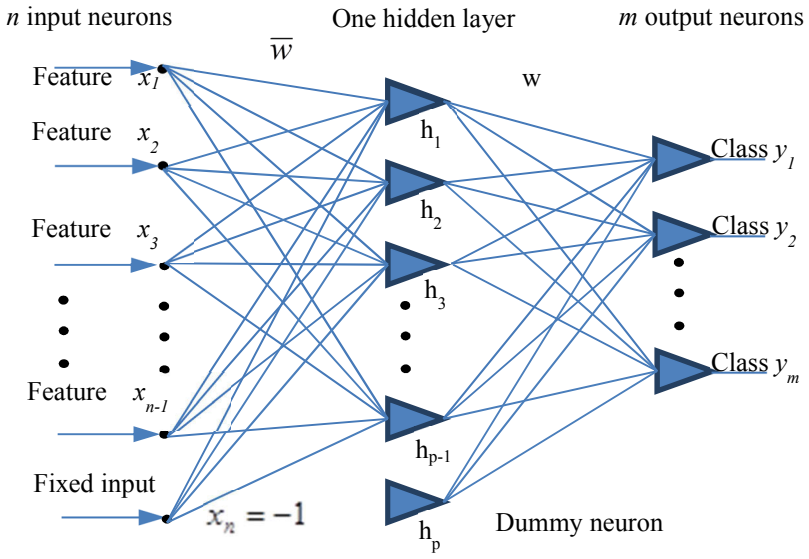

Figure 4.3. Structure of a layered feedforward neural network.

The number of nodes in the hidden layer, denoted as p, needs to be chosen by trial and error. In general, it should be large enough to guarantee the convergence of the network in training, but it cannot be too large to avoid the over-mapping problem. In this study, n=3, p=45, m=11 are defined. The network equation for this two-layer feedforward network is given by Bipolar logistic function as

$$h = f(\overline{w}x) \tag{4.2}$$

$$y = f(wh) \tag{4.3}$$

where w and $\overline{w}$ represent the $n_m \times n_p$ and $n_{p-1} \times n_n$ weighting matrices for the output and hidden layers, respectively, and

$$f(v) = \frac{2}{1+e^{-v}} - 1 = \frac{1-e^{-v}}{1+e^{-v}} \tag{4.4}$$

The weighting matrices w and $\overline{w}$ of the feedforward network will be adjusted by using a back-propagation method, which will be discussed in this chapter.

4.4.2.Feature extraction

As the input signals to the NNs are suspension deflections and the outputs are mode-ratios, the direct mapping between them may not be easily and accurately established because the target mode-ratios are calculated by the MEM, which needs more information about state vector and ground inputs rather than suspension deflections. To enhance the mapping capability of the NNs, a feature extraction part, which extracts the similar information to MEM from the input displacements, is added to the NNs before the NNs are trained.

Take the pitch-plane NN as an example (the roll-plane NN uses the same structure), in the feature extraction part, the input suspension deflection vector for the pitch-plane NN, $s=[s_1,\ s_2]$, and its differentiation $\dot{s}=[\dot{s}_1,\ \dot{s}_2]$ will be used as inputs. By defining the coefficient matrices L and T as

$$L = \begin{bmatrix} l_1 & 1 & -1 & 0 \\ -l_2 & 1 & 0 & -1 \end{bmatrix}, \quad T = \begin{bmatrix} 0 & 0 & 1 & 0 \\ 0 & 0 & 0 & 1 \end{bmatrix},$$

the input suspension deflection vector can be processed as follow

$$q_d = (L\Psi)\backslash \begin{bmatrix} s_1 \\ s_2 \end{bmatrix}, \quad q_v = (L\Psi)\backslash \begin{bmatrix} \dot{s}_1 \\ \dot{s}_2 \end{bmatrix} \tag{4.5}$$

where vector q_d and q_v each contains four elements: $q_d = [q_{d1} \quad q_{d2} \quad q_{d3} \quad q_{d4}]$ and $q_v = [q_{v1} \quad q_{v2} \quad q_{v3} \quad q_{v4}]$, corresponding to four motion-modes that a half-car model has. As we only consider the two primary body motion-modes, that is, pitch and

bounce, the first two corresponding elements are used in the following energy feature calculation. The energy feature extracted from the suspension deflections signals is defined as

$$\sigma_i = sum\left\{\frac{1}{2}\begin{bmatrix} H & 0 \\ 0 & M \end{bmatrix}\left[\begin{bmatrix} L \\ T \end{bmatrix} c_i \right]^2\right\},\ i = 1,2 \tag{4.6}$$

where M and H are the mass matrix and stiffness matrix for energy calculation, specified as

$$M = \begin{bmatrix} M_s & 0 \\ 0 & M_u \end{bmatrix},\quad H = \begin{bmatrix} K_s & 0 \\ 0 & K_t \end{bmatrix} \tag{4.7}$$

and

$$c_i = real(\phi_1 q_{di}),\ v_i = real(\phi_1 q_{vi}),\ i = 1,2 \tag{4.8}$$

Energy feature σ_i will be sent to the NN for training. As the energy feature σ_i show some similarities to the energy calculated by the MEM, the mapping between this energy feature and the target mode-ratios will be easily established.

4.5 Neural network training

For training the NNs, we need to generate an input vector and a corresponding target vector for NNs. A schematic diagram for generating these training data sets is illustrated in Figure 4.4.

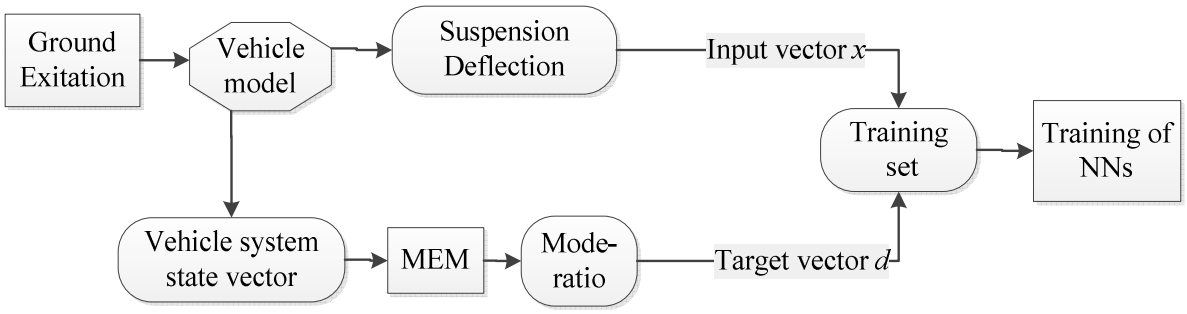

Figure 4.4. Schematic diagram for generating the training data sets.

It can be seen from Figure 4.4 that the suspension deflections and the system state are vectors obtained from the responses of the half-car models under certain ground excitation. In Figure 4.4 the input vector x is the vehicle suspension deflections (note that the input vector will be further processed to extract its feature as discussed in the previous sub-section) and the target vector d is formed from the mode-ratios calculated by the MEM in terms of the obtained system state vector and the ground excitation. And then the input vector x and the target vector d are combined together to form the training data sets and sent to the NNs for training.

Note that the output of each NN is the mode-ratio. The mode-ratio is actually a continuous number in the range of [0, 1], where 0 means a pure bounce motion-mode and 1 means a pure pitch or roll motion-mode. As it is impractical to take an infinite number to form the training targets, we discretise the target ratio value into 10 sections with 11 nodes, and define the set of [0, 0.1, ⋯, 0.9, 1] as the training target vector d. To generate this training target vector, the appropriate excitation signals will be defined and applied to the vehicle models so that the mode-ratios calculated by the MEM will match the values in the vector. In the training of the NNs, the difference between the target vector d and the actual NN output vector y is defined as the error function:

$$\Xi = \frac{1}{2}\sum_{i=1}^{m}(d_i - y_i)^2 \tag{4.9}$$

where $m = 11$ represents the total number of elements inside the target vector, and the weighting matrices will be updated by

$$(w^*, \overline{w}^*) = (w, \overline{w}) - \tau \frac{\partial \Xi}{\partial (w, \overline{w})} \tag{4.10}$$

where $(w^*, \overline{w}^*)$ represents the updated weighting matrices during training according to the delta training rule, and τ is the learning constant.

4.6 Result interpretation

As we use two NNs to represent the pitch- and roll-plane models, respectively, and the output of each NN is a value reflecting its mode-ratio, we need to interpret the mode-ratio of each NN in one plane and then combine them together to provide the final mode-ratio in terms of the bounce, pitch, and roll motion-modes.

For each NN, the interpretation block contains an algorithm to project the NN's output onto an *m*-dimensional space, *m*=11, according to the discretised training target classes. The distance between the actual output and each class is defined by the following equation

$$r_i = 1 - \frac{\sqrt{\sum_{j=1}^{m}\left(y_j - d_{ij}\right)^2}}{2\sqrt{2}} \tag{4.11}$$

where y is actual NN's output, d_i (i=1,…11) is the pre-defined 11 target classis, and distance r_i represents the similarity between y and d_i. By the normalization of r_i, we

gain the probability vector $\hat{p}_i$ to show the likelihood of NN's output belonging to target class d_i.

$$\hat{p}_i = \frac{r_i}{\sum_{j=1}^{m} r_i} \tag{4.12}$$

The multiplication of the target ratio vector [0, 0.1, ⋯, 0.9, 1] and its probability vector $\hat{p}_i$ provides the output mode-ratio for one set of given input data. After obtaining the mode-ratio between pitch and bounce from pitch-plane NN and between roll and bounce from roll-plane NN, we can obtain the mode-ratios for pitch, roll, and bounce motion-modes.

4.7 Numerical examples on a full-car model

After finishing the training of the NNs, the weighting matrices of the NNs are fixed and the NNs can be used as the mapping from the input suspension deflections to the mode-ratios. To validate the accuracy of the built mapping, numerical examples on the 10-DOF nonlinear full-car model (presented in Chapter 3) will be provided to validate the effectiveness of the proposed method. This full-car model includes three primary body motion-modes, that is, bounce, roll, and pitch, and this model has not been used for training the NNs. The parameter values for the 10-DOF model are compatible with the pitch-/roll-plane half-car models. The validation will be done for the following three typical cases.

4.7.1. Under ground excitation

This case shows the NNs can detect the three motion-modes when the vehicle is under excitation from the ground. The excitations to the wheels are described in the following equations:

$$z_{gi}(t) = A_i \sin(2\pi f), \quad i = 1,\ 2,\ 3,\ 4 \tag{4.13}$$

where $A_1 = -0.5A_2 = A_3 = -0.5A_4 = 0.01m$ and $f = 2Hz$.

The measured suspension deflections are presented in Figure 4.5, based on which the proposed NNs method will detect the three vehicle body motion-modes. The dynamic mode-ratios of the three primary motion-modes, which are calculated by the MEM, are shown in Figure 4.6(a), and the detected mode-ratios by NNs are shown in Figure 4.6(b). Through the comparison, we can see NNs have a similar performance with MEM in representing the mode-ratios of the vehicle under the given ground excitation.

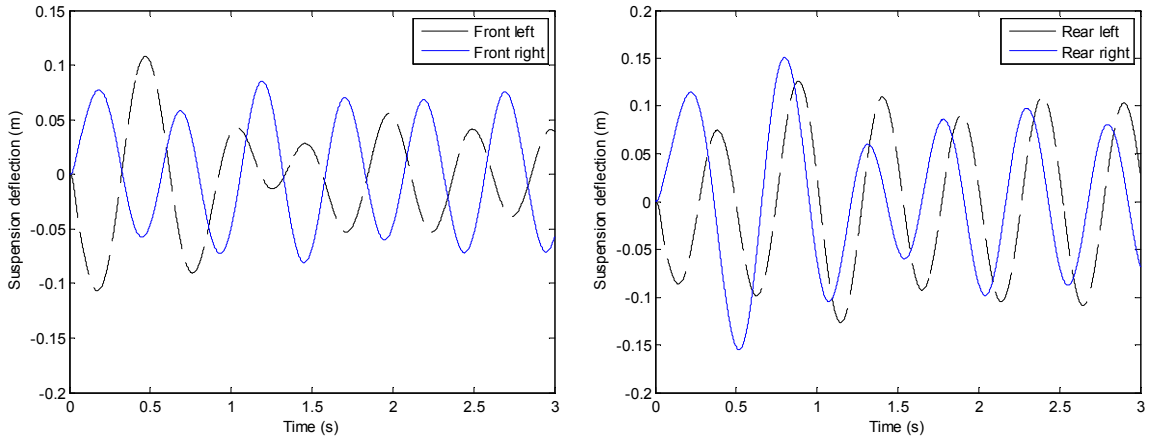

(a) (b)

Figure 4.5. Suspension deflections: (a) Front; and (b) Rear.

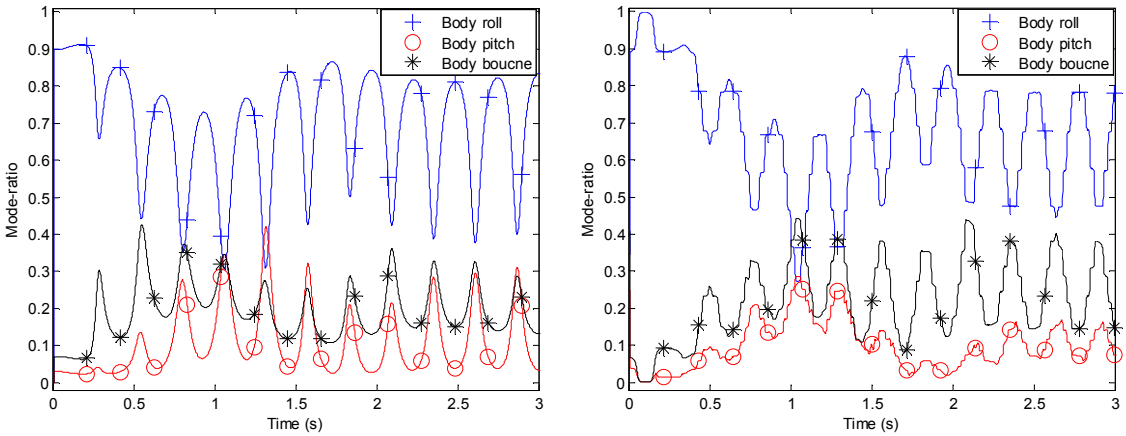

(a) (b)

Figure 4.6. Comparison of mode-ratios of the vehicle under ground excitation, detected by: (a) MEM; and (b) NNs.

4.7.2.Under fishhook manoeuvre

This case is to show how the proposed NNs perform when the vehicle is driving under a typical steering wheel input. The test is set up with a vehicle entering a fishhook manoeuvre at 75 km/h on a smooth road. The steering wheel input and the motion-mode energy distribution calculated by MEM are presented in Figure 4.7. The measured suspension deflections are presented in Figure 4.8. The motion-modes, calculated by MEM and NNs respectively, are presented in Figure 4.9 for comparison. From Figure 4.9, it can be seen that the vehicle body roll motion-mode is becoming the dominate mode after the vehicle starts to enter the manoeuvre at 0.5 seconds, and the results given by the proposed NNs method are in good agreement with the results obtained by the MEM.

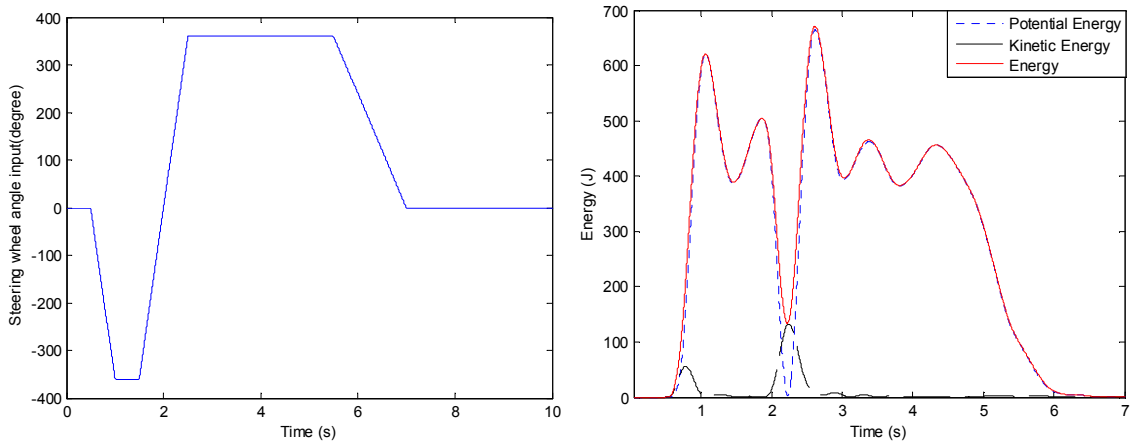

(a) (b)

Figure 4.7. Motion-mode study of a vehicle in the dynamic event of a fishhook manoeuvre: (a) steering wheel angle input; and (b) motion-mode energy by MEM.

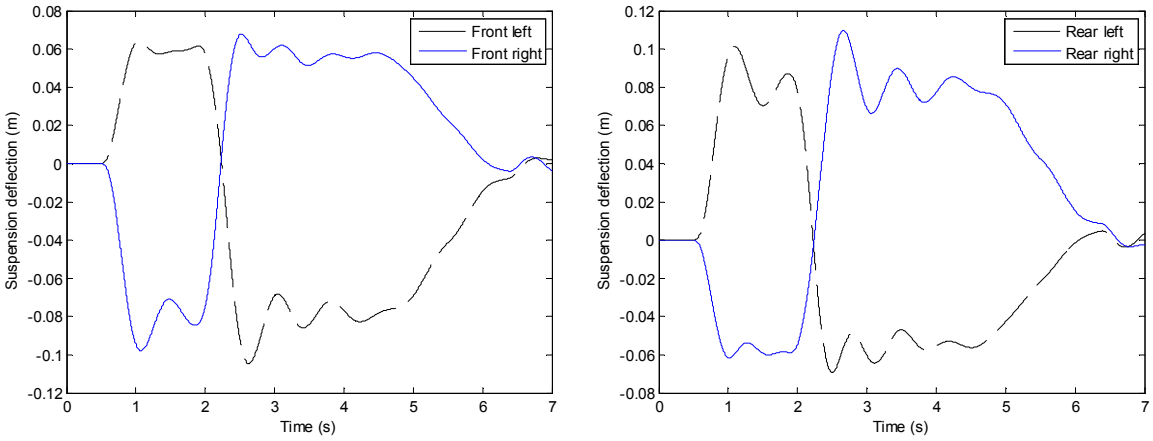

(a) (b)

Figure 4.8. Suspension deflections: (a) Front; and (b) Rear.

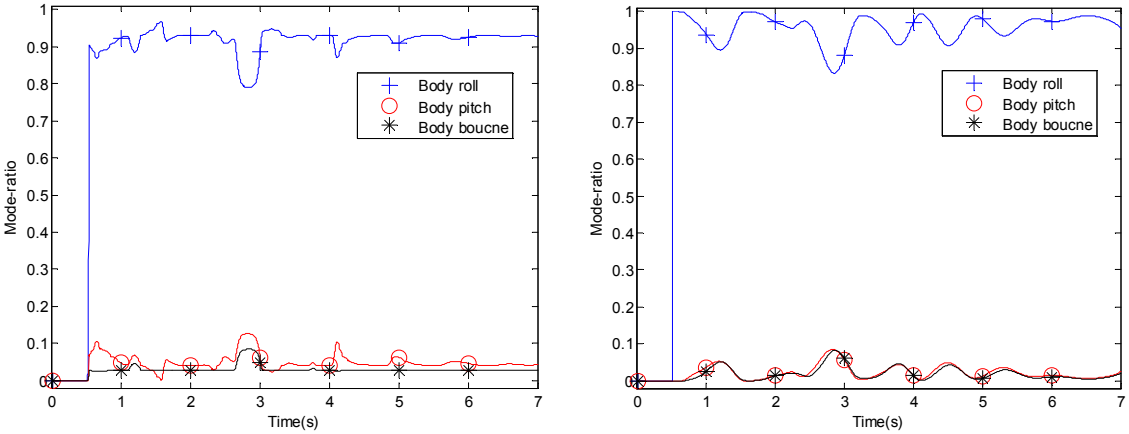

Figure 4.9. Comparison of mode-ratios of the vehicle under fishhook manoeuvre, detected by: (a) MEM; and (b) NNs.

4.7.3.Under a combined braking and steering operation

In this case, a combined operation of steering and braking of a vehicle when exiting from a highway is considered. The test is set up with a vehicle running on a smooth road surface with an initial speed of 80 km/h, then applying a steady brake (corresponding to a steady-state longitudinal deceleration of 0.4 g) for the first 4 seconds and applying a 30º step steering wheel input after 2 seconds of braking. Therefore, braking and steering operations are both executed during the period of 2~4s.

The measured suspension deflections are presented in Figure 4.10, and mode-ratio is presented in Figure 4.11. We can see from Figure 4.11(b) that, the NNs method indicates a dominate body pitch motion-mode throughout the braking operation (the first 4 seconds), and after that, the pitch motion-mode is overtaken by body roll motion-mode. The NNs method captures the sequence of the change of these three motion-modes, and the NNs' result shown in Figure 4.11(b) well matches the MEM's in Figure 4.11(a).

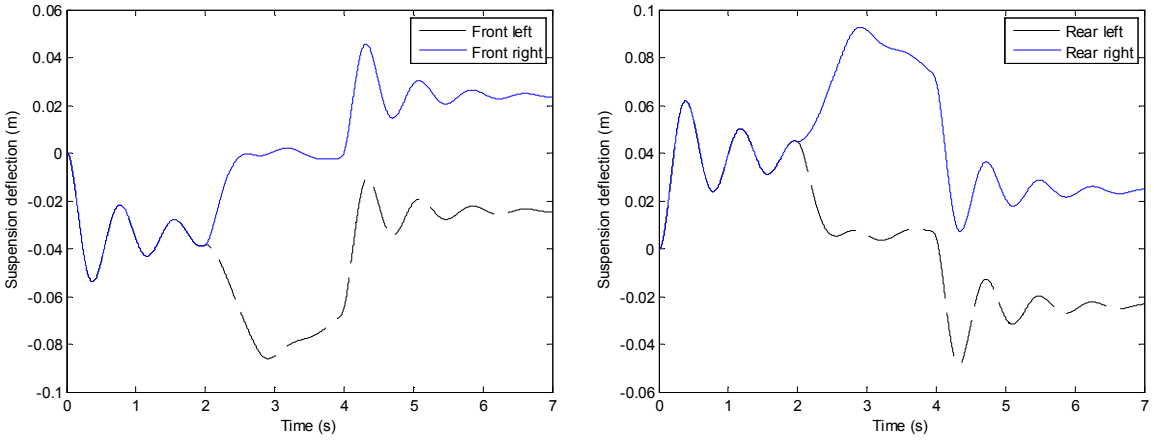

(a) (b)

Figure 4.10. Suspension deflections: (a) Front; and (b) Rear.

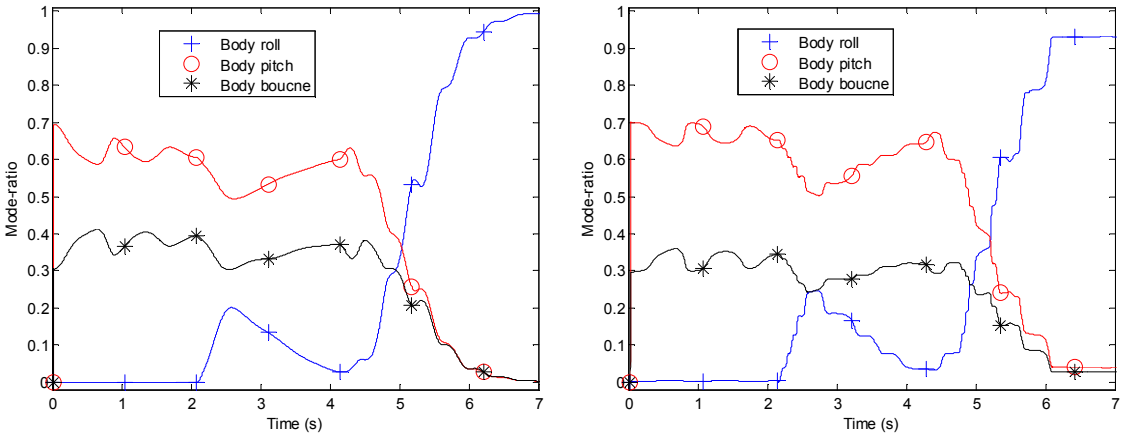

(a) (b)

Figure 4.11. Comparison of mode-ratios of the vehicle under braking and steering with an initial speed of 80 km/h, detected by: (a) MEM; and (b) NNs.

The test is then repeated again with a higher vehicle initial speed of 120 km/h. In this case, the suspension deflections are presented in Figure 4.12, and the comparison of mode-ratios is provided in Figure 4.13. Under the same steering angle, higher vehicle speed enhances the energy in vehicle roll motion-mode, and it becomes the dominating one over the other two motion-modes during the overlap period 2~4 s. This is indicated by both the MEM and NNs method in Figure 4.13.

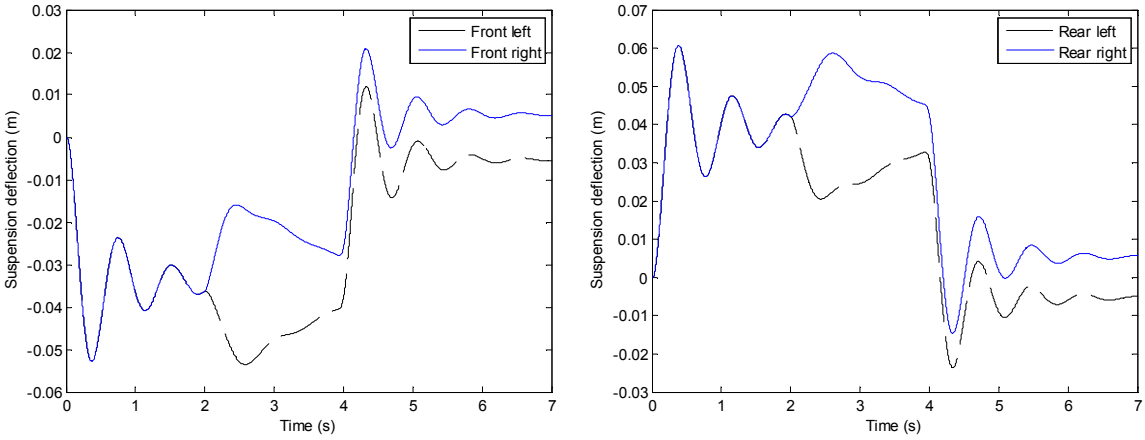

(a) (b)

Figure 4.12. Suspension deflections: (a) Front; and (b) Rear.

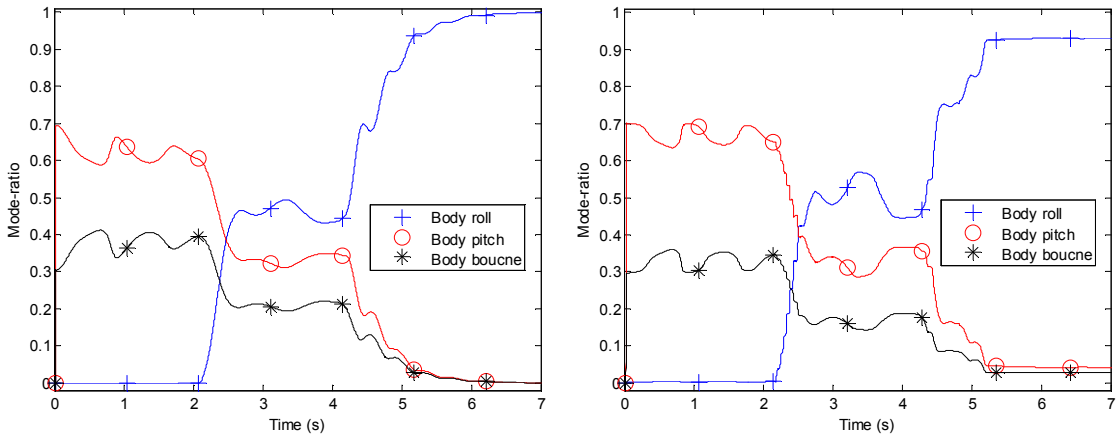

(a) (b)

Figure 4.13. Comparison of mode-ratios of the vehicle under braking and steering with an initial speed of 120 km/h, detected by: (a) MEM; and (b) NNs.

The presented three examples confirm the effectiveness of the proposed method under different scenarios with different input excitation sources. It can be seen from these examples that the NNs can recognise the mode-ratios in the dynamic events with multiple excitations. As the trained NNs method can predict the mode-ratios with acceptable accuracy without further learning process, this method can be applied to detect motion-modes in real-time.

4.8 Discussion

In this section, the recognition accuracy of the proposed method is investigated through empirical analysis. In general, for the samples that are not in the training sets of NNs, there is no guarantee that NNs can provide an accurate approximation even if the network training error can approximate to zero [97]. The empirical approach taken here is to use the new samples, of which mode-ratios are not in the training target classes, to test the recognition error of the NNs. The maximum recognition error is expected from samples with mode-ratios in the class of [9.5, 8.5, ⋯ 0.5], and therefore these samples are used to check the NNs in the worst scenario. By testing with 4000 data points, the error distribution of the NNs method is presented in Figure 4.14.

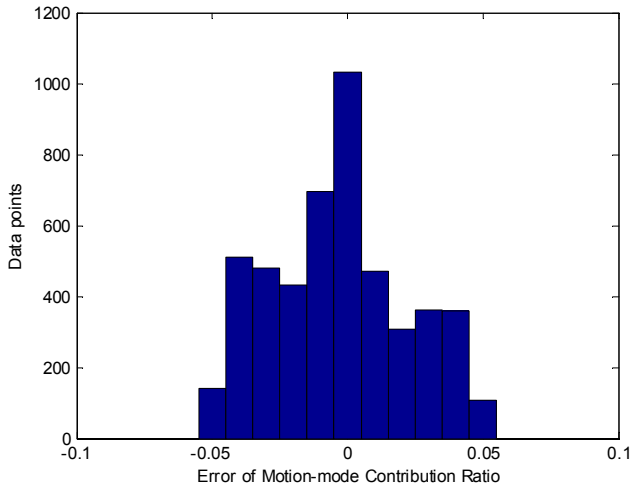

Figure 4.14. Error distribution of the NNs method.

As it is seen from Figure 4.14 that the error data set does not appear to be normally distributed, we accordingly use the non-uniform distribution method to calculate the confidence interval $[\hat{\theta}_1\ \hat{\theta}_2]$. With the confidence level at 95%, the recognition error lies in the confidence interval [-4.2%, 5%], and the average error is about 0.26%. As the sample size of n=4000 is used, it is considered to be adequate for this error distribution evaluation.

4.9 Summary

This chapter proposes an NN based approach to detect vehicle primary motion-modes with acceptable accuracy. This method only requires the measurement of vehicle suspension deflections. The feed-forward NNs with one hidden layer are employed and two half-car models in roll- and pitch-planes are used to generate the training data sets for these two NNs, respectively. To simplify the NNs' training process and enhance its recognition capability, a feature extraction algorithm is proposed. The empirical analysis of the recognition error shows that the NNs can achieve an acceptable accuracy. Several simulation examples are used to verify the effectiveness of the proposed NNs on the 10-DOF nonlinear vehicle model. The NNs method is compared with the MEM in three cases with different excitations including ground excitation, steering wheel input, and braking. The results confirm that the detected mode-ratio is applicable to vehicle motion-mode-based suspension control. The extension of the method to the detection of important wheel motion-modes, such as, the articulation mode, can be further considered in the future work.

CHAPTER 5 SWITCHED CONTROL OF VEHICLE SUSPENSION BASED ON MOTION-MODE DETECTION

5.1 Introduction and rationale

In this section, an attempt is made to structure an overall architecture of MEM-based switched control, covering vehicle dynamic parameter variation to multi-mode control stability, including five processes: signal process, parameter and state estimation, MEM, actuating reconfiguration, and multi-mode control. The motivation behind this architecture is to minimise the energy consumption of active control by identifying and controlling the dominant dynamic aspect of a vehicle at each time instant.

The architecture begins with the vehicle model estimation and employs online algorithm to detect its parameter variation. A moderate complex vehicle model (7-DOF) is directly derived through mode reduction method from the sensing signals, and its parameters are kept updated with the vehicle's working condition (e.g., loaded/unloaded). Next, based on the derived model, the MEM analysis is performed to detect the dominating motion-mode by rating their energy contribution. Following this, the active HIS system reconfigures its configuration to control the detected motion-mode.

To ensure the system is stable during the mode-switch, an H∞ optimal controller is designed for each motion-mode with the use of a common quadratic Lyapunov function. A three-mode switched control is briefly introduced which covers a vehicle's body-dominated bounce, pitch, and roll motion-modes. The obtained results offer further confirmation that the MEM can provide the basis for primary mode detection and control.

5.2 Real-time system architecture for active suspension control

The performance of modern control theories are often subject to the mathematical modelling of the plant. For a complex dynamic system such as a vehicle, to derive a single mathematical model to accurately capture all of its dynamic behaviours under different working conditions is rather difficult, if not impossible. Even if this model exists; it will possess a considerably large number of DOF and becomes inapplicable to deriving controllers. Furthermore, for a running vehicle, not only its working condition changes frequently (e.g., off-road / urban driving), but also its physical parameters (e.g., inertial property, tire pressure) change as well.

To address the uncertainty of the modelling, it is necessary to monitor the change of driving conditions and the change in vehicle physical parameters, and then update the vehicle model for deriving controllers that are more appropriate for this time point. From the dynamic responses collected from the deployed sensors on a vehicle, a vehicle model can be estimated to cover the primary dynamic modes of the system. Since the structure of a vehicle is fixed after its production, this model estimation process only needs to be conducted once, and an example is provided in Chapter 7. Furthermore, real-time parameter monitoring methods (e.g., random decrement technique [98]) are considered to monitor the parameter variation and to update the model. As a result, more effective and accurate controllers can be expected from this adaptive model. The schematic diagram of the real-time system architecture is presented in Figure 5.1.

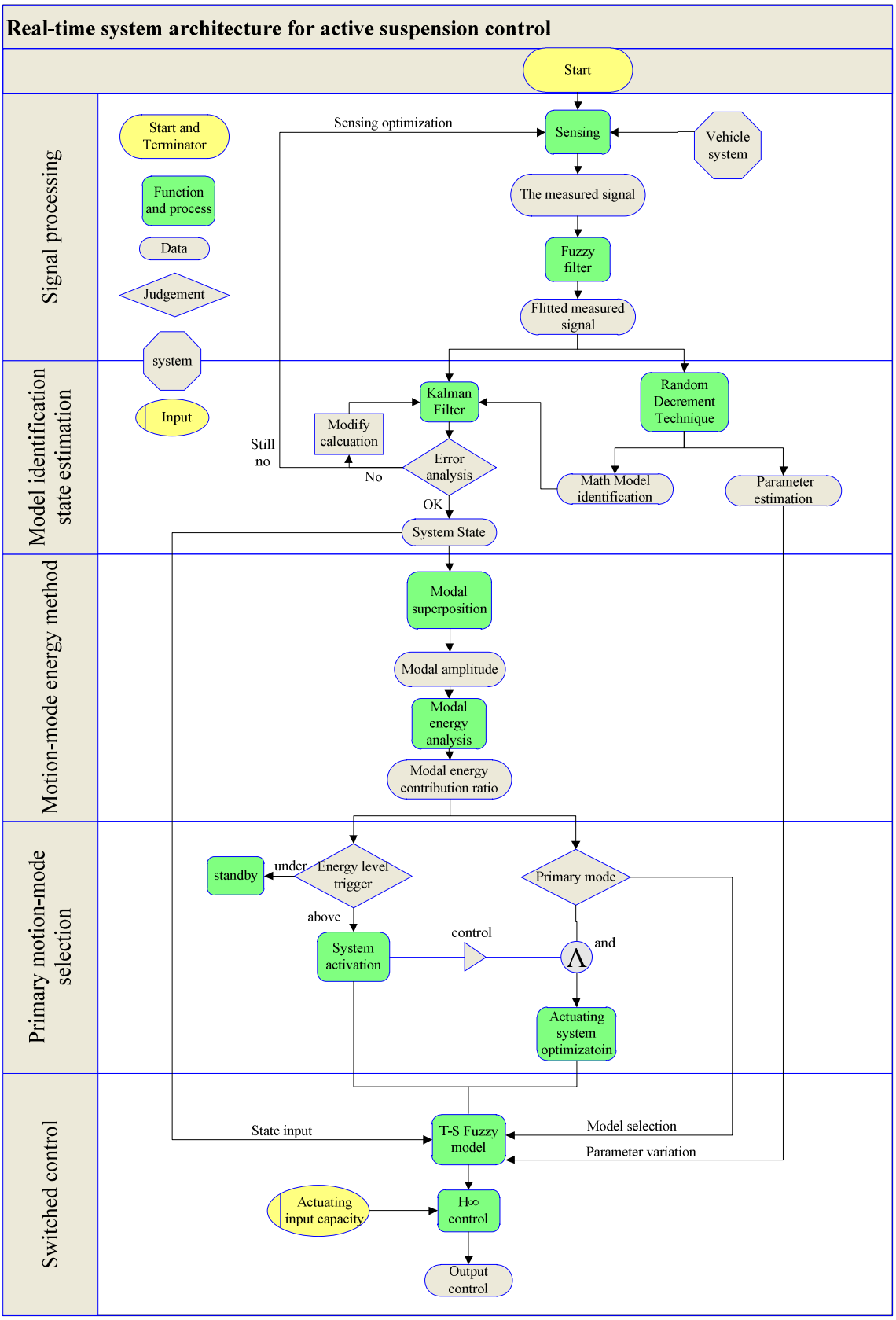

Figure 5.1. Real-time system architecture for active suspension control.

State vector is required by the MEM for detecting dominating motion-mode. Therefore, it is necessary to estimate the system state vector based on input signals from limited sensing channels. Variable methods are available for this state vector observation. The most commonly used method is the Kalman filter, which has been applied to vehicle state estimation and has reasonable performance [99]. However, due to the assumption used in its estimating algorithm, the Kalman filter has difficulty in coping with unknown impacts (e.g., force input) to a system. Although H∞ filter may address the impact issue better, its functionality and performance in a vehicle application needs to be further confirmed [100, 101]. Since state estimation is not the focus of this thesis, here we assume that the vehicle state is known to carry on the MEM analysis for primary mode detection.

Since the preliminary requirements for performing MEM are met (the model of the object system model and its state vector need to be known), the vehicle dynamics can be assessed by the energy level of its motion-modes based on the updated model and its state. Once the energy level in one motion-mode triggers the actuating system, the active HIS will reconfigure itself and apply the according control in this mode. H∞ optimal controller for each motion-mode will be designed with the use of a common quadratic Lyapunov function, which guarantees the stability of the switched system under arbitrary switching functions.

The architecture in Figure 5.1 has two levels of model reduction. The first model reduction is to simplify a vehicle into to a mathematical full-car model that covers its primary vibration modes. This model represents the major dynamics of the system. The purpose of having this full-car model is to perform state estimation and mode superposition for the MEM. The second model reduction happens when applying active control after real-time primary motion-mode detection. Once the dominating motion-mode is locked (e.g., roll mode), the full-car model is further downsized to a

half-car model to cover the primary motion-mode dynamics only (e.g., a roll-plane half-car model). The reason for the second model reduction is that in order to be computational practical, optimal control derivation usually requires a much simpler vehicle model than dynamic analysis requires; moreover, since the control is only applied to one motion-mode, the model used to derive this controller is not necessary to cover other motion-modes. Having these two model reductions makes the computation affordable in real time while also guaranteeing that each level of process has enough accuracy.

The architecture also has the sensing system optimisation and the actuating system optimisation. The optimisation of the sensing system needs to balance the performance and cost, to determine how many sensors are needed and where should they be deployed. Since the sensing systems hold the responsibility of model parameter variation detection and vehicle state estimation, therefore, the errors of the estimation process can be used as the criteria for this optimisation.

The principle of the MEM-based actuating system optimisation is to focus the control energy on the dominating dynamic aspect only. To be energy conservative while maintaining a high control performance, optimising the way that an actuating system responds is the key to locating control resources more efficiently. Some discussion on how to achieve a higher performance/power ratio can be found in [102]. In order to do so, the actuating system has to be able to physically reconfiguring its interconnecting hydraulic circuits to switch from one motion-mode to another, when the control focus shifts. This mechanism is detailed in the prototype design of the reconfigurable HIS test rig in Chapter 6.

5.3 Three-mode switched control

An example of the three-mode switched controller is cited from a recent work by Du in [103] to validate the feasibility and stability of the proposed switched-control strategy on a vehicle. The control concept and some simulation results are briefly presented here and for other details please refer to [103]. The presented switched control law focuses on three body motion-modes: bounce, pitch, and roll. The model used for the study is the 7-DOF full-car model presented in Chapter 3. The state variables are the input to performing the MEM analysis and also to each individual controller. The disturbance is road irregularity and the performance indices include sprung mass's acceleration in bounce, roll and pitch direction, suspension deflection and the road holding ability.

An H∞ optimal controller is designed for each motion-mode with the use of a common quadratic Lyapunov function [30, 104, 105], which guarantees the stability of the switched system for arbitrary switching functions. The designed controllers (K_1, K_2, K_3) can be switched according to the detected motion-mode. In this method, the vehicle dynamic energy for bounce, pitch, and roll motion-modes is calculated by MEM and used to provide a switching signal for the above designed control law. The dominant motion-mode is the motion-mode that has the highest level of energy relative to other motion-modes at one time instant. Furthermore, to reduce the effect of discontinuity when switching between different configurations on ride comfort, a soft switching strategy is applied. This strategy is implemented by linearly interpolating the switched controllers as

$$K = \eta_1(t)K_1 + \eta_2(t)K_2 + \eta_3(t)K_3 \tag{5.1}$$

where $\eta_1(t)+\eta_2(t)+\eta_3(t)=1$, thus the stability of the system can be guaranteed [104] and the impulse effect on the transient response is reduced. The overall control system block diagram is shown in Figure 5.2.

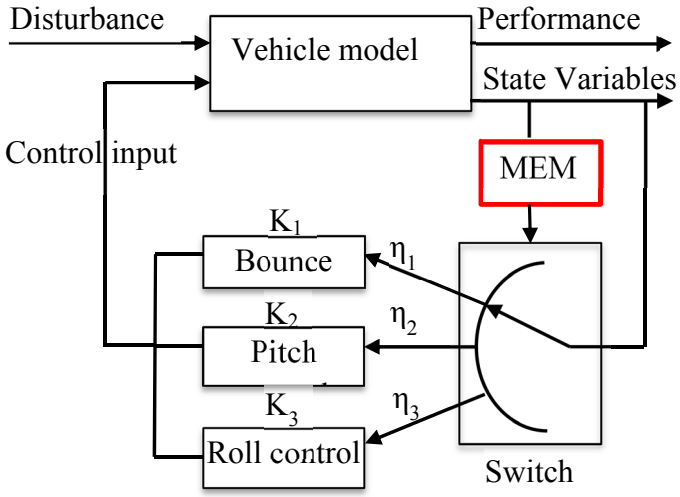

Figure 5.2. Block diagram of switched control system structure.

The effectiveness of the proposed suspension control system for improving ride comfort is evaluated by numerical simulations. The bump road profile will be used to test the system performance. The ground displacement for an isolated bump in an otherwise smooth road surface is given, and the road inputs to four wheels are shown in Figure 5.3.

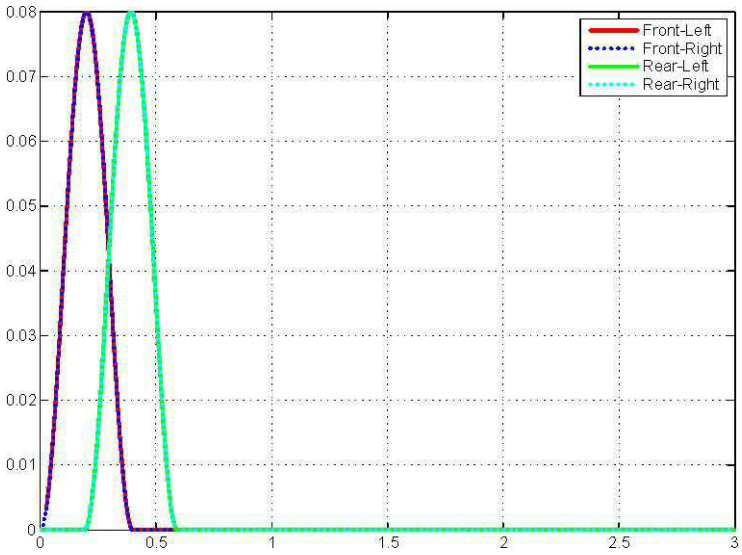

Figure 5.3. Bump road input.

The energy contribution ratio of each motion-mode shown in Figure 5.4 is the result of the passive suspension, which has no control system installed. It can be seen from this figure that the pitch motion, which has a bigger ratio value, is dominated at the beginning when the front wheels touch the bump, and then the bounce motion becomes dominant when the rear wheels pass over the bump. The ratio for the roll motion-mode is always zero since no roll motion is excited by the applied road input. As the energy contribution ratio is consistent with the physical analysis of the vehicle dynamics response, it confirms the effectiveness of the developed motion-mode detection method. The energy contribution ratio for each motion-mode of the designed active suspension under the same bump road input is shown in Figure 5.5. Similar analysis results can be obtained in terms of the ratio values for the dominant motion-mode. According to the detected dominant motion-mode, the designed controllers will be switched to achieve better suspension performance.

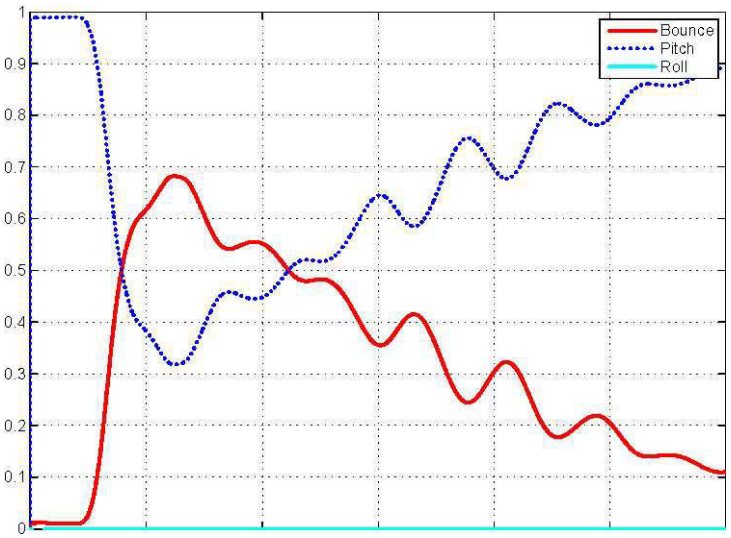

Figure 5.4. Energy distribution ratio of passive suspension under bump road input.

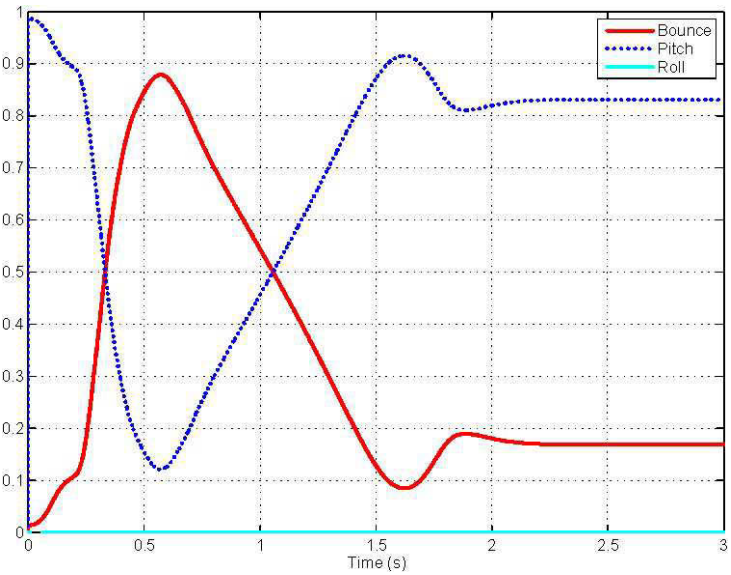

Figure 5.5. Energy distribution ratio of active suspension under bump road input.

The bump responses of the sprung mass vertical acceleration for the passive suspension and the designed active suspension are compared in Figure 5.6. The sprung mass pitch acceleration and roll acceleration are compared in Figure 5.7 and Figure 5.8, respectively. It can be seen from Figure 5.6 and Figure 5.7 that an improved performance on ride comfort in terms of the maximum peak values of vertical and pitch accelerations is obtained by the designed active suspension when compared to the

passive system. As the roll motion is not excited under this road input, roll accelerations for both passive suspension and active suspension are all zero as shown in Figure 5.8.

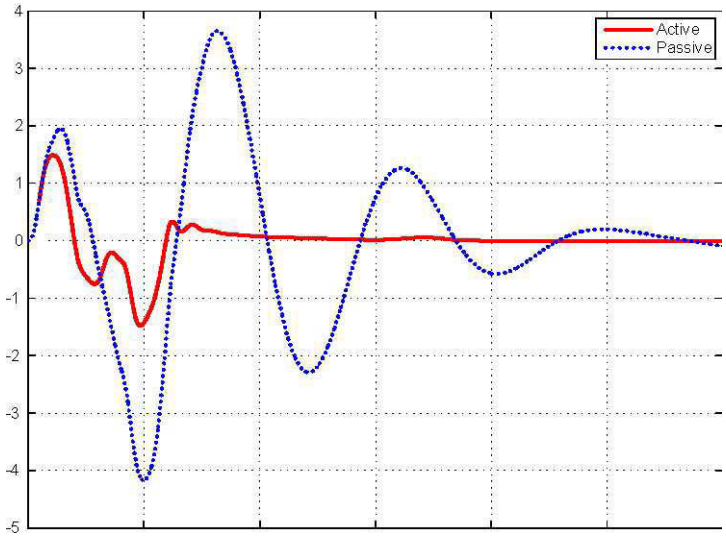

Figure 5.6. Bump response of sprung mass vertical acceleration.

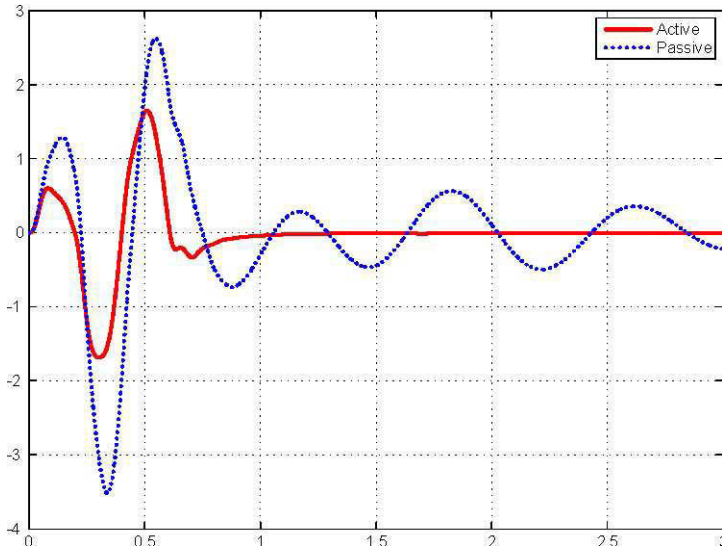

Figure 5.7. Bump response of sprung mass pitch acceleration.

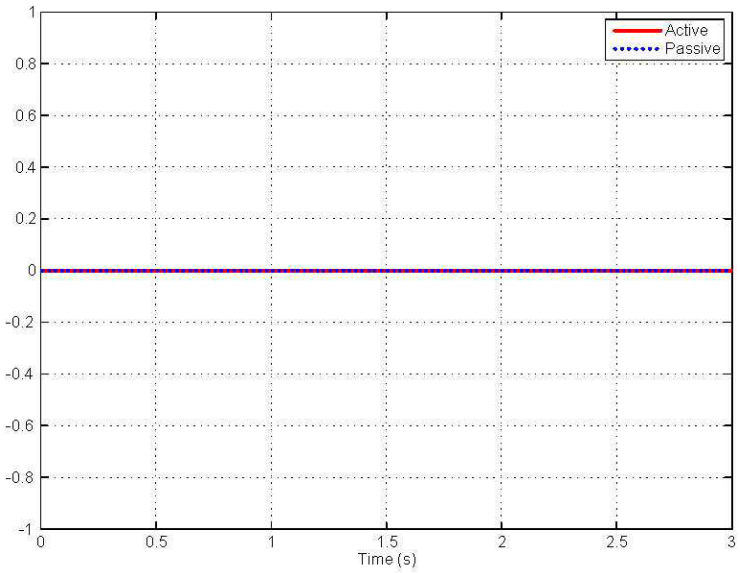

Figure 5.8. Bump response of sprung mass roll acceleration.

The comparison on suspension deflections is shown in Figure 5.9, from which we can see that the designed active suspension generates less or similar suspension deflections compared to the passive suspension because the constraint on the suspension deflection limitation has been considered in the controller design process. Further comparison on the tyre dynamic loads is shown in Figure 5.10. It can be seen that the designed active suspension generates less tyre dynamic load than the passive suspension. This means that the designed active suspension has good road holding performance compared to the passive suspension and it achieves better ride comfort performance.

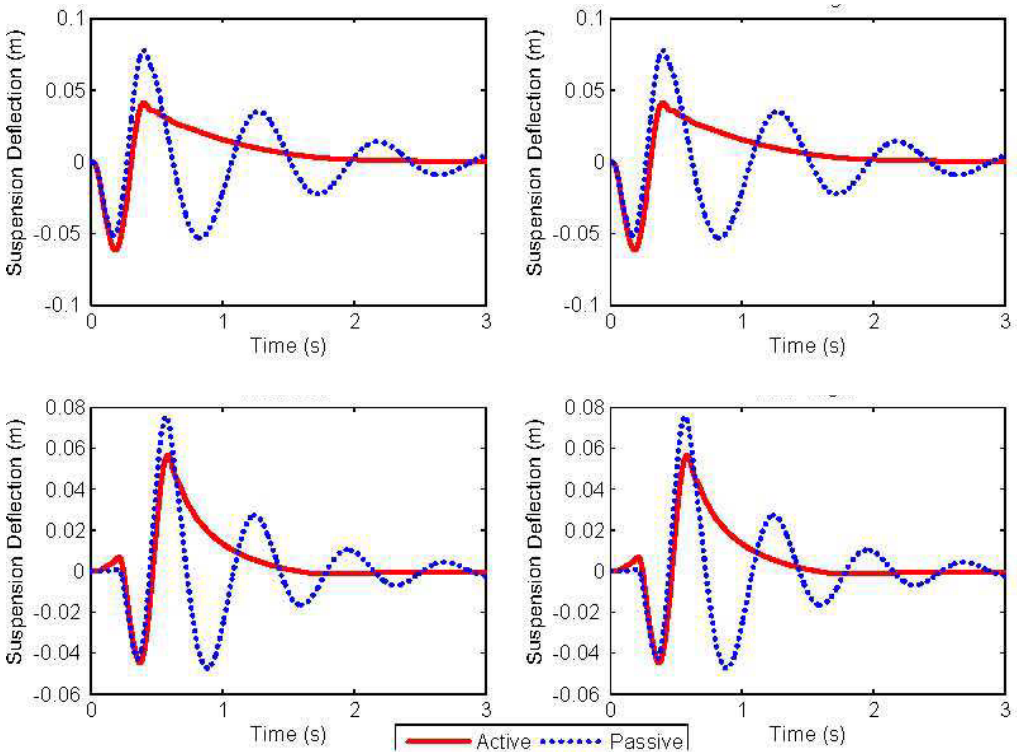

Figure 5.9. Bump response of suspension deflection.

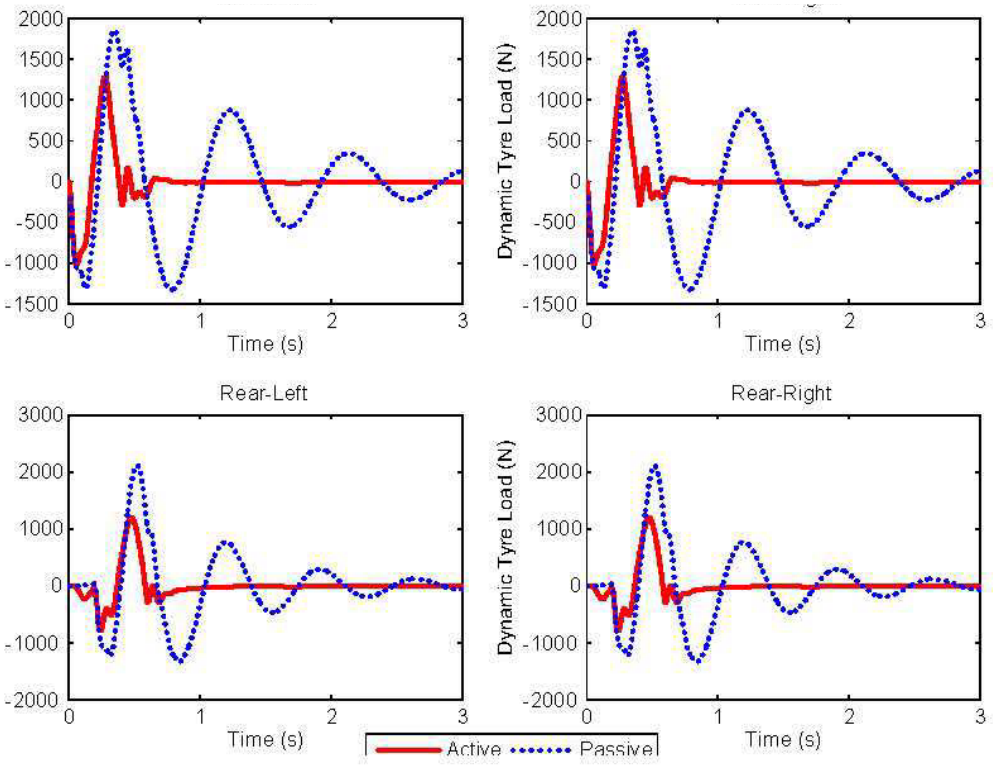

Figure 5.10. Bump response of tire dynamic load.

5.4 Summary

This chapter provides a roadmap of deriving a cost effective controller for a time variable system, from model estimation, primary mode detection, to the derivation of switched control with stability. The parameters of the working controller are determined by the vehicle operating state and its physical parameter variations, which are updated in real-time, to enhance the controller performance. Based on the detected dominant motion-mode by MEM, the active HIS system can be switched to a specific mode to control this particular motion-mode more effectively and more energy efficiently. To ensure the system is stable during the mode-switch, an H∞ optimal controller is designed for each motion-mode with the use of a common quadratic Lyapunov function.

Numerical simulations are used to validate the performance of this switched control strategy based on a three-mode scenario. The results offer further confirmation that the MEM can provide the basis for primary mode detection and control. The results also show that the active-HIS fitted vehicle system achieves good performance and is stable during the mode-switch. To further develop the research on the active HIS system, experimental investigation on prototypes with real vehicles is needed for better understanding the system's switching dynamic character between modes. In the next chapter, several test rigs are built for experimental studies, and a preliminary test of a single mode controller on an active HIS fitted vehicle is provided in Chapter 7.

The presented real-time system architecture may be applicable to a generalised unknown system which has time variable structure or parameters, e.g., a distributed flight array [106]. Based on the primary mode control concept, optimised control strategies can be derived for this kind of systems to efficiently locate control resources. This is recommended for the future studies.

CHAPTER 6 TEST FACILITY DEVELOPMENT

6.1 Introduction and rational

This section presents the test facilities that have been developed in this project for the study of active hydraulically interconnected suspension (HIS). Developing the circuit reconfigurable HIS involves a significant amount of engineering practice. Up to date, there are three test facilities have been designed, assembled and tested, namely, a six-channel vehicle dynamic test rig, a multi-functional anti-roll HIS test rig and a reconfigurable HIS test rig. The three test rigs lay the foundation for the development of the active HIS system and form the platform for the prototype development and experimental study. The design and specification details are provided in this chapter and test results are presented in the following chapter.

The three test rigs, specifically designed at the University of Technology, Sydney (UTS), are novel in terms of their specified functions.

- The six-channel test rig is, to the author's knowledge, unique in being a full-scale full-car stimulating rig, which can perform vehicle full-car parameter estimation, represent road arbitrary irregularity, and apply a yaw moment or a centrifugal force to a vehicle. Four channels out of six have been completed and employed in tests, and the rest of two channels are under assemblage.
- The multi-functional anti-roll HIS test rig, installed to a test vehicle, can be manually switched to individual mode to perform: passive HIS test, semi-active HIS test, fully-active HIS test, and demonstration of active suspension for teaching purposes. In this way, by simply switching a pair of ball valves, different types of HIS systems can be easily compared, without the need of physically disclosing any part of the enclosed hydraulic system. It saves

enormous effort and time especially when conducting the comparison tests between passive and active HIS systems. This test rig has been completed and involved in several tests in Chapter 7.

- The reconfigurable HIS test rig is purposely developed to study the transient dynamics of mode switching. As mentioned in Chapter 5, the stability of mode-switch is a main criterion for controller design, and this HIS test rig could bring valuable insights of the circuit reconfiguring dynamics. Moreover, the developed various switching strategies could also be designed, tuned, and compared on this test rig before implementing on real cars. This test rig has been completed.

The relation matrix of the task and facility is summarized in Table 6.1, illustrating the usage of test rigs and the tests. The detail description of each test rig is provided as afterwards.

Table 6.1. Relationship matrix of task and facilities.

Task & Facility	Parameter estimation	Passive anti-roll system testing	Active suspension testing
Six-channel vehicle dynamic test rig	yes	yes	yes
Multi-functional HIS test rig		yes	yes
Reconfigurable HIS test rig			yes

6.2 Six-channel vehicle dynamic test rig

The six-channel vehicle dynamic test rig is evolved from a four-poster shaker rig by adding another two channels to stimulate the roll and yaw motions of a vehicle. The test facility is intended to be used for:

- performing vehicle suspension experiments (by research staff & students);

- identifying vehicle system parameters (for research and industrial customers);
- researching on vehicle handling, stability, and ride comfort (e.g., in collaboration with the government etc.);
- teaching subjects such as machine dynamics, mechanical vibration and measurement, and vehicle design for the University.

The four-poster shaker rigs have been employed in the passenger car industry for validation, durability, buzz, squeak and rattle (BSR), and noise, vibration and harshness (NVH) testing for years, since they allow for more precise evaluations of body and suspension dynamics than running on road. A four-poster shaker rig typically consists of four ground-up-mounted hydraulic actuators with hydrostatic bearings and flat pans for vehicle tires to sit on and support the car. An optional X-Y positioning system is also necessary for the shaker rig to host four-wheel-vehicles with different chassis dimensions. Arbitrary wheel positions can be realised through the four-poster test rig, and the outputs of a four-poster rig commonly are harmonic sine waves or representations of real roads.

The four-poster test rigs can possibly be upgraded to include seven vertically mounted hydraulic cylinders, where four cylinders hold and excite the upsprung masses and the remaining three are attached to vehicle sprung mass for tilting vehicle body in roll, pitch or bounce direction. These tests rigs are particularly good for testing racing vehicles.

However, two things that the shaker rigs cannot perform are: 1) simulating lateral forces; and 2) simulating yaw moment. This is because the shaker rigs can only apply vertical forces to sprung and unsprung masses, examining vehicle dynamic aspects from a vehicle-fixed coordination frame. Vehicle planar dynamics and associated inputs such as lateral force and yaw moment cannot be applied to the test vehicle.

Applying lateral excitation to a test vehicle is important for evaluating the performance of its anti-roll system. During cornering of a vehicle, the friction forces between its tyres and the ground produce the essential centripetal force for it to turn. In detail, the resultant cornering dynamics consist of two components: a lateral force on the vehicle centre of gravity to conduct cornering, and a roll moment applied to the rotating centre to tilt the vehicle. Therefore, the lateral exciting test rig would be the ideal test facility for the study of vehicle roll dynamics, and it can produce the most direct and convincing result for validating and comparing the performance of the anti-roll systems.

In additional to the obvious need of having excitation in the lateral direction, having excitation in the yaw direction is also important to vehicle dynamic study and should be included in the test rig. The yaw-directional excitation is essential for vehicle parameter estimation of the yaw inertial property and the yaw-directional equivalent tire shear stiffness. These parameters are widely required by vehicle dynamic models for handling and safety analysis purposes.

Therefore, the author proposes a compact yaw/roll multi-functional stimulator design combined with the four-poster shaker rig. The combined facility, named as the six-channel vehicle dynamic test rig, consists of six hydraulic cylinders in total. Four of them are vertically mounted to the ground as a four-post rig to provide road excitation, and another two installed horizontally to provide roll/yaw stimulations, as shown in Figure 6.1. The two horizontally mounted cylinders, supported by two vertical standing posters in the front and rear of the test vehicle, are connected to the front and rear points of the vehicle in line with its centre of gravity (CG), through universal ball joints. The synchronising of the two horizontal cylinders can yield: (1) a resultant lateral force when cylinders are in-phase; (2) a resultant yaw moment when cylinders are out-of-phase.

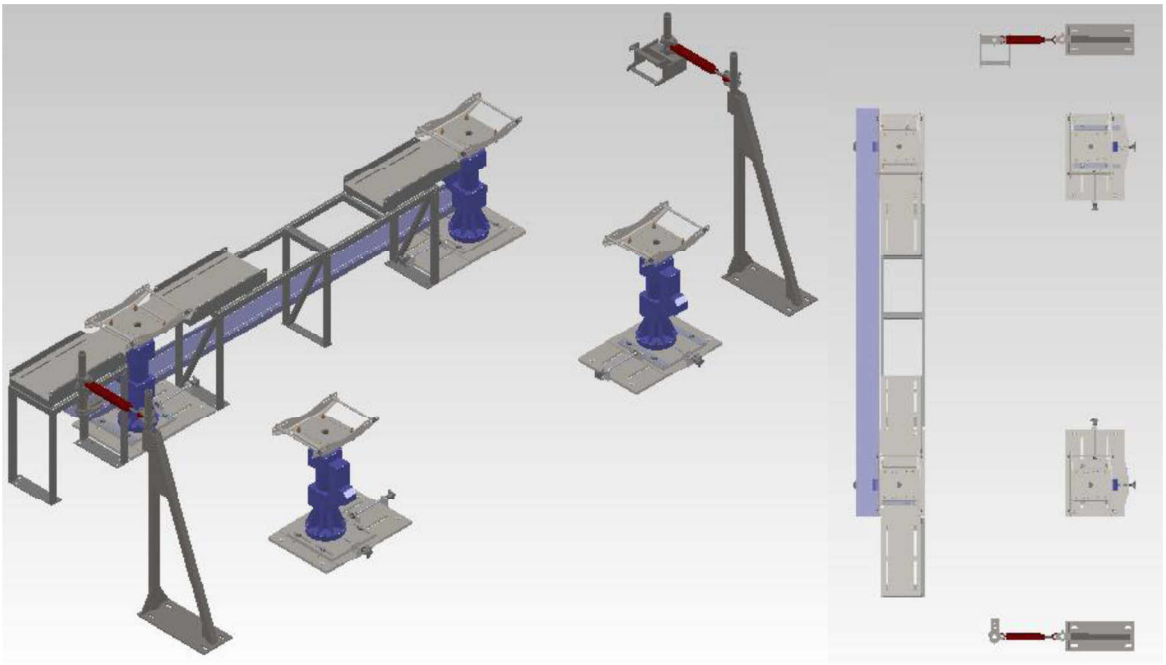

Figure 6.1. 3D design of the six-channel vehicle dynamic test rig.

Figure 6.1 presents the structural design of this six-channel test rig, and Figure 6.2 shows the hydraulic circuits that control the two lateral cylinders. The ground excitation hydraulic circuit and planar excitation circuit are kept separated to eliminate the potential interference between the two. Figure 6.3 shows a photo of two of the finished cylinders and Figure 6.4 shows a photo of the motor-pump unit. Figure 6.5 presents a photo of a test vehicle sitting on top of the test rig and Figure 6.6 shows the controller developed in Labview.

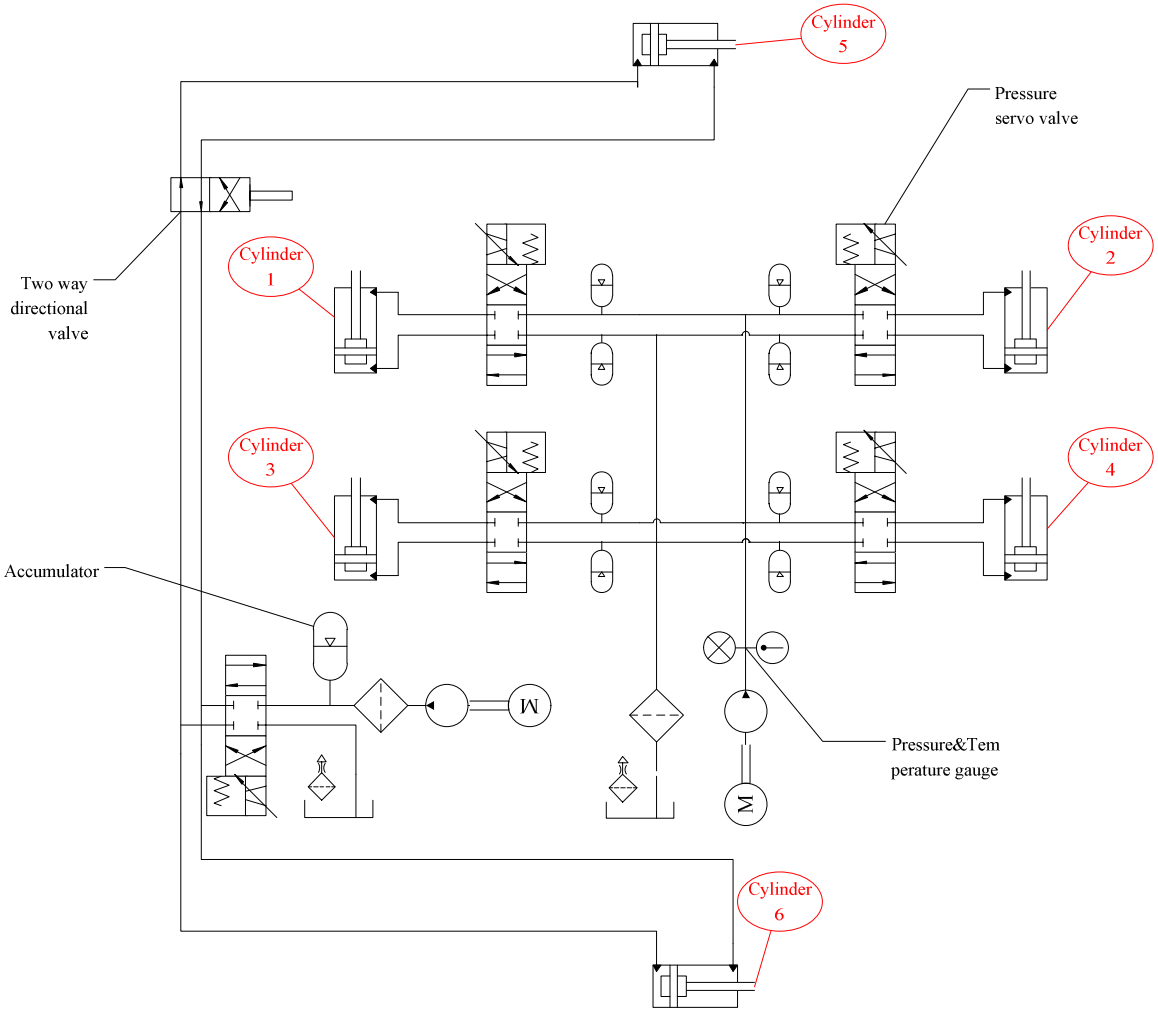

Figure 6.2. Hydraulic circuits of the six-channel vehicle stimulating test rig.

Figure 6.3. Finished cylinders with their motor-pump of the test rig.

Figure 6.4. One motor-pump unit of the test rig

Figure 6.5. A test vehicle sits on the four finished cylinders.

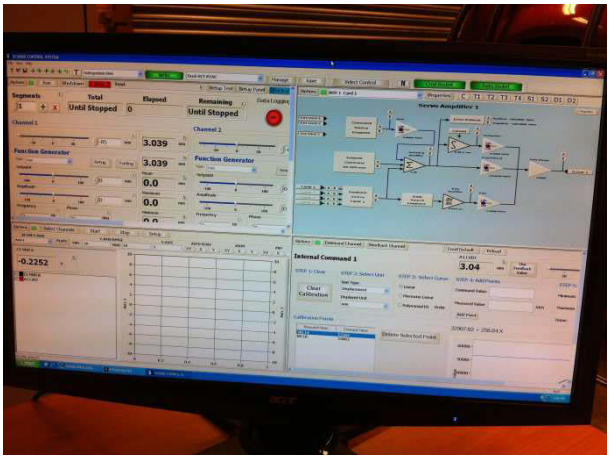

Figure 6.6. The control software of the test rig.

The six-channel test rig presents a unique research and teaching facility, second to none amongst Australian research institutions. The system specifications are summarized in Table 6.2.

Table 6.2. Six-channel test rig system specifications.

Vehicle weight (max.)	3000 kg
Wheel base adjustment range	2450 - 2890 mm
Track width adjustment range	1460 - 1720 mm
Actuator:	
Force (rated max.)	+/- 40 kN (equal area)
Displacement	+/- 76 mm
Velocity (max.)	0.4 m/s
Acceleration (max.)	20 g
Frequency range	0.1 - 60 Hz
Typical unsprung mass (per actuator)	75 kg
Typical sprung vehicle mass	1700 kg
Base mount	independent x-y positioning mechanism for easy adjustment of track width & wheel base
Wheel pan	rectangular design for easy roll-on; safety skirt to prevent vehicle roll-off; provision for load cell
Control System:	
Servo controller	roll & bounce modes; independent excitation

6.3 Multi-functional hydraulically interconnected suspension test rig

The research and development of different hydraulically interconnected suspension systems, the active HIS in particular, requires a developing platform as the common test bed for design, tuning, validation and comparison. A multi-functional developing platform on a test vehicle is proposed and built, which is capable of performing: the passive HIS suspension test at different pressure settings, the active HIS test with different controllers, and the semi-active HIS test with pressure compensating or adjustable features. The test rig in its full-scale, named as the multi-functional hydraulically interconnected suspension test rig, MHIS in short, can be easily converted into different HIS configurations without the need of re-plumping. This provides significant benefits for experiment set up and testing. Otherwise, to convert between a passive HIS and an active one on the test vehicle would require replacing the accumulators and the hoses with the active hydraulic manifold. In this process, air and dirt could enter the enclosed hydraulic system and they may have a detrimental effect on the valves and actuators.

The MHIS saves the repetitive effort of re-plumping and the major benefits of this design include: 1) no extra cost while different HIS systems are sharing the common components; 2) takes no more than 2s to switch from one type of HIS to another; 3) switching without disassembling any part of the hydraulic system. The hydraulic diagram of MHIS is shown in Figure 6.7. The switching menu is shown in Table 6.3.

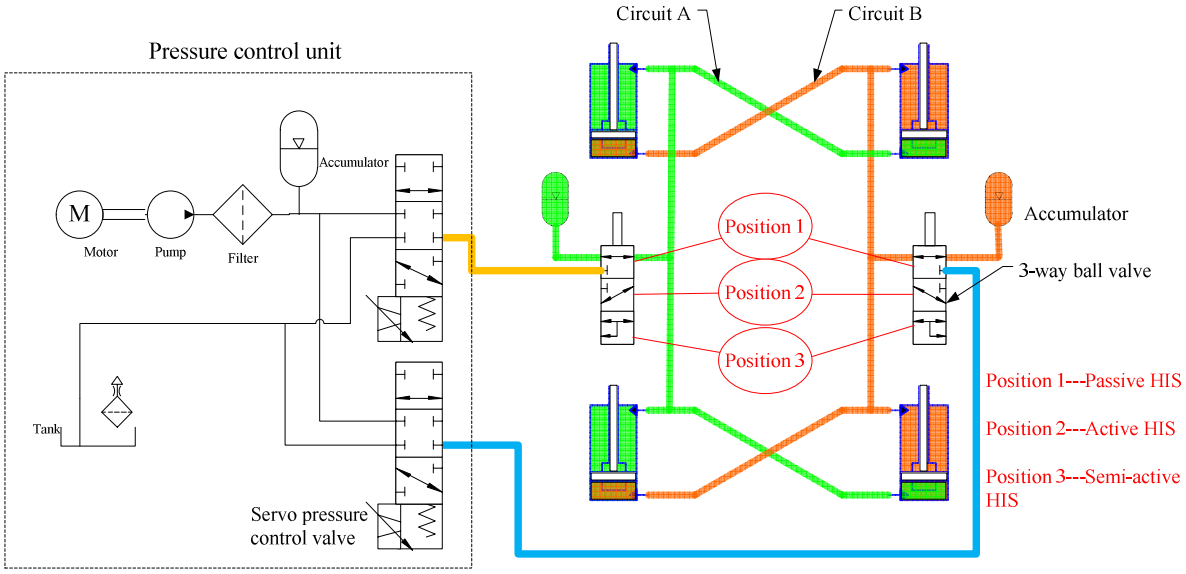

Figure 6.7. Hydraulic circuits of the multi-functional hydraulically interconnected suspension test rig.

Table 6.3. Configuration of the MHIS test rig.

Mode	Position of the ball valves	Control
Passive HIS	1	No
Active HIS	2	Auto-control
Semi-active HIS	3	Demand-control

The MHIS test rig consists of a typical roll-plane interconnected configuration with two hydraulic circuits (A and B), four cylinders, accumulators, ball valves and a pressure control unit. The pressure control unit is composed of a motor-pump, an accumulator, two pressure control servo valves and other necessary accessories such as a tank and a filter. By switching the two ball valves to position 1, 2 or 3, as marked in Figure 6.7, the test rig is turned into a passive, an active or a semi-active HIS system. These functions are detailed as the following and illustrated in Figure 6.8, Figure 6.9, and Figure 6.10, separately.

6.3.1.Passive HIS mode

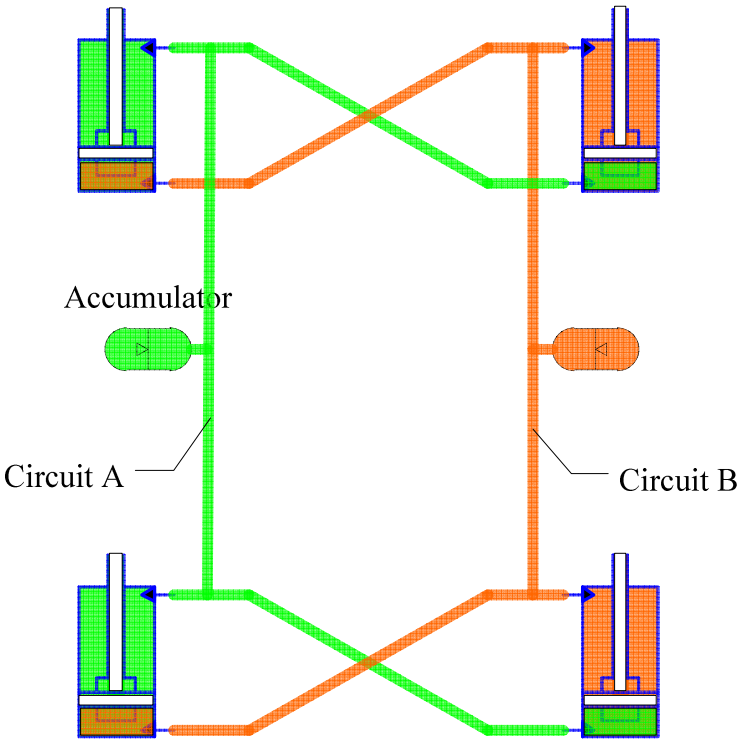

Figure 6.8. Hydraulic circuits of the passive anti-roll HIS system.

The passive HIS system consists of two identical hydraulic circuits, as shown in Figure 6.8. The two hydraulic circuits are coupled with each other kinetically via four double acting cylinders. Each of the hydraulic circuits has a nitrogen-filled diaphragm accumulator, and hydraulic pipeline elements.

Within the two hydraulic circuits, the cylinders are mounted between the car body and the wheel stations. The dynamic interaction between the hydraulic system and the sprung and unsprung masses can be described as such: relative velocities in the suspension struts cause changes in pressure in both circuits, which lead to changes in suspension strut forces through all four cylinders. As a result, vehicle body and wheel motions occur, which, in turn, affect the hydraulic system. This mechanic-hydraulic interaction will continue until the system reaches a new equilibrium.

The passive HIS system is considered as a replacement of anti-roll bars to provide essential roll stiffness to a vehicle. The pair of accumulators in the HIS system functions as a torsional spring to provide reacting force to suppress the vehicle body's roll motion. The passive HIS system needs to be pre-charged to a certain working pressure in order to provide this roll stiffness. The higher the passive HIS's working pressure is, the stiffer it is in the roll plane, and vice versa.

6.3.2.Active HIS mode

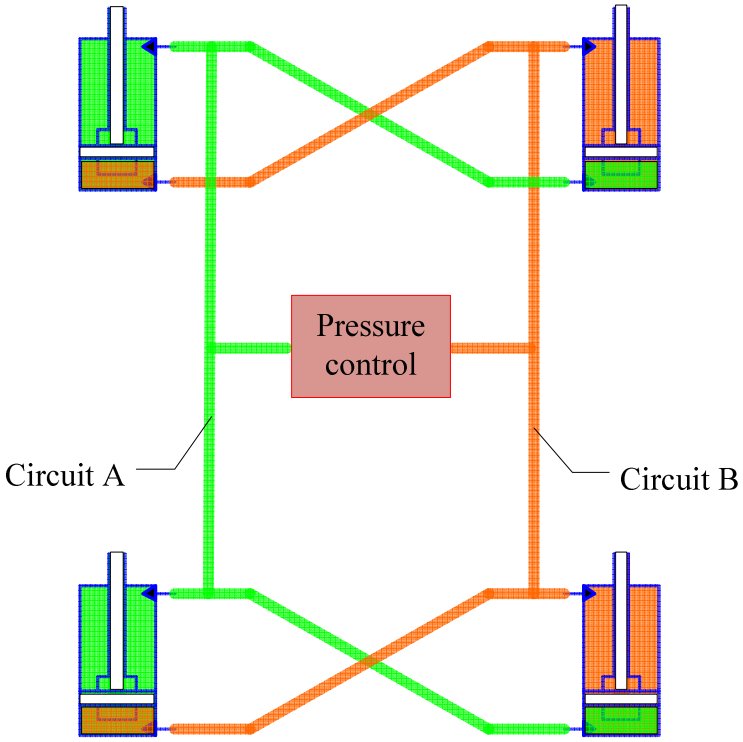

Figure 6.9. Hydraulic circuits of the active anti-roll HIS system.

Similar to the passive HIS system, the active HIS system also consists of two hydraulic circuits interconnecting four cylinders in the roll-plane, but without accumulators in the circuits. Unlike the passive system which provides the reacting force from its pair of accumulators, the active system provides an optimised control force (calculated by

the given control algorithm) to counteract the vehicle body's motion. The pressure control unit is responsible for providing the required pressure in circuits *A* and *B*, and also delivers any flow if required. The active HIS is more flexible in control and should have superior performance than the passive HIS, though its cost is higher than the passive system.

When roll motion of the vehicle body occurs, the control unit estimates the roll angle and controls the pressure of fluid circuits to provide an anti-roll moment to the vehicle body. For example, during sharp cornering, the body of a vehicle experiences a large roll motion and rolls to its left, the active suspension will title the vehicle body to the opposite side for compensation. The left suspension needs to extend while the right needs to compress in order to maintain the vehicle body's levelling. In this circumstance, the pressure control unit will need to pump oil into circuit *A* to increase its pressure, while reducing the pressure (if not tank pressure) in circuit *B*. The pressure difference of circuit *A* and *B* forms an anti-roll moment to the vehicle body through four cylinders. With active suspension, zero titling during cornering is possible.

6.3.3. Semi-active HIS mode

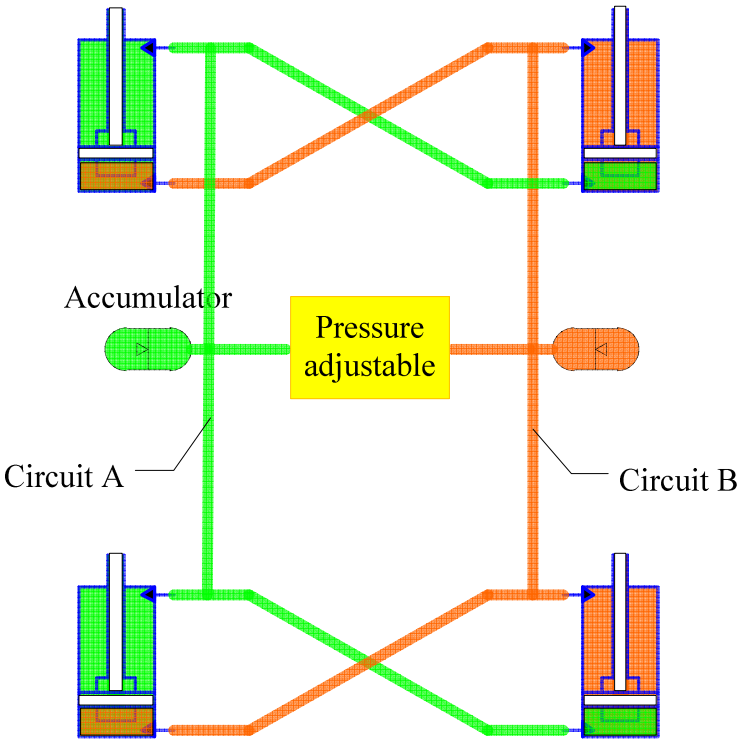

Figure 6.10. Hydraulic circuits of the semi-active anti-roll HIS system.

The semi-active HIS system is motivated by the desire of making a cost effective passive system with pressure adjustable features. In literature, similar systems are called smart passive system; however, in this work, the semi-active system is defined as any system between purely passive and fully active. Passive HIS systems are appreciated for their effectiveness, reliability and low cost, but there are two arising concerns with them in practice. One issue is the fluid leakage of the enclosed system, which causes the shifting of the working point of the system. Another issue, which is shared with all passive systems, is that none of its parameters can be changed after production, e.g., once the pre-charged working pressure is determined, it cannot be further adjusted during driving.

The pressure adjustable semi-active HIS system can control the working pressure of hydraulic system by pumping/releasing oil into/from the HIS circuits. The roll stiffness of the HIS system is determined by its working pressure. The semi-active HIS system senses the driving condition and changes its stiffness accordingly, e.g., on a high way drive, its stiffness can be reset to "*High*" to enhance the handling; on a rough road drive, the working pressure can be reset to "*Low*" to tolerate the uneven ground and reduce vehicle body movement. The proposed semi-active design offers flexibility and reliability to the existing passive HIS system and makes it more adaptable. The semi-active HIS is not the focus of this thesis and is recommended in future studies.

6.3.4.Implementation

The MHIS was designed and assembled onto an SUV in the Dynamics Laboratory at the University of Technology, Sydney. The standard anti-roll bars were removed from this vehicle and were replaced by the MHIS system. Dimensional parameters of the HIS system are determined by geometric measurement of the car, e.g., the stroke of the hydraulic cylinder, the pipe length. Some design details are provided here. The experimental vehicle has a double wishbone front suspension and independent rear suspension. The shock absorbers of conventional independent suspensions are kept with the car to minimise the change to the chassis. To mount the MHIS cylinders onto the car, ball joints are used for all hydraulic cylinders, to ensure each cylinder end has 3 DOF.

At the front, the top of the cylinder is pivoted on the vehicle body and the cylinder rod end shares a pin point with the original shock absorber on the lower control arm of the wishbone suspension, shown in Figure 6.11(a). The stroke of the cylinder does not limit suspension travel and the geometric location of the cylinder does not affect wheel turning. At the rear, the cylinders are installed beside the original coil springs, mounted

to the vehicle body at the top, and attached to the control arm at the bottom, shown in Figure 6.11(b). Flexible hoses are used to connect the inlets/outlets of the four cylinders to the rigid piping system to accommodate the movement of the cylinders. The configuration of a rear cylinder, hoses and some piping are shown in Figure 6.12(a). The piping system, running underneath the vehicle chassis, interconnects the hydraulic cylinders into two circuits.

Each circuit connects to a ball valve which further links to an accumulator and/or the pressure control unit. A photo that shows the mounting of the ball valve and its connections is presented in Figure 6.12(b). As a safety measure, a mechanism is installed to lock the valve handle in any one of its configurations, to prevent unintentional triggering of the valve when in operation. The completed assembly of the pressure control unit is shown in Figure 6.13(a); and its mounting on the car is shown in Figure 6.13(b).

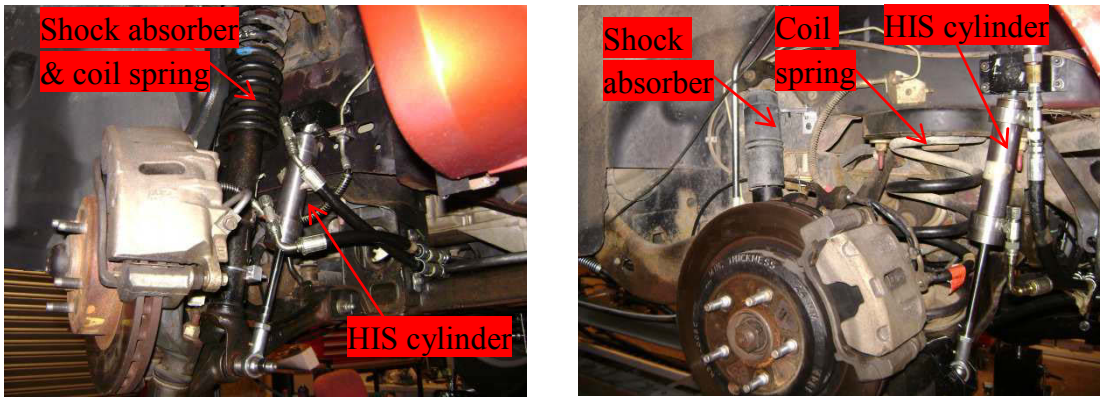

(a) (b)

Figure 6.11. Mounting of MHIS cylinders at: a) the front; and b) the rear.

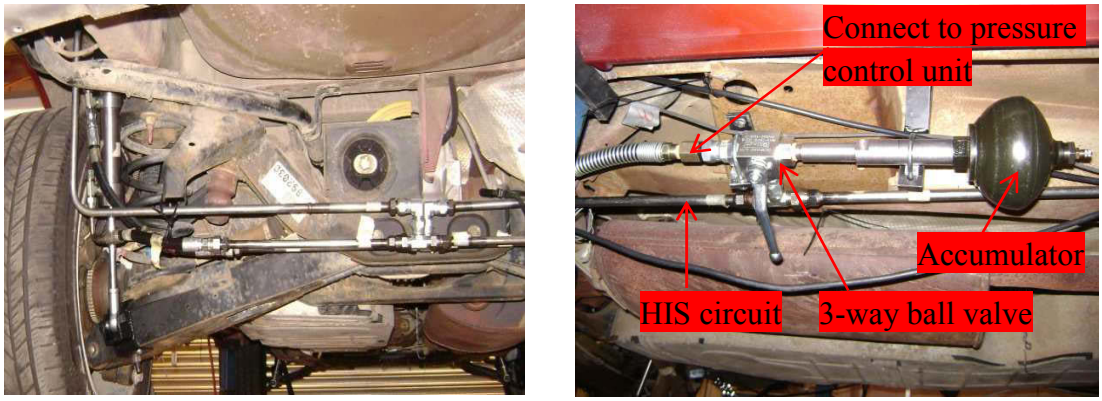

(a) (b)

Figure 6.12. Mounting of MHIS system: a) cylinder, hose and piping at rear left; and b) mounting of a 3-way ball valve.

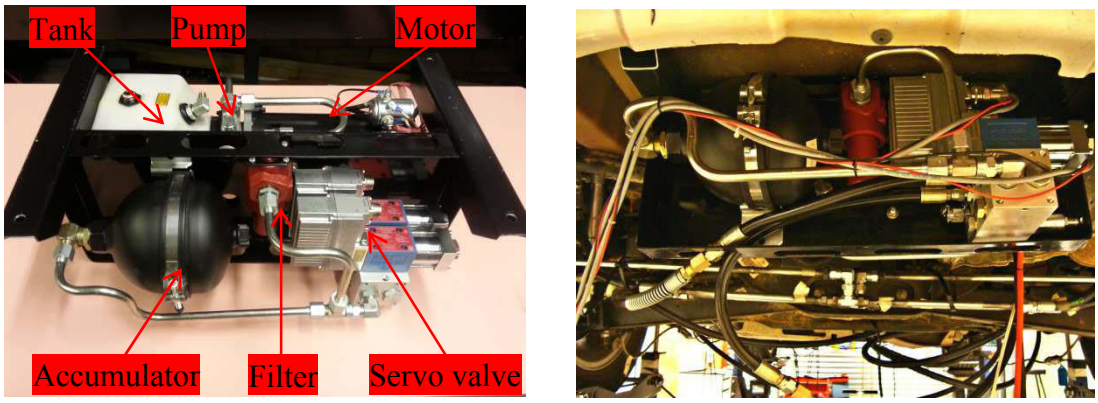

(a) (b)

Figure 6.13. MHIS pressure control unit: a) assembled pressure control unit; and b) installation of the pressure control unit on the test car.

The sensing system, considered as an important part of the test rig, collects responses from the HIS system and the test vehicle. The data acquisition system consists of a National Instrument (NI) data acquisition board, a computer with Labview, and a number of transducers, including up to eight accelerometers, four linear displacement transducers, two pressure transducers, and two Gyroscopes. Three accelerometers are installed underneath the storage box between the two front seats, which is at the CG

(centre of gravity) of the vehicle, to measure the vertical, lateral and longitude acceleration, respectively. Another four accelerometers are installed onto the four wheel hubs to measure the wheels' acceleration. As shown in Figure 6.14, four linear variable differential transformer (LVDT) displacement transducers, mounted besides the coil-spring in each wheel station, measure the relative motions between vehicle body and wheels, which are defined as suspension deflection in this thesis. Two pressure sensors are installed into two hydraulic circuits to monitor the hydraulic system response; the mounting is shown in Figure 6.14. There are a few more accelerometers, which can be made mobile to be deployed at other spots of interest on the car depending on the particular study focus.

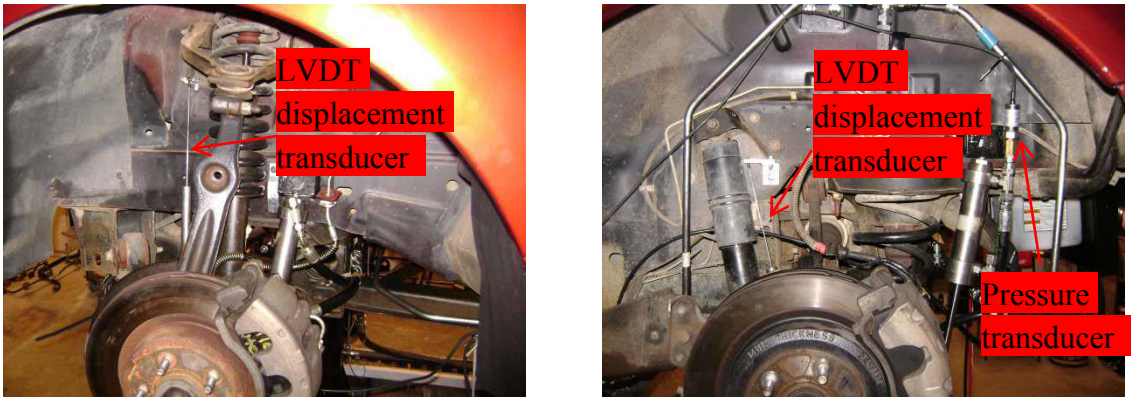

(a) (b)

Figure 6.14. Mounting of LVDT and pressure sensors at: a) the front; and b) the rear.

The controller-developing platform supports the real-time communication between the computer Matlab workspace and the physical test rig. Through this platform, different controllers from the Matlab toolbox can be efficiently implemented, tested and compared on the test rig. Note, although the current MHIS only enables control in the roll-mode, it can be easily upgraded from the single-mode control to the full-mode control by adding a set of direction valves to its cylinders. Once this upgrade is effected, the MHIS will be able to perform anti-pitch control, anti-bounce control, and

anti-articulation control on the same test vehicle without affecting existing functions. This upgrade could be carried out in the future once the research interest expands.

6.4 Reconfigurable hydraulically interconnected suspension test rig

To realise the proposed motion-mode based active switchable control, it is necessary to develop a prototype and experimentally investigate the switch dynamics during the hydraulic circuit re-configuration. A separated test rig is proposed for studying transient dynamic study of the mode-switch control and the development of switching strategies.

The reconfigurable hydraulically interconnected suspension test rig (RHIS) is disconnected from the test vehicle to eliminate the mechanical-hydraulic dynamic coupling effect, in order to focus on the transient hydraulic dynamics within the HIS system itself. The hydraulic circuit diagram of the RHIS system is shown in Figure 6.15. The RHIS system consists of a pressure control unit mainly including a pressure servo valve, a circuit reconfigure unit of three direction valves, four cylinders and necessary piping and hosing. With the circuit reconfigure circuit, the system can be switched into four modes: bounce, roll, pitch, articulation, and then the pressure control unit will take action to regulate the system pressure.

Two pressure transducers are installed in the pressure control unit to measure the transient pressure response during the switching of directional valves. A computer connected with an NI data acquisition board is employed to measure the system dynamic responses. Another computer installed with Labview software is used to communicate with the test rig to perform the pressure control and mode-switch control.

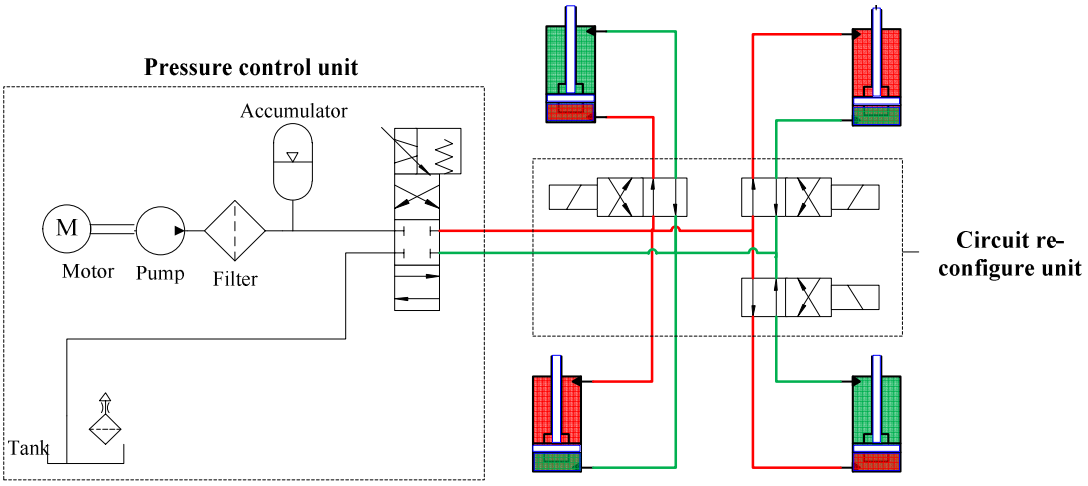

Figure 6.15. Hydraulic circuits of the RHIS test rig.

Figure 6.16. Photo of the finished RHIS test rig.

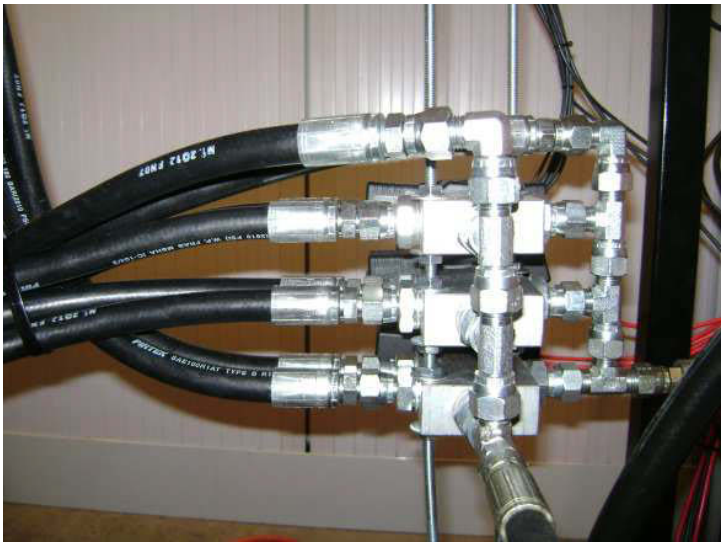

Figure 6.17. RHIS directional valve set.

Figure 6.18. RHIS pressure control unit.

Figure 6.16 shows the assembled multi-modes active HIS test rig. The photo of the circuit reconfigure unit is shown in Figure 6.17, and the pressure control unit is shown in Figure 6.18.

Based on the developed RHIS test rig, several potential projects can be carried out in the future: investigation of time delay in the pressure control unit and the circuit

reconfigure unit, development of a switch strategy to synchronize the four cylinder's motions, a study of the pressure impulse during directional valve switch, and development of a new compact reconfigure unit.

CHAPTER 7 EXPERIMENTAL INVESTIGATION OF THE HYDRAULICALLY INTERCONNECTED SUSPENSIONS

7.1 Introduction and rationale

This section presents the experimental investigations that have been conducted in this project which includes:

- the vehicle parameter estimation and modelling;
- the passive HIS laboratory test;
- the passive HIS filed test;
- the preliminary active HIS laboratory test with an H∞ controller.

To be able to conduct any computer-based analysis of the dynamics of a vehicle or HIS systems, it is necessary to obtain their physical parameters in advance. These physical parameters of a vehicle include the sprung mass, the unsprung mass, the inertial properties of the sprung mass, the stiffness and damping coefficient of suspension, the tire stiffness, etc. This session starts with the experiments to estimate these parameters through the employment of the State Variable Method [107]; then uses the obtained value to construct a half-car model for mathematical analysis. The anti-roll bars and the passive HIS anti-roll system are compared over their equivalent roll stiffness based on this half-car model using the same parameter estimation method. In addition to the laboratory tests, field tests are also provided to compare these two anti-roll systems under different types of manoeuvres. Based on the solid understanding of the passive HIS system, the active HIS suspension has been designed and tested on the vehicle dynamic test rig that has been developed in the previous chapter.

7.2 Vehicle parameter estimation

The first task to start the experimental investigation of this project is to obtain the vehicle parameters from the test vehicle. Vehicle parameters include modal and physical parameters. Modal parameters are natural frequencies, damping ratios and mode shapes; and physical parameters include inertial parameters, stiffness and damping coefficient. A novel approach is proposed in this session to test and estimate vehicle physical parameters in time domain. A set of specified full-car drop tests are designed to obtain the free decay responses from different primary vibration modes, such as bounce, roll and pitch. Then a combined State Variable Method (SVM) [8-9] and numerical inverse-eigenvalue method is proposed to process the time domain signal. The data process involves two stages: firstly obtaining system modal parameters from vehicle free decay response through the SVM method; then estimating the physical parameters of the vehicle by solving the so called inverse problem [10-11].

The proposed parameter estimation approach has several unique advantages to others, which usually require special test rigs and strict testing conditions. Firstly, it is a time domain method and is relatively cost effective in practice, compared to frequency domain methods. Secondly, the estimation process does not require the measurement of the excitation (force or displacement input) to the test vehicle. Thirdly, the testing process does not require special testing facilities and thus is easy to set up.

A 4-DOF half-car model is employed for this parameter estimation in the roll-plane. Since the merits of having anti-roll systems is to provide essential roll stillness to vehicle during cornering, the installed anti-roll system (e.g., anti-roll bar, HIS) on the test vehicle is modelled as a torsional spring attached to vehicle roll centre. In this way, the parameters of the vehicle and the parameters of the anti-roll systems can be

estimated separately; moreover, the different anti-roll systems can be compared for their equivalent roll stiffness.

7.2.1.Vehicle modelling

A bilateral symmetry half-car model with 4 DOF is employed for the study. The vehicle model consists of sprung and unsprung mass, connected by springs and dampers, shown in Figure 7.1. An additional torsional spring is connected to the roll centre of vehicle body to represent any anti-roll system.

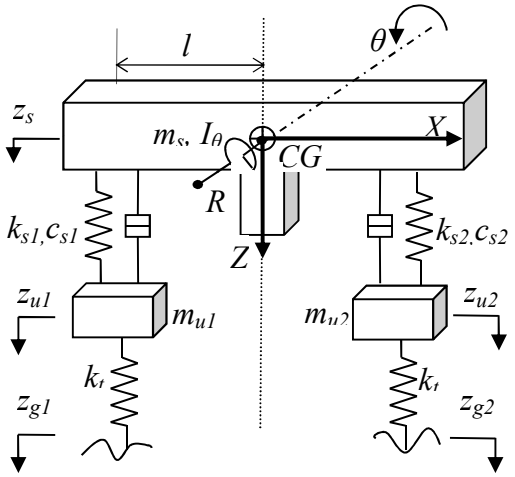

Figure 7.1. A 4-DOF half-car model.

In Figure 7.1, point *CG* is the centre of the gravity (CG) of the sprung mass which rotates around rolling centre *O*. In *X* axis direction, a torsional spring is connected to the rolling centre *O* of the sprung mass with a roll stiffness k_{tr}. Restrain point *R* can move in the *Z* axis direction freely to cope with vehicle's bounce motion. The test vehicle is a Ford Territory and its parameters are listed in Table 7.1.

Table 7.1. Model parameters of the Ford Territory.

Notation	Description	Units	Values
I	Sprung mass inertia	Kg·m^2	Unknown
m_v	Total half-car mass	Kg	980
m_s	Sprung mass	Kg	Unknown
m_u	Unsprung mass	Kg	Unknown
k_s	Suspension stiffness	N/m	Unknown
c_s	Suspension damping coefficient	N s/m	Unknown
k_{tr}	Torsional spring stiffness	N/rad	Unknown
k_t	Tire stiffness	N/m	Unknown
CG	Height of Centre of Gravity	m	0.637
O	Height of Centre of rolling	m	0.487
l	Distance between left and right wheels	m	1.15
h	Distance between CG and O	m	0.15
z_s	Displacement of sprung mass in Z direction	m	------
θ	Roll angle of sprung mass	rad	------
z_{u1}	Displacement of left unsprung mass	m	------
z_{u2}	Displacement of right unsprung mass	m	------
z_{i1}	Input displacement to left tire	m	------
z_{i2}	Input displacement to right tire	m	------

The differential equations for the heave and roll movements of the vehicle body, and the heave movements of the two wheels are given as follows.

$$m_s\ddot{z}_s = -k_s(2z_s - z_{u1} - z_{u2}) - c_s(2\dot{z}_s - \dot{z}_{u1} - \dot{z}_{u2}) \tag{7.1}$$

$$I\ddot{\theta} = lk_s(z_{u1} - z_{u2} - 2\theta l) + lc_s(\dot{z}_{u1} - \dot{z}_{u2} - 2\dot{\theta}l) + \theta k_{tr} \tag{7.2}$$

$$m_u\ddot{z}_{u2} = -k_t z_{u2} + k_s(z_s - \theta l - z_{u2}) + c_s(\dot{z}_s - \dot{\theta}l - \dot{z}_{u2}) \tag{7.3}$$

$$m_u\ddot{z}_{u1} = -k_t z_{u1} + k_s(z_s + \theta l - z_{u1}) + c_s(\dot{z}_s + \dot{\theta}l - \dot{z}_{u1}) \tag{7.4}$$

Based on the differential equations, we obtain the following state equation of the half-car model:

$$M\ddot{Z} + C\dot{Z} + KZ = 0 \tag{7.5}$$

where $Z = [\theta \quad z_s \quad z_{u1} \quad z_{u2}]^T$,

$$M = \begin{bmatrix} I & 0 & 0 & 0 \\ 0 & m_s & 0 & 0 \\ 0 & 0 & m_u & 0 \\ 0 & 0 & 0 & m_u \end{bmatrix}, \quad C = \begin{bmatrix} 2l^2c_s & 0 & -lc_s & lc_s \\ 0 & 2c_s & -c_s & -c_s \\ -lc_s & -c_s & c_s & 0 \\ lc_s & -c_s & 0 & c_s \end{bmatrix},$$

$$K = \begin{bmatrix} 2l^2k_s - k_{tr} & 0 & -lk_s & lk_s \\ 0 & 2k_s & -k_s & -k_s \\ -lk_s & -k_s & k_s + k_t & 0 \\ lk_s & -k_s & 0 & k_s + k_t \end{bmatrix}.$$

7.2.2. Flow chat of vehicle parameter estimation

The parameter estimation in practice is always with difficulties. The proposed estimation approach is simple and cost effective. It has two steps as shown in Figure 7.2: (1) estimation of the modal parameters of a vehicle from its free decay responses; (2) estimation of the physical parameters of the vehicle from its modal parameters by solving the inverse problem.

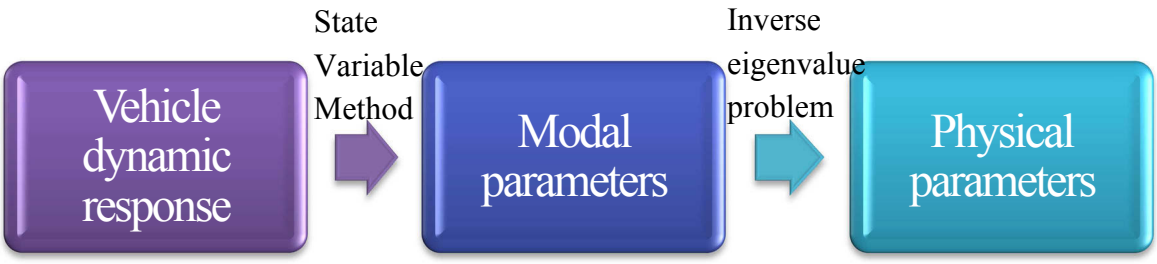

Figure 7.2. Flow chart of the procedure of vehicle parameter estimation.

The first step of estimation employs the SVM to extract the transition matrix of the vehicle system from its free decay responses. By solving the eigenvalues problem of the derived transition matrix, the modal parameters of the vehicle system can be obtained, such as its natural frequencies and damping ratios. The next step is to reconstruct the system characteristic matrix from the obtained eigenvalues, which is the so-called inverse eigenvalues problem. As the system matrix certainly exists in this case, and its form is known from the modelling, a numerical solution is developed to estimate the mass-spring parameters in the vehicle model.

7.2.3. Procedure of the drop test

The test to obtain the dynamic response of the test vehicle is straightforward: the vehicle free decay responses are stimulated by simultaneously dropping a particular group of the vehicle tires from blocks to flat ground, according to different motion-modes, as shown in Figure 7.3. Theoretically, we can stimulate the vehicle in such a way that its response contains all of four motion-modes; however, when processing the data, the noise mode may overwhelm the four motion-modes. To enlarge the signal-noise ratio, both bounce and roll tests are performed separately to obtain more accurate results. For instance, the vehicle roll mode can be stimulated by rolling one side of the tires off the blocks together and the bounce mode can be stimulated by rolling four tires off the blocks together.

The vehicle's free decay responses are obtained by accelerometers mounted on the strong point of the vehicle chassis, away from the engine and flexible structures. Several potential locations are indicated in Figure 7.4.

Figure 7.3. The test vehicle upon blocks.

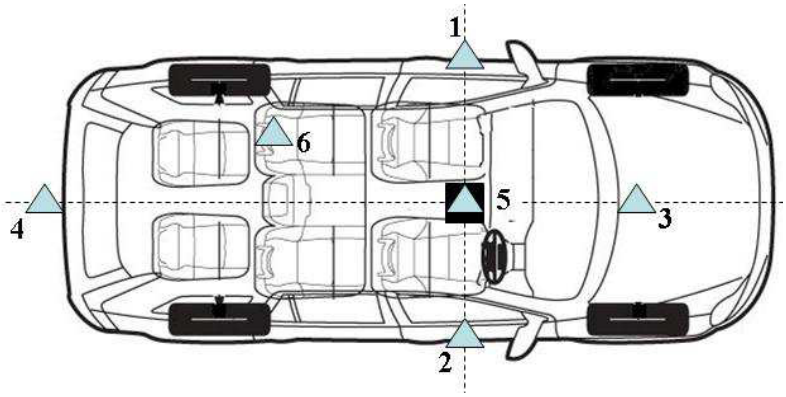

Figure 7.4. The diagram of accelerometer location.

Figure 7.4 shows several possible locations for accelerometers on the vehicle chassis. Location 6 is sensitive to all vehicle body modes but in practice we found none of the modes can be highlighted properly in this location. Better results can be obtained by locating sensors to the position which is sensitive to a particular mode, e.g., location 5, the centre of the gravity for bounce test, location 1 and 2 for roll test. Vehicle roll

angular acceleration is calculated by the accelerations measured from these two locations.

7.2.4. Modal parameter estimation

The anti-roll bar has been taken off from the test vehicle. The vertical acceleration and angular acceleration of the vehicle body in both time and frequency domain are presented in Figure 7.5 and Figure 7.6, representatively. The angular acceleration is calculated from the vertical acceleration of the left and right side of the vehicle chassis.

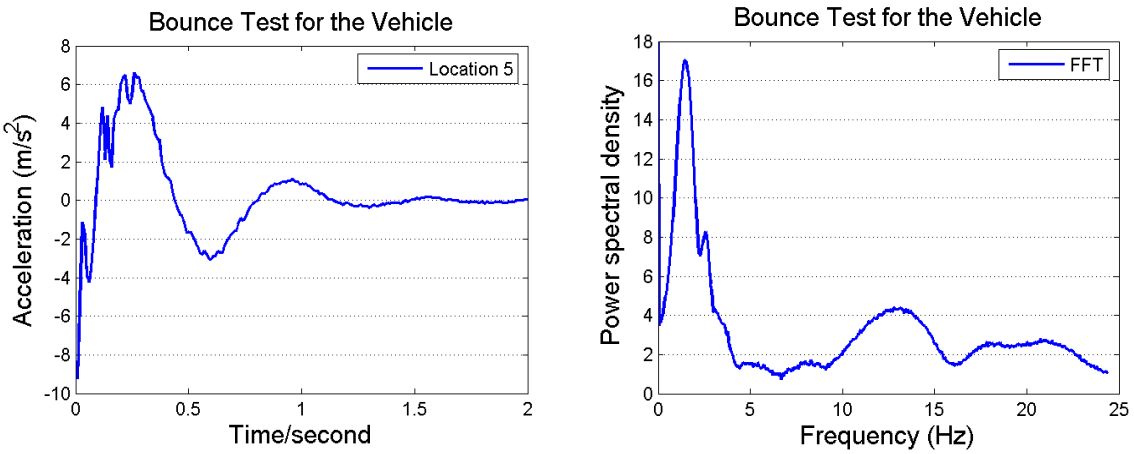

(a) (b)

Figure 7.5. Bounce test -- sprung mass acceleration in (a) *time domain*; and (b) *frequency domain*.

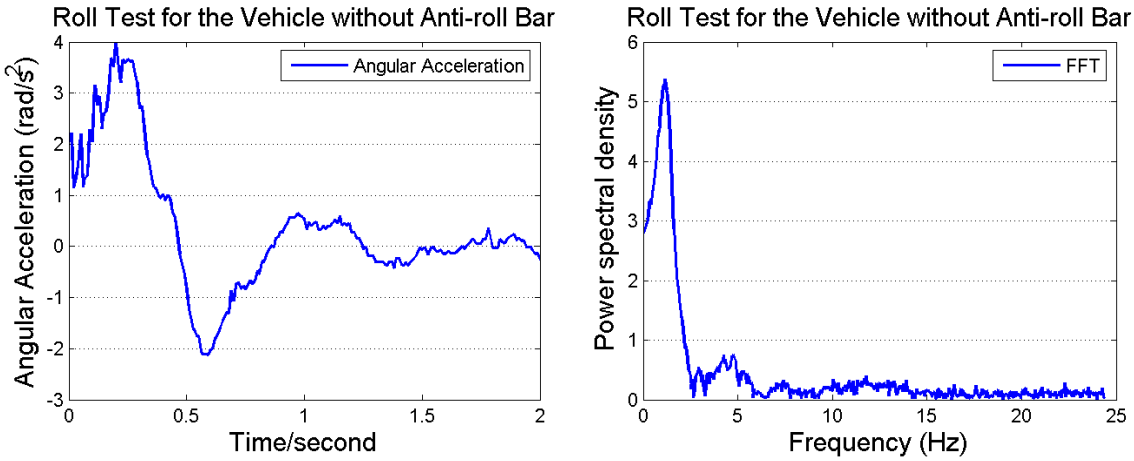

(a) (b)

Figure 7.6. Roll test -- sprung mass angular acceleration in (a) *time domain*; and (b) *frequency domain*.

The acceleration signal is a single-channel data in the discrete time domain. In the SVM method, this single-channel data is reconstructed into a data string with eight arrays to cover the four DOF of the roll-plane model, and the system transition matrix of eight dimension can be determined from this data string by taking advantage of the least squares method. After solving its eigenvalues problem, we can obtain four pairs of modal parameters, in terms of damped frequencies ω_d, natural frequencies ω_n, and damping ratios ζ. The SVM estimation results are presented in Table 7.2.

Table 7.2. Estimated modal parameters of the vehicle.

	FFT ω_d (Hz)	SVM ω_d (Hz)	Error ε (%)	SVM ω_n (Hz)	SVM ζ
Sprung mass bounce	1.465	1.420	3.1%	1.469	0.2548
Sprung mass roll	1.172	1.189	1.4%	1.245	0.2991
Unsprung mass 1&2	13.09	13.79	5.3%	13.81	0.0595

In Table 7.2, ω_d is the damped natural frequency. It can be obtained through both FFT and SVM methods. The difference between the estimation results of those two methods is defined as ε in percentage. From the table we can see the errors are small. ω_n and ζ refer to the natural frequencies and the damping ratios of the four motion-modes of the test vehicle. Then we can solve the inverse problem to estimate the physical parameters of the vehicle from its modal parameters.

7.2.5. Physical parameter estimation

The statement of inverse eigenvalues problem is: given a list of a set of complex numbers $\lambda = \{\lambda_1, \lambda_2, \lambda_3, \lambda_4\}$, finding a 4x4 matrix with eigenvalues λ. From the mathematical perspective, the inverse eigenvalues problem has been a challenging research problem for over half a century and still questions remain [10-11]. However, in this particular application case, the system matrix A_0 certainly exists and its form is known from the modelling. The total weight of the vehicle is also known. Therefore, a numerical approach can be employed to obtain the approximate values of each physical parameters, including the weight distribution of sprung mass and unsprung mass, suspension and tire stiffness. By assuming that the suspension shock absorber is the only damping device in the system, the numerical solution of the damping coefficient of the shock absorber can be obtained as well. The outcomes of the estimation are presented in Table 7.3.

Table 7.3. Estimated physical parameters of the Ford Territory vehicle with the anti-roll bar removed.

Notation	Description	Units	Estimated Values
I	Sprung mass inertia	Kg·m^2	388
m_s	Sprung mass	Kg	900

m_u	Unsprung mass	Kg	40
k_s	Suspension stiffness	N/m	44e3
m_s	Suspension damping coefficient	N s/m	2.5e3
k_t	Tire stiffness	N/m	270e3
k_{tr}	Torsional spring stiffness	Nm/rad	0

To verify the parameter estimation approach, the test results are compared with the simulation results of the mathematical modelling. By using the above estimated parameters, the simulation results match the measured response of the vehicle well in both bounce and roll tests. The agreements between the simulation and the tests are shown in Figure 7.7.

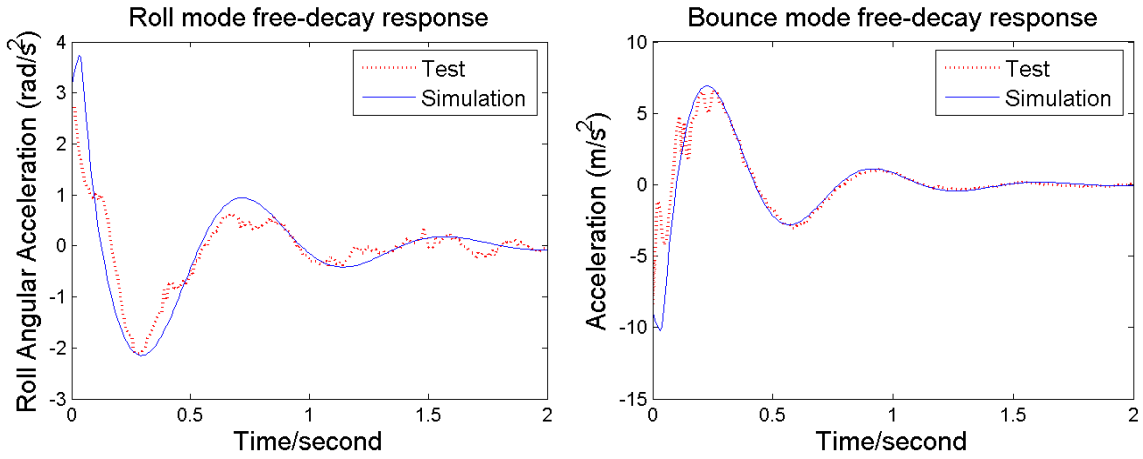

(a) (b)

Figure 7.7. Simulations and test results of vehicle roll (a) and bounce (b).

In simulation, the free decay responses of the vehicle are stimulated by the force impulses to a certain group of tires, to represent the experiment conducted in Figure 7.3. The red dotted line in Figure 7.7(a) is the angular acceleration of vehicle body from the test, while the blue solid line represents the simulation results. Figure 7.7(b) is

the free decay response of the vehicle body in its bounce mode; the dotted line is the acceleration at the vehicle centre of gravity from the test, and the solid line is the simulation result. The agreements between the simulation and the tests are good and it verifies the proposed method of vehicle modelling and parameter estimation.

The major advantage of the proposed estimation method is that it does not require any special testing facility. Thus it can be easily applied to various applications, e.g., vehicle flaw detection, vehicle condition evaluation and comparison after modification. Another advantage of this method is that its errors are limited from the system level. The estimating error of each individual component does not add up but rather cancel out after assembled together, because the estimation process is conducted from the modal analysis perspective in the full-car level. The limitation of this method is that the estimated property of each component may not be high enough for some applications where the degree of accuracy is critical, such as the component design.

7.2.6. Estimation of roll stiffness of the passive HIS system

By using the parameter estimation method, different anti-roll systems can be compared for their equivalent roll stiffness through a set of drop tests. The standard anti-roll bars and the passive HIS system are in turn installed in the test vehicle and tested under the same conditions. The processed data are shown in Figure 7.8 to Figure 7.10. The roll stiffness of the HIS depends on the pre-set system pressure. Therefore, the 20-bar HIS and 30-bar HIS are tested separately for comparison.

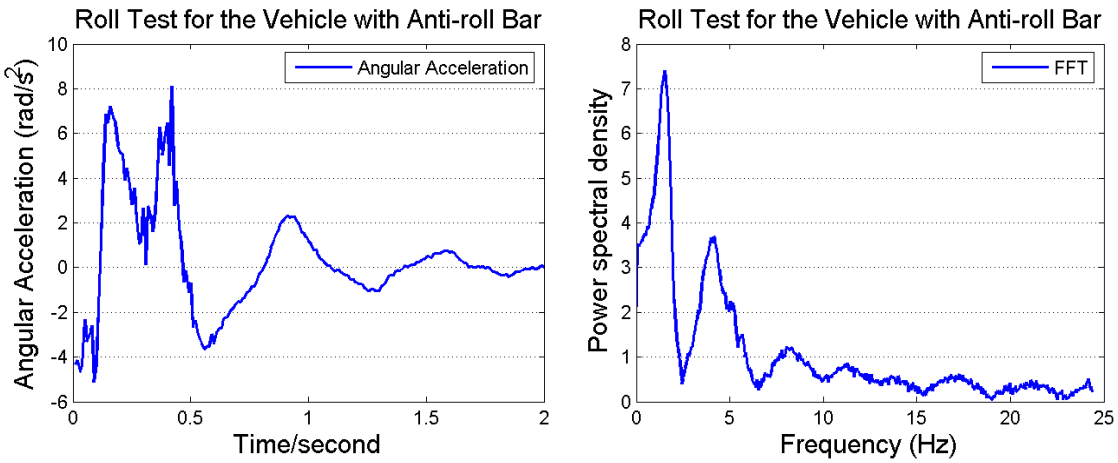

(a) (b)

Figure 7.8. Roll angular acceleration of the anti-roll bar test: (a) *time domain result*; and (b) *FFT results*.

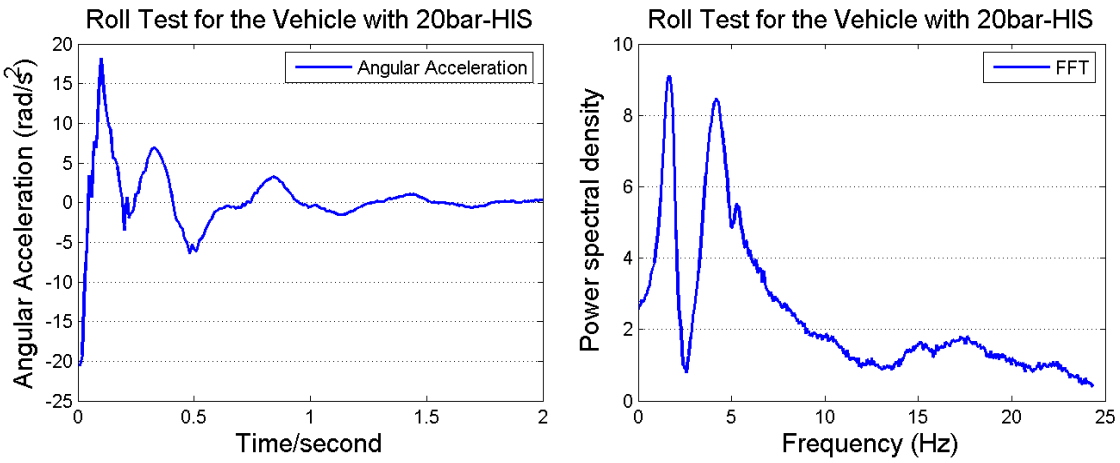

(a) (b)

Figure 7.9. Roll angular acceleration of the 20-bar HIS test: (a) *time domain result*; and (b) *FFT results*.

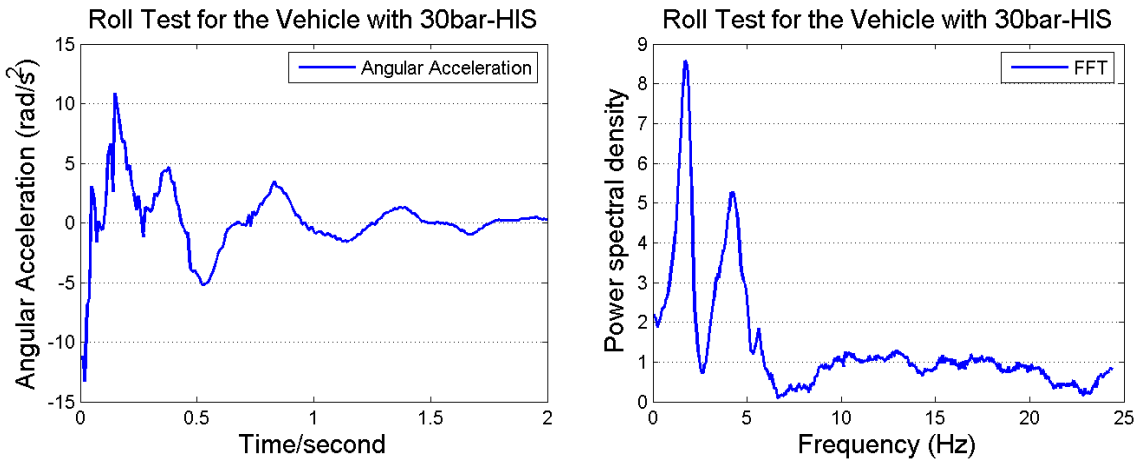

(a) (b)

Figure 7.10. Roll angular acceleration of the 30-bar HIS test: (a) *time domain result*; and (b) *FFT results*.

Table 7.4. Modal parameters of the vehicle with different anti-roll systems.

	FFT ω_d (Hz)	SVM ω_d (Hz)	Error ε (%)	SVM ω_n (Hz)
Vehicle	1.1719	1.1885	1.2455	0.2991
V Anti-roll bar	1.5140	1.5999	1.6221	0.1648
V 20bar HIS	1.6620	1.7221	1.7465	0.1666
V 30bar HIS	1.7090	1.7472	1.8157	0.143

By comparing the updated vehicle modal parameters in Table 7.4 with the benchmark data in Table 7.2, we can see that by adding different anti-roll means (anti-roll bar, 20-bar HIS, 30-bar HIS), the vehicle's modal parameters have changed as expected. The effects of these systems are also shown in terms of the increased vehicle natural frequency and decreased damping ratio. The estimated equivalent roll stiffness and suspension damping coefficient are provided in Table 7.5.

Table 7.5. Estimated equivalent roll stiffness and suspension damping coefficient.

	k_{roll} (kNm/rad)	k_{tr} (kNm/rad)	Δk_{roll} (%)	c_s (Ns/m)	Δc_s (%)
Vehicle	23.74	0	0%	2507	0%
V Anti-roll bar	40.26	16.5	69.6%	1970	-21.2%
V 20bar HIS	46.67	22.9	96.6%	2144	-14.2%
V 30bar HIS	50.45	26.7	112%	1913	-23.6%

The installation of anti-roll systems increased the vehicle's equivalent roll stiffness. In Table 7.5, k_{roll} represents the vehicle overall equivalent roll stiffness; k_{tr} represents the increased equivalent vehicle roll stiffness; Δk_{roll} shows the increased percentage; c_s is the calculated shock absorber damping coefficient; and Δc_s is the change of c_s. The anti-roll bar increases the roll stiffness by 69.6%; the 20-bar HIS increases it by 96.6%; and the 30-bar HIS is 112%. The increased roll stiffness enhances the vehicle handling performance and improves cornering safety.

Shock absorber has nonlinear characteristic and the measured damping coefficient decreases when shock absorber travels less. The anti-roll systems increase the whole vehicle roll stiffness, thus under the same test condition the vehicle body travels less, and therefore the calculated damping coefficient has a trend to decrease.

To summarise, three advantages of the passive HIS systems stand out. The first is that its roll stiffness can be adjusted by changing the working pressure of the hydraulic system. The second is that the damping of the HIS system can be controlled conveniently by installing damper valves. The last one is that the HIS does not affect

the wheel-ground contact capability in the articulation mode, which will be further explained in the following session.

7.3 Passive HIS field test

Field tests and rig tests are provided in additional to previous tests to investigate the handling and ride comfort of the test vehicle with the passive HIS system. The model employed in this study includes a 9-DOF full-car model and a 34-DOF HIS model, which are dynamically coupled together through boundary conditions. To validate the model and to further enhance understanding of the passive HIS in practice, companionable experiments have been carried out and the test results are presented in the session.

A set of slalom and fishhook manoeuvre tests is conducted on a smooth road to evaluate the handling performance of the HIS system by comparing a vehicle fitted with: 1) no anti-roll system (benchmark); 2) the HIS system; and 3) anti-roll bars.

7.3.1.Anti-roll bar in vehicle handling

Vehicle roll mode needs to be sufficiently stiff in order to possess good handling and road safety. To stiffen roll mode whilst maintaining a soft bounce mode for ride comfort, it is necessary to employ anti-roll systems in additional to spring-damper systems in suspension design. For example, the anti-roll bar, a mechanically interconnected system, is widely accepted as a standard configuration on today's road vehicles. The employment of stiff anti-roll bars can suppress a vehicle's roll angle to some extent and improve the roll stability at the cost of reduced ride comfort [108, 109], particularly on rough roads. The anti-roll bar transmits the force of one wheel to the other because it connects wheels on the opposite sides of the vehicle together.

During very hard cornering, this mechanism causes the lateral load transfer to the outer tires and may cause the inside wheels to lift off the ground. Stiffer front anti-roll bars may cause the static understeer margin to become more negative and lead to over steering, which is undesirable. Moreover, since the anti-roll bars cannot provide sufficient damping to match the increased stiffness in vehicle roll motion-mode, there is a limitation to the stiffness that the anti-roll bars can provide. To address this matter, active anti-roll bars have been proposed which can help to realise a better functionality, but at the cost of complexity and weight [46, 71].

Furthermore, anti-roll bars are not uncoupled in all four motion-modes and thus bring effects to other motion-modes. For instance, anti-roll bars will undesirably stiffen the articulation motion-mode. This is because a stiff articulation motion-mode has negative effects on a vehicle during the passage over uneven surfaces. The stiff articulation motion-mode will increase the torsional torque applied onto the vehicle chassis, as a large torsional torque may even bring damage to the chassis, and can also limit the wheels' tire-ground contact ability and affect handling.

Sport utility vehicles (SUV) are designed to allow the passage over uneven terrains in off-road driving and commonly have a higher centre of gravity (CG). Due to their high CG, they are more susceptible to body roll motion during sharp cornering. Hence, the stiff anti-roll bars are conventionally considered indispensable for SUVs, despite the fact that anti-roll bars undesirably stiffen the articulation mode and compromise the off-road passage capability. To be specific, during a rough-road drive, the anti-roll bars bring large torsional torque to the vehicle body/chassis, and due to the unevenly distributed vehicle weight across four wheels, one wheel may lift up. Therefore, during an off-road drive, some designs disengage the vehicle's anti-roll bars to soften the articulation mode, but at the cost of compromising the anti-roll ability, e.g. Kinetic Dynamic Suspension System (KDSS).

In contrast, as a potential replacement of anti-roll bars, the HIS system can provide the desired roll stiffness during cornering without stiffening the articulation mode and thereby enhancing a vehicle's ability over various surfaces and speeds. This is particularly meaningful for SUVs and military vehicles, which require high handling performance as well as decent capability on uneven surfaces. In this session, a set of manoeuvre tests on the road have been conducted to investigate the effectiveness of the HIS system on different aspects of vehicle dynamics, including roll stability, lateral and vertical dynamics. Moreover, a set of articulation tests has been conducted on a four-poster test rig to study and compare the HIS system and anti-roll bars in the articulation mode. Test data are collected from three cases for comparison, where a car is fitted with: (a) nothing but spring-damper suspension, (b) standard anti-roll bars, and (c) an HIS.

7.3.2.Modelling of vehicle and HIS

The design and implementation of the HIS system please refer to the MHIS test rig in chapter 6. A brief description of the HIS is provided here in order to give a complete background of the system dynamics. A lumped-mass 9-DOF full-car model, as shown in Figure 7.11, is employed in this study. The sprung mass is considered to have 5 DOF (bounce, roll, pitch, yaw and lateral) and each of the unsprung masses has only 1 DOF in vertical direction. The vehicle suspension system consists of conventional suspension (spring and damper), and a typical anti-roll HIS system. The Magic-Formula tire model is used to calculate the tyre/ground contact forces [81]. The set of parameters presented in Table 7.6 has been estimated from the vehicle's dynamic response from a large-motion drop test through modal analysis method [110]. Therefore, the produced simulation results are in good agreement with the test results, particularly in larger motions.

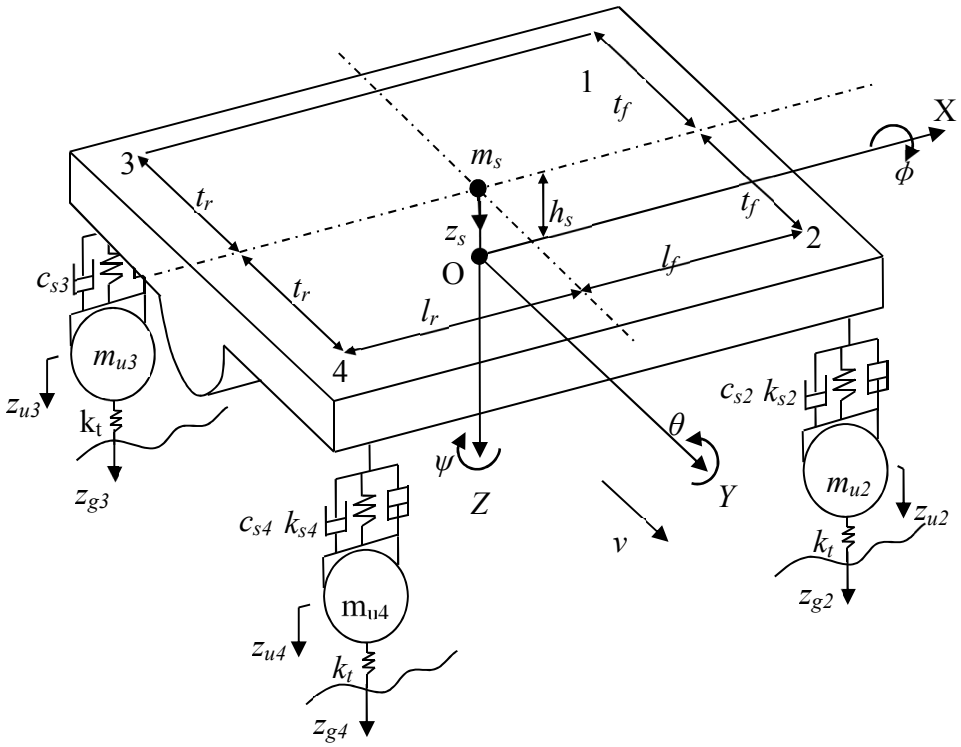

Figure 7.11. Schematic diagram of a car with an HIS.

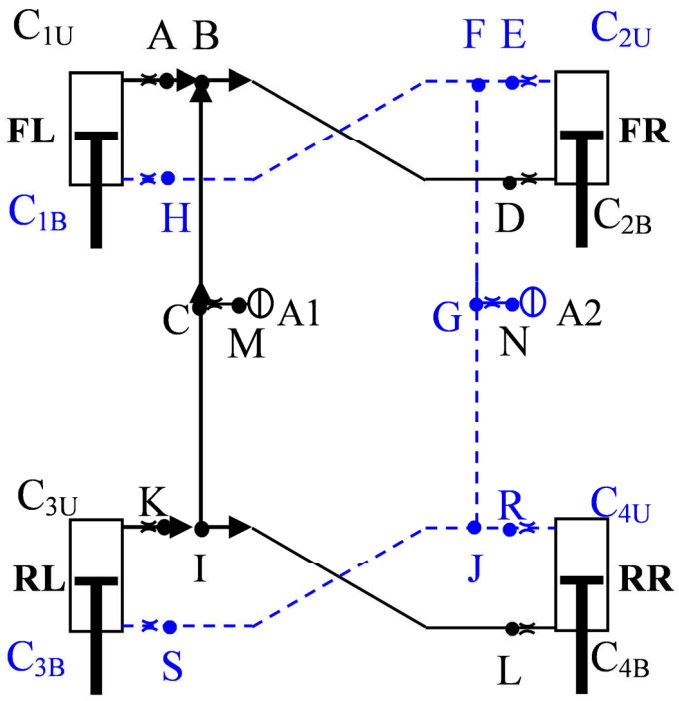

Figure 7.12. Schematic diagram of the HIS.

Table 7.6. Properties of the 9-DOF mechanical multi-body subsystem.

Symbol	Value	Units	Description
m_s, m_{ui}	2000/40	kg	Sprung / unsprung mass (i =1, 2, 3, 4)
I_ϕ	780	kg m^2	Sprung mass moment of inertia about the x-axis
I_θ,	3800	kg·m^2	Sprung mass moment of inertia about the y-axis
I_ψ	4050	kg·m^2	Sprung mass moment of inertia about the z-axis
l_f	1.37	m	Distance from sprung mass CG to the front axle
l_r	1.48	m	Distance from sprung mass CG to the rear axle
t_f, t_r	0.575	m	Half axle width at the front/rear of the vehicle
h_s	0.33	m	Height of sprung mass CG above the roll axis
h_{ra}	0.3	m	Height of roll axis above ground
k_{si}	40	kN·m^{-1}	Suspension spring stiffness (i =1, 2)
k_{si}	46.5	kN·m^{-1}	Suspension spring stiffness (i =3, 4)
k_t	270	kN·m^{-1}	Tire spring stiffness
c_{si}	2500	Ns·m^{-1}	Suspension damping coefficient (i =1, 2, 3, 4)

The installed HIS system for this application consists of two identical hydraulic circuits, as shown in Figure 7.12. The two hydraulic circuits are coupled with each other kinetically via four identical double acting cylinders. The dynamic interaction between the hydraulic system and the sprung and unsprung masses can be described as such: relative velocities in the suspension struts cause changes in pressure in both circuits, which lead to changes in suspension strut forces through all four cylinders. As a result, vehicle body and wheel motions occur, which, in turn, affect the hydraulic system. This mechanic-hydraulic interaction will continue until the system reaches a new equilibrium.

The derivation of motion equations of the combined vehicle multi-body system and hydraulic circuits for transient analysis can be found in [57]. Here the governing equations for hydraulic elements are briefly presented to illustrate the modelling method.

7.3.3.Fluidical component modelling

Accumulator - As shown in Figure 7.12, the HIS system features gas-pressurized hydraulic accumulators which provide roll-plan stiffness to the vehicle and also reduce shock pressure loading due to system inputs. The accumulator consists of a pressure housing divided into two chambers by an elastomeric diaphragm. One chamber is filled with gas and the other with hydraulic fluid. The accumulator is modelled by assuming an adiabatic process.

$$P_a V_a^r = P_p V_p^r = const \tag{7.6}$$

where P_a and V_a are the pressure and volume at any time in the accumulator, respectively, while P_p and V_p refer to the pre-charge values. The adiabatic gas law is used to model the accumulator pressure as a function of gas volume at a pre-charged pressure. Taking the partial time derivative of Equation 7.6, noting that the flow into the accumulator Q is given by $Q_a = -\partial V_a / \partial t$, the pressure gradient of the accumulator with respect to time can be written as a nonlinear function of pressure P,

$$\dot{P}_a = \frac{\gamma Q_a P_a}{V_p} \left(\frac{P_a}{P_p} \right)^{1/\gamma} \tag{7.7}$$

Pipelines - A lumped parameter model is developed by dividing the fluid pipelines into several elements. Each fluid pipeline of constant diameter is handled as one element. The mean pressure and mean flow in each element is assumed as an arithmetic mean of the pressure and flow rate at both ends of the pipe. Assuming the

pressure losses due to viscosity are proportional to the mean flow rate, the momentum equation can be written as

$$\frac{\rho l_i}{A_i}\dot{Q}_i = (P_{i1} - P_{i2}) - R_i l_i Q_i \tag{7.8}$$

where the viscous loss $R_i = 8\pi\rho / A_i^2$, ρ is the fluid density, l_i the pipe length, and A_i the pipe cross-sectional area. The continuity equation for the pipeline is written as

$$\dot{P}_i = \frac{\beta(p)}{V_i}(Q_{i1} - Q_{i2}) \tag{7.9}$$

where $\beta(p)$, the bulk modulus, is expressed as a function of mean pressure p. The mean pressure and mean flow rate of the pipe element are given as the arithmetic mean at both ends of the element, shown in the following equation

$$P_i = \frac{1}{2}(P_{i1} + P_{i2}) \text{ and } Q_i = \frac{1}{2}(Q_{i1} + Q_{i2}) \tag{7.10}$$

It is noted that piping equations apply to each pipe element. Substitution of these equations results in one coupled first order differential equation governing the pressures at defined nodal points of the suspension fluid circuits.

7.3.4.State space equations

The description of the assembled dynamic model in state space form is provided here. The notation list is provided in the appendix. The state vector that describes the motion of the sprung and unsprung lumped multi-body subsystem is defined as

$$X_M = \begin{bmatrix} Z^T & \dot{Z}^T \end{bmatrix}^T \tag{7.11}$$

where $Z = \begin{bmatrix} v & z_s & z_{u1} & z_{u2} & z_{u3} & z_{u4} & \varphi & \theta & \psi \end{bmatrix}^T$

The state vector that describes the dynamic states of the hydraulic subsystem is defined as

$$X_H = \begin{bmatrix} p_U^{C1} & p_A^{AB} & p_B^{AB} & q_B^{AB} & p_M^{A1} & p_C^{BC} & q_C^{BC} & q_C^{CI} & p_I^{CI} & q_I^{CI} & q_I^{IL} & p_L^{IL} & p_B^{C4} & p_U^{C2} & p_E^{EF} & p_F^{EF} & q_F^{EF} \cdots \\ p_N^{A2} & p_G^{FG} & q_G^{FG} & q_G^{GJ} & p_J^{GJ} & q_J^{GJ} & q_J^{JS} & p_S^{JS} & p_B^{C3} & p_D^{CD} & p_B^{C2} & p_U^{C3} & p_K^{KI} & p_H^{GH} & p_B^{C1} & p_U^{C4} & p_R^{RJ} \end{bmatrix}^T$$

.

Combining the vehicle subsystem vector (18 elements) and hydraulic subsystem vector (34 elements) gives the system vector of a vehicle fitted with an HIS:

$$X = \begin{bmatrix} X_M^T & X_H^T \end{bmatrix}^T \qquad (18+34=52 \text{ elements})$$

By using free body diagram approach and applying Newton's second law, the full car system state space equation is derived as

$$T\dot{X} = SX + F \tag{7.12}$$

which can be further written as

$$\begin{bmatrix} I & 0 & 0 \\ 0 & M & 0 \\ 0 & 0 & T_H \end{bmatrix} \begin{bmatrix} \dot{Z} \\ \ddot{Z} \\ \dot{X}_H \end{bmatrix} = \begin{bmatrix} 0 & I & 0 \\ -K & -C & S_{H2M} \\ 0 & 0 & S_H \end{bmatrix} \begin{bmatrix} Z \\ \dot{Z} \\ X_H \end{bmatrix} + \begin{bmatrix} 0 \\ F_m \\ F_h \end{bmatrix} \tag{7.13}$$

where M, K, C are the mass, stiffness and damping coefficient matrices respectively; T_H and S_H are the coefficient matrices determining the hydraulic dynamics of the HIS system. S_{H2M} is the coupling matrix which conveys hydraulic forces to the lumped mechanical system. F_m contains the external excitation from the ground and some nonlinear components of the 9-DOF vehicle model which cannot be included in T or S matrices. F_h is another coupling matrix which converts mechanical disturbance (relative displacement and velocity between chassis and wheels) to hydraulic system inputs for HIS sub-model. Due to the nonlinear characteristics of this coupling, F_h is included in the right hand side to keep the equation formatting clear.

7.3.5.Slalom manoeuvre field test

The slalom test is performed by driving test vehicles around a series of traffic cones which are placed 10 m apart, at a vehicle speed of 30 km/h. To obtain a lateral acceleration that is sufficiently large, and also to ensure the safety of the test driver, a testing plan of having larger steering angle at lower speed is strategically adopted. The lateral acceleration measured from these tests reached 0.7 g which is sufficient according to the literature, where most vehicles tested for handling evaluation experience a lateral acceleration up to 0.8 g [24, 25].

Test data are collected from three cases when a car is fitted with: (a) only spring-damper suspension, (b) standard anti-roll bars, and (c) HIS. Cases (a) and (c) are performed on the experimental vehicle. Case (b) is performed on another vehicle fitted with anti-roll bars, referred to as the standard vehicle, shown in Figure 7.13. These two vehicles are assumed identical in dynamic parameters. These scenarios are named as following: the experiment vehicle fitted with spring-damper suspension only is referred to as the "Spring-damper car", the same experimental vehicle fitted with the HIS system pre-charged with 40 bar pressure is referred to as the "HIS car", and the standard vehicle with anti-roll bars is referred to as the "Anti-roll-bar car". The vehicles are driven by the same driver through the same path at the same speed. To validate the obtained results, each test is conducted twice to ensure repeatability; in addition to this, verification tests at different vehicle speeds are also conducted to check the consistency of the findings.

(a) (b) (c)

Figure 7.13. Vehicle fitted with: (a) *only spring-damper suspension*; (b) *anti-roll bars*; and (c) *HIS*.

The data acquisition system consists of a LabJack data acquisition board, a laptop running Labview, and a number of transducers, including four accelerometers, four linear displacement transducers and two pressure transducers. Two accelerometers are installed underneath the storage box between the two front seats, which is at the CG (centre of gravity) of the vehicle, to measure the lateral and longitude acceleration, respectively. The other two accelerometers are installed onto the left and right chassis edges in the roll plane that crosses the CG point, to measure vertical acceleration. The linear displacement transducers, mounted besides the coil-spring in each wheel station, measure the relative motions between vehicle body and wheels, defined as suspension deflection. Two pressure sensors are installed at point K and R, to monitor the hydraulic system response, as shown in Figure 7.12. The steering wheel angle and vehicle speed from the experiment are used as inputs to the HIS-vehicle model for drive event re-construction. Figure 7.14 shows the testing and analysing process.

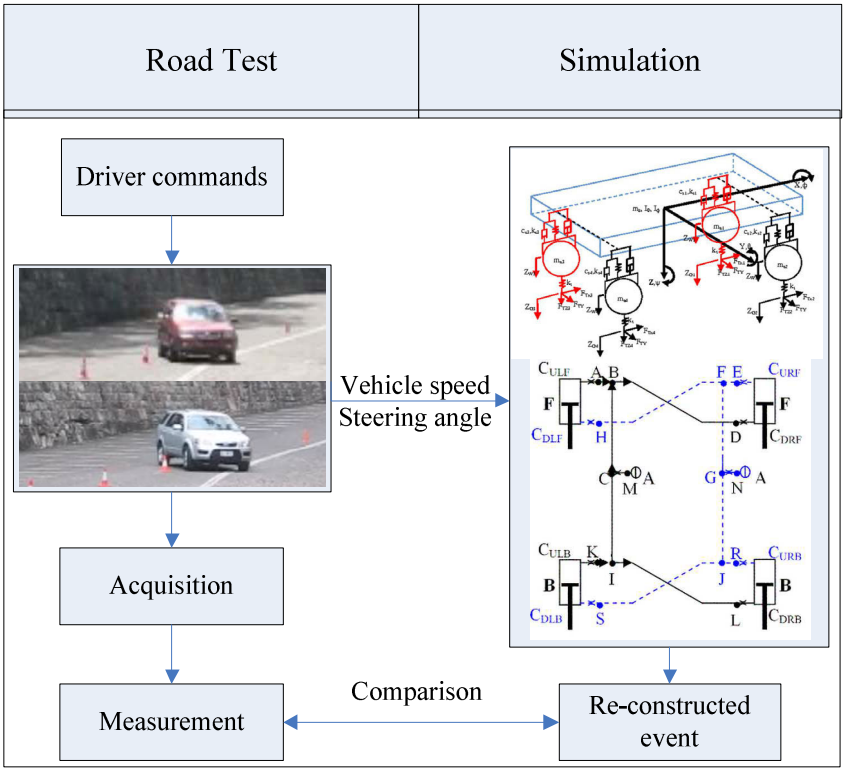

Figure 7.14. Test-Simulation interactive configuration.

Steering input

The handling manoeuvres are executed by the human driver and therefore deviations in the steering input for different tests are expected. The steering inputs for three tests are presented in Figure 7.15 as a reference for assessing the resulting vehicle dynamics.

In the case of the HIS car, the drive event re-construction is performed on computer to verify the dynamic model. The obtained vehicle speed and steering wheel input are used as input to the simulation. In Figure 7.16, the comparison of the simulation and the test result of the HIS car lateral acceleration shows good agreement between the two and confirms that the developed vehicle-HIS model captures the major features of the real vehicle dynamic characteristics in the lateral direction. In addition, the comparison of HIS hydraulic responses from the simulation and the test is presented in the following sections.

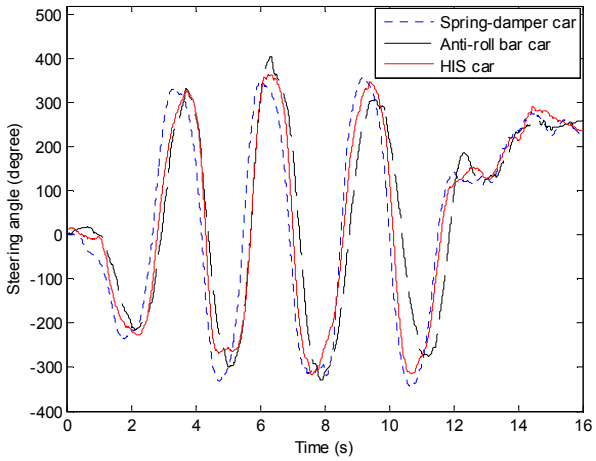

Figure 7.15. Steering wheel input for three tests.

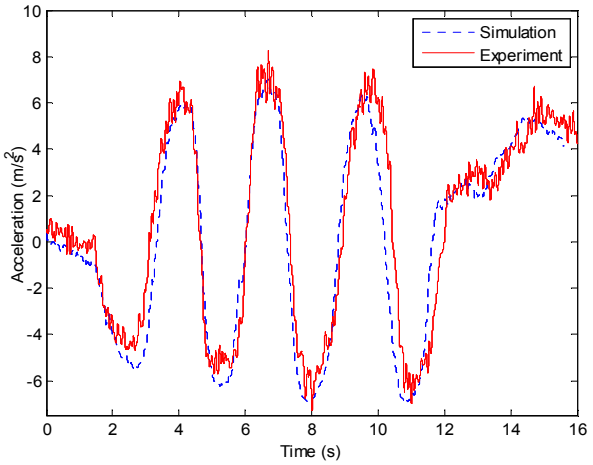

Figure 7.16. Lateral acceleration comparison of test result and simulation of the HIS car.

Vehicle lateral dynamics

The lateral motion is important to vehicle stability control. Once the centrifugal force during cornering exceeds the friction force that the vehicle's tire/ground contact can generate, sliding and yaw motions occur. The lateral acceleration data obtained from the three individual tests are presented into two pairs of comparison graphs, shown in Figure 7.17(a-b).

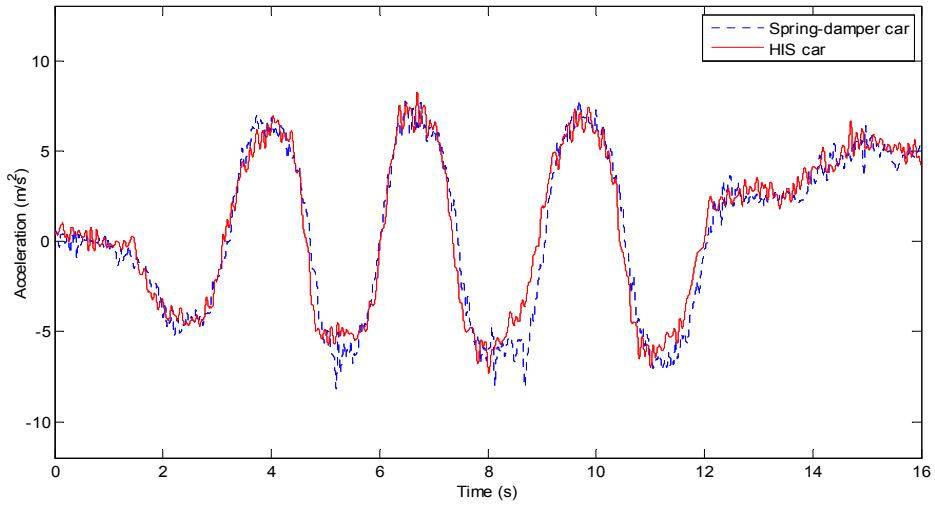

(a)

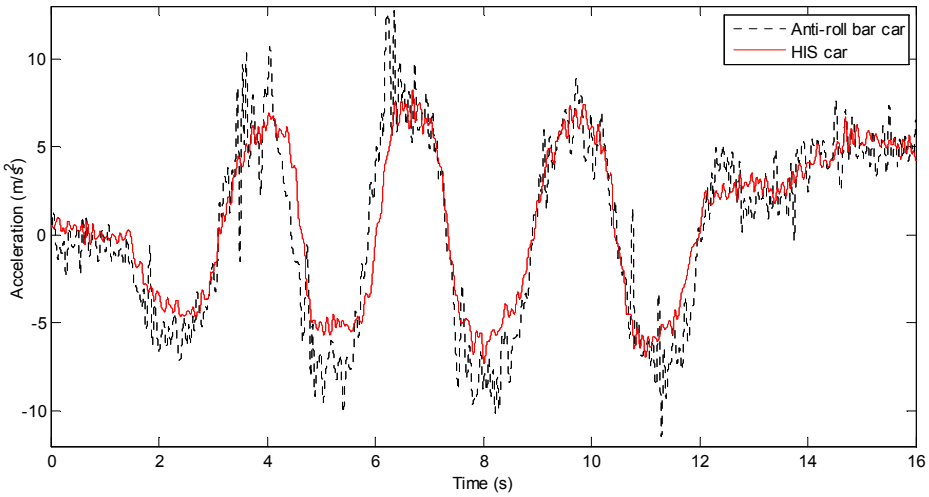

(b)

Figure 7.17. Comparison of Lateral acceleration: (a) *HIS car and Spring-damper car*; and (b) *HIS car and Anti-roll-bar car.*

Figure 7.17(a) provides the lateral acceleration comparison of the Spring-damper car and the HIS car, the responses of which approximately overlap each other. In contrast, in Figure 7.17(b), the comparison of the Spring-damper car and the Anti-roll-bar car shows the Anti-roll-bar car experiences larger oscillations around the peak value. Overall, the lateral acceleration range of the HIS car, [-7.19 8.21] m/s^2, is 36.13% less than that of the Anti-roll-bar car, [-11.40, 12.71] m/s^2. The oscillations of the lateral

acceleration signal in the three cases are compared in the frequency domain in Figure 7.18.

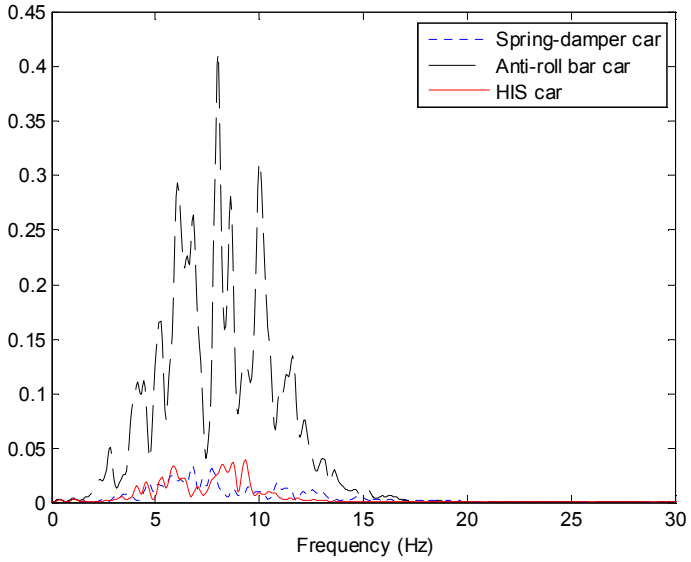

Figure 7.18. Comparison of vehicle CG lateral acceleration of three cases in frequency domain: *Spring-damper car*; *HIS car and Anti-roll-bar car*.

Vehicle lateral motion is governed by the vehicle's lateral friction forces which are generated from wheel/ground contact points. At given driving and road conditions, the friction forces are limited by tire normal forces. Therefore, the oscillation observed in the lateral acceleration measurement suggests that the tire normal forces are fluctuating, in which the suspension system has an important role to play. Since this oscillation is not observed from the Spring-damper car and the HIS car, the author suspects it is the result of the action of anti-roll bars.

Vehicle roll dynamics

In vehicle roll dynamics, the sprung mass roll angle is the direct evidence to evaluate the performance of anti-roll bars and the HIS system. The sprung mass roll angle is calculated from the measured suspension travel and estimated tire deflection, and the

comparison of three cases in the slalom test is presented in Figure 7.19. The Spring-damper car is shown in the dotted blue line, and due to the lack of an anti-roll system, the largest vehicle roll motion is expected in this case. The anti-roll bars suppress sprung mass roll angle by 23.48% from the test data, reducing the peak value from 4.94° to 3.78°, shown in the dashed black line. The HIS system remarkably condenses the roll angle peak down to 1.23°, resulting in a 75.10% improvement compared to the Spring-damper car, shown in the solid red line.

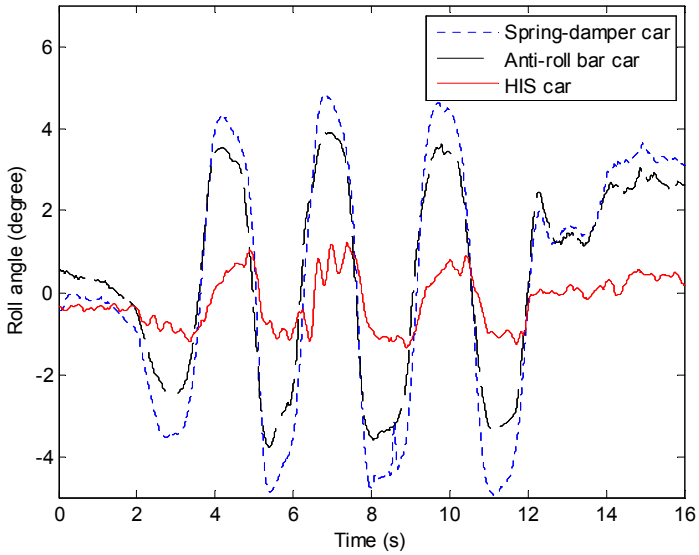

Figure 7.19. Vehicle roll angle in slalom test.

Vehicle vertical dynamics

Ideally, anti-roll systems should not compromise vehicle vertical dynamics, but in reality different anti-roll systems have different effects on bounce mode due to their different mechanisms. The comparison of measured vehicle vertical suspension deflection (the average of left and right side suspension) is presented in Figure 7.20(a). The Spring-damper car and the HIS car show slightly larger sprung mass movement in the vertical direction in comparison with the Anti-roll-bar car, as shown in the period of 6-12 s from the time history. This indicates the HIS system does not bring

restrictions to the sprung mass in the vertical direction and allows it to travel freely as in the Spring-damper car.

Vertical acceleration is another important dynamic aspect for vehicle dynamics evaluation. The comparison of the measured CG acceleration of three cases is presented in Figure 7.20(b). The HIS system reduces the acceleration peaks and thus the HIS car has a lower energy level overall. The root mean squares (RMS) of these data are provided: 0.5234, 0.4192, 0.3551 (m/s2), for Spring-damper car, Anti-roll-bar car, and HIS car, respectively. The HIS car has the lowest vertical acceleration RMS of the three cases.

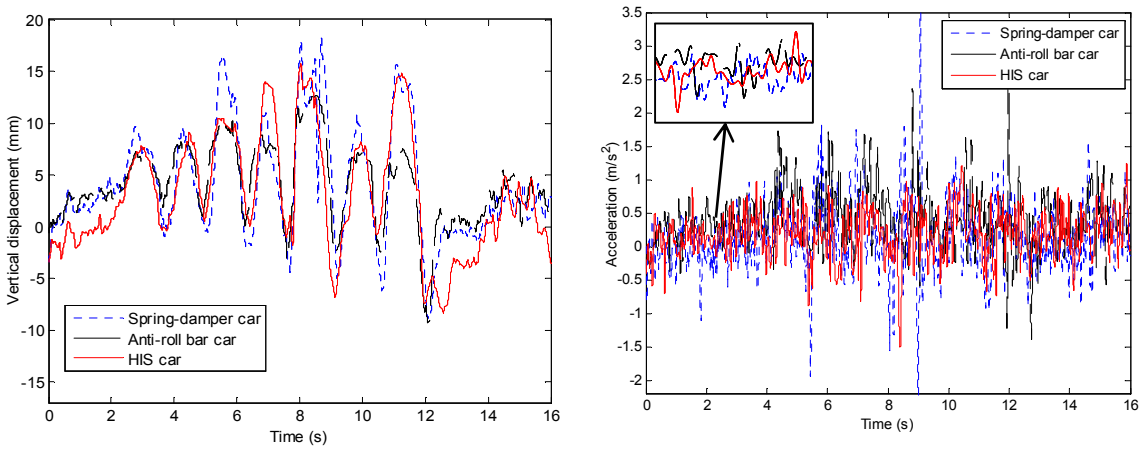

(a) (b)

Figure 7.20. Comparison of vehicle vertical dynamics of three cases at: (a) *the vertical suspension by averaging four suspension deflections*; and (b) *CG vertical acceleration*.

The frequency domain comparison of the CG acceleration from three cases is provided in two pairs of comparison. In Figure 7.21(a), the HIS car shows a lower energy level than the Spring-damper car overall, particularly in the frequency range of 1-3 Hz and 4-8 Hz. The former refers to the car body motion's roll, heave, and pitch natural frequency and the latter corresponds to human sensitive frequency range. The reason is that due to the fluid viscosity, the HIS system adds some damping effect to the bounce

mode and absorbs the vibration energy in a vertical direction. Other tests we performed suggest that this damping effect increases with the HIS system working pressure. The comparison of the Anti-roll-bar car and the HIS car in Figure 7.21(b) shows the HIS car has a lower energy intensity.

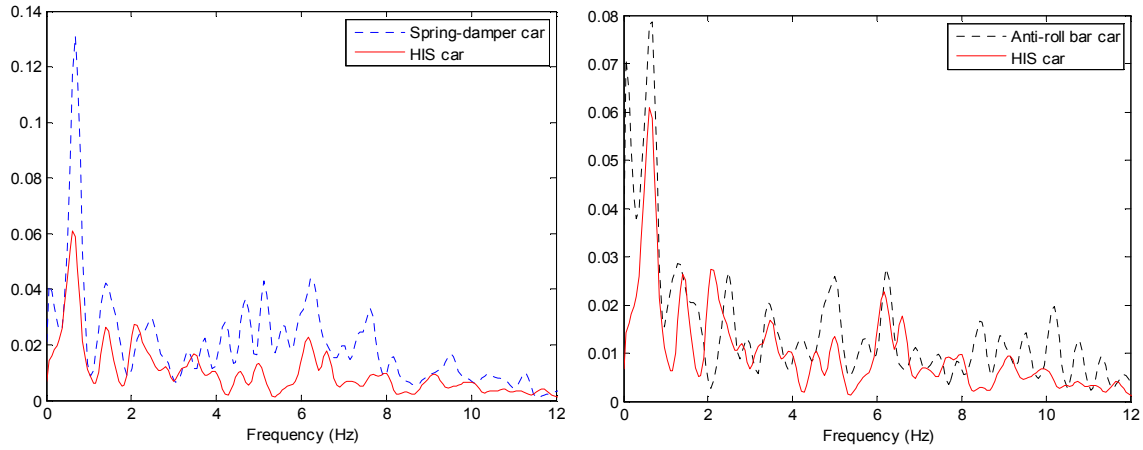

(a) (b)

Figure 7.21. Comparison of vehicle CG vertical acceleration of three cases in frequency domain: (a) *HIS car and Spring-damper car*; and (b) *HIS car and Anti-roll-bar car*.

Overall in the vertical dynamics (bounce mode), the test data comparison shows that the Anti-roll-bar car has a less vertical sprung mass displacement but larger CG acceleration RMS value than the HIS car, suggesting that the anti-roll bars restrain the sprung mass in a vertical direction while the HIS system adds damping into the bounce mode during cornering.

Hydraulic system responses

As part of the drive event re-construction, the calculated HIS hydraulic response is provided and compared with the pressure transducer measurement. Figure 7.22 presents the pressure comparison at point K of the HIS system, referring to Figure 7.12. The simulation captures the nonlinearity characteristics of the hydraulic system's response and matches the test data well.

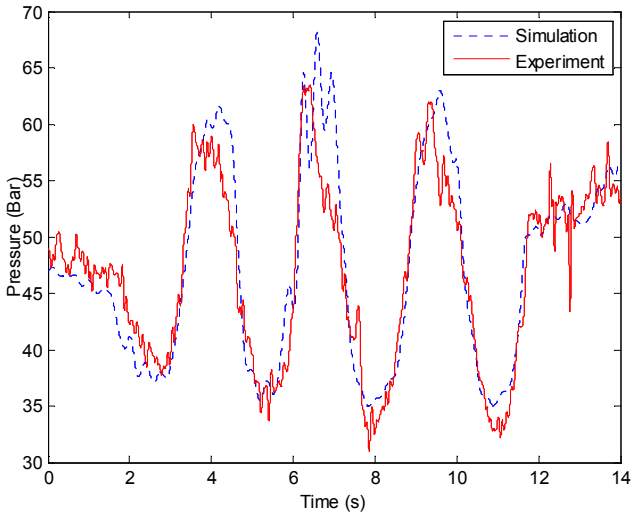

Figure 7.22. Pressure comparison of the HIS system at point K.

7.3.6.Fishhook manoeuvre field test

The set of comparison tests are repeated on the testing vehicles under the fishhook manoeuvre. The simulated vehicle lateral acceleration is presented in Figure 7.23, compared with the measured lateral acceleration data. The graph shows a good agreement between the simulation and the test.

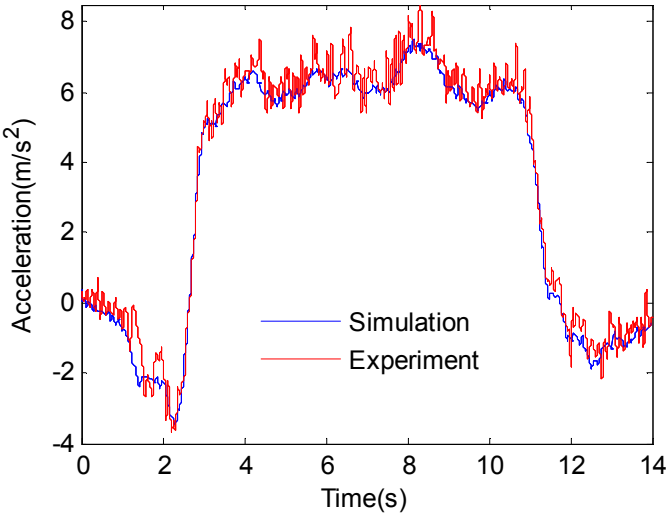

Figure 7.23. Lateral acceleration comparison of test result and simulation of the HIS car.

Vehicle lateral dynamics

The lateral acceleration data obtained from three individual tests are presented in two pairs of comparison graphs in Figure 7.24, respectively.

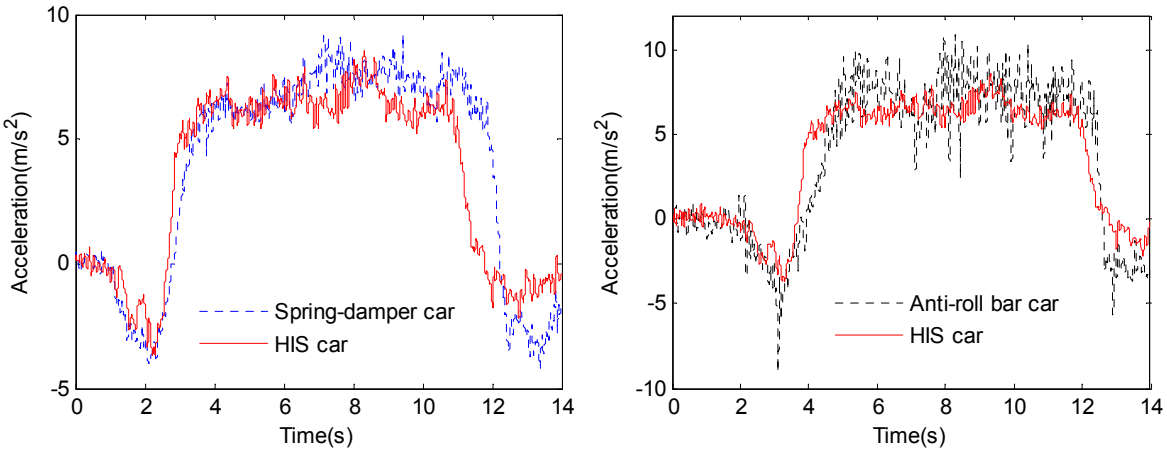

(a) (b)

Figure 7.24. Comparison of Lateral acceleration: (a) *HIS car and Spring-damper car*; and (b) *HIS car and Anti-roll-bar car.*

In Figure 7.24(a), the HIS system is examined against the benchmark case of the conventional spring-damper suspension, where they share a similar appearance in vehicle body lateral acceleration. Figure 7.24(b) presents a comparison of the HIS car and the Anti-roll-bar car. The average values of two curves remain similar but the Anti-roll-bar car experiences larger oscillation around the peak value.

In Figure 7.24(b), the lateral acceleration range of the HIS car is [-3.69, 8.54] m/s^2, but for the Anti-roll-bar car, the range is [-9.09, 10.72] m/s^2, which is 61.96% more. In the same figure, at 3.1 s during the over-correction steering, the resultant lateral acceleration reaches its peak. The HIS car reaches -3.69 m/s^2, while the Anti-roll-bar car soars to a maximum negative value of -9.09 m/s^2, which is 2.46 times of the HIS car. By reducing the peak lateral acceleration, the HIS system has a better chance to

reduce the propensity of vehicle rollover. The findings from the fishhook test are consistent with the result of the Slalom test.

Vehicle roll dynamics

Figure 7.25 compares the performance of the HIS system with anti-roll bars. The Anti-roll-bar car, shown in the dashed black line, is able to suppress vehicle body roll to some extent, thereby reducing the peak roll angle of vehicle body from 5.65° to 4.04°. Overall the reduction ratio is 28.49%. The HIS car, shown in the solid red line, reduces the peak roll angle from 5.65° down to 2.42°, which results in a 57.17% improvement. In this case, the HIS system has approximately doubled the Anti-roll bars' roll reduction performance. The findings from the fishhook test are again consistent with the result of the slalom test.

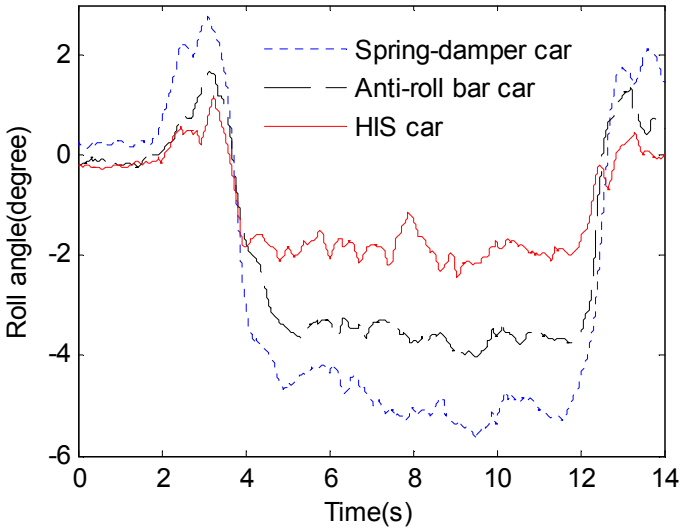

Figure 7.25. Vehicle body roll angle in the fishhook test

Vehicle vertical dynamics

Figure 7.26 shows the body's vertical displacement and acceleration of three cases. The HIS car shows a slightly larger movement of the vehicle body in the vertical direction, and the black dashed line of the Anti-roll-bar car shows a noticeable suppression between 6 to 12s. The HIS system reduces the acceleration frequency peak and has a lower energy level overall. The RMS for evaluation: Spring-damper car, 0.6376 m/s^2; Anti-roll-bar car, 0.5272 m/s^2; and HIS car, 0.4046 m/s^2. It shows that the HIS car has better ride comfort during cornering, which is consistent with the previous test.

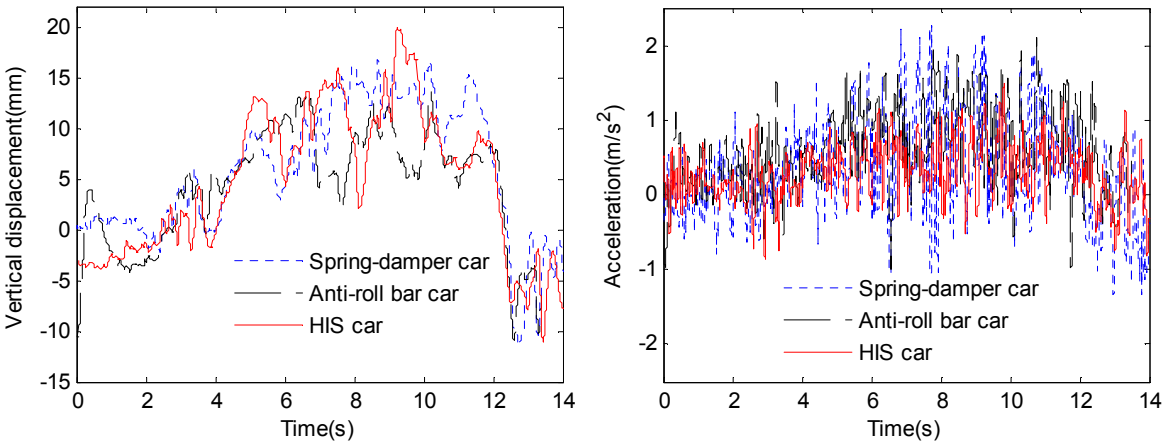

(a) (b)

Figure 7.26. Comparison of vehicle vertical dynamics of three cases at: (a) *the vertical suspension by averaging four suspension deflections*; and (b) *CG vertical acceleration*.

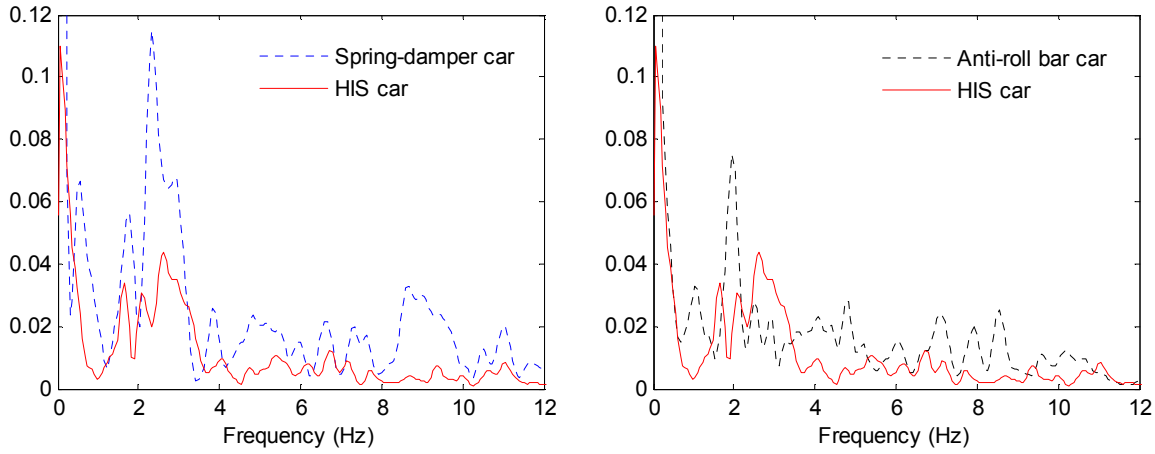

Figure 7.27. Comparison of vehicle CG vertical acceleration of three cases in frequency domain: (a) *HIS car and Spring-damper car*; and (b) *HIS car and Anti-roll-bar car*.

7.3.7.Articulation mode analysis

A stiff articulation mode has negative effects on vehicle handling and chassis structure. For handling, it worsens the uneven weight distribution of four wheels, and may lead to a wheel lifting up under severe cases. The lift of driving wheels causes the loss of forward driving torque, and the lift of steering wheels reduces steering and handling ability. The articulation effect on vehicle chassis can be decomposed as a pair of roll moments, which are opposite to each other in direction and are applied to the front and rear parts of the chassis separately. As a result, the two opposite roll moments form a torsional torque to twist vehicle chassis along the X axis. Once this X-axis torque exceeds a critical level, damage to the chassis occurs.

Due to the fact that anti-roll bars are only interconnected from left to right but not connected from front to rear, they increase the front and rear roll stiffness separately and result in a stiffened articulation mode. In contrast, the HIS system interconnects the front and rear without providing any stiffness to the articulation mode. As the anti-roll bars tend to equalize the left and right suspension deflection and minimise the

relative roll motion between wheels and body, when the left wheel's inputs are out of phase with the right wheels (ground roll excitation), the anti-roll bars tilts vehicle body to match the sloped road surface, but when the front wheel's inputs are also out of phase with the rear wheels (ground articulation excitation), the anti-roll bars twist the car body along the X axis.

Since the articulation mode can only be excited by uneven road surfaces in practice, the four-poster test rig from Chapter 6, shown in Figure 7.28(a), is employed to study the articulation mode property change between the three test cars. In addition to the transducers mentioned in the slalom test, gyroscopes in the roll and pitch directions are installed at the vehicle CG to measure the angular velocity.

As the articulation mode most likely affects the vehicle's handling at low frequency, the test is set up at 1 Hz articulation input, and the excitations to the wheels are shown in Figure 7.28(b) and defined as

$$z_{gi}(t) = Amp_i \sin(2\pi ft) \tag{7.14}$$

where $Amp_1 = -Amp_2 = -Amp_3 = Amp_4 = 0.015\text{m}$; $f = 1Hz$.

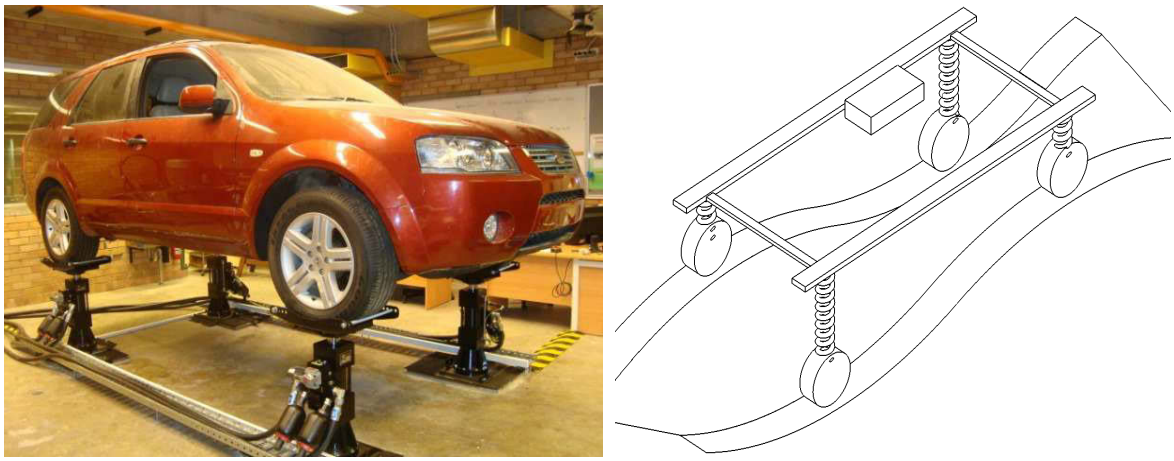

(a) (b)

Figure 7.28. a) the four-poster test rig for vehicle dynamics study; and b) the articulation mode excitation.

The comparison of suspension deflections at front left and rear right wheels and the comparison of sprung mass roll/pitch velocity are presented in Figure 7.29 and Figure 7.30, respectively. The independent spring-damper suspension system is considered to have a soft articulation mode, and thus used as a reference for the articulation softness comparison.

It can be seen that the HIS car behaves in a very similar manner to the Spring-damper car in the articulation mode, and the agreement is evidenced by the solid line and dotted line in Figure 7.29(a-b). The agreement between the HIS car and the Spring-damper car indicates that the HIS car has an articulation mode that is as soft as it could be in the Spring-damper car.

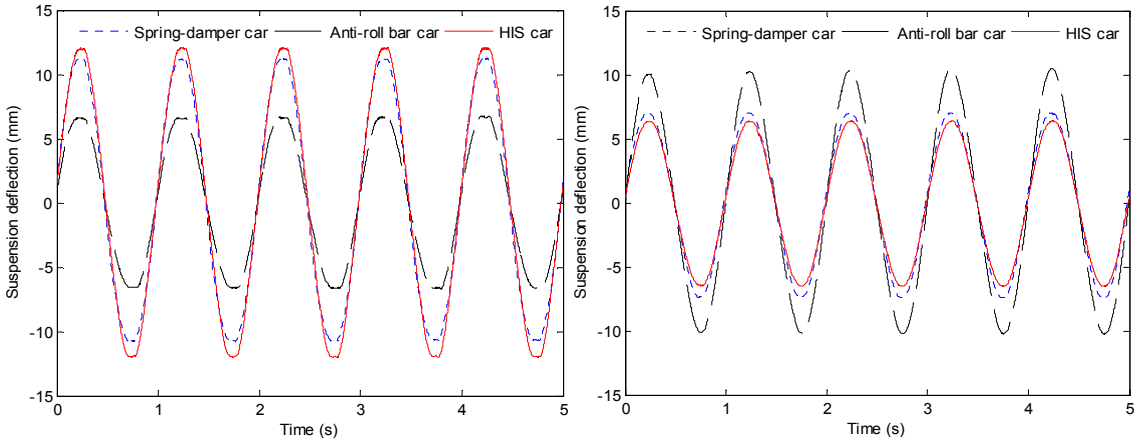

(a) (b)

Figure 7.29. Vehicle suspension deflection measured in: a) *front left wheel station*; and b) *rear right wheel station*.

The Anti-roll-bar car has anti-roll bars installed in the front and rear, but the front anti-roll bar is much stiffer than the rear anti-roll bar and provides the major anti-roll stiffness to the vehicle. As shown in Figure 7.29(a), the front left wheel suspension travel has been significantly limited by 44%, owing to the installation of the front anti-roll bar. Since the front anti-roll bar pushes the vehicle body rotating according to the front wheels' input but against the rear wheels' motions, the rear suspension deflection increases, as shown in Figure 7.29(b). This means the anti-roll bars heavily concentrate the vehicle load at the two diagonal wheels where the spring-coils are already under compression, but further diminish the normal force of other two wheels which already have the tendency to lift up. Consequently, under articulation excitation, anti-roll bars worsen the weight distribution of four wheels and reduce the vehicle road-holding ability.

Due to the stiffness difference of front and rear coil-springs, vehicle body roll and pitch motions are also excited to some extent under the articulation excitation. Comparisons of roll and pitch velocity of vehicle body are presented in Figure

7.30(a-b). The finding in roll/pitch velocity comparison is consistent with the result from the suspension deflection comparison. The roll and pitch velocity of the HIS car match the spring-damper car well, and this confirms that the HIS system decouples the roll and articulation mode in principle, providing no observable effect on the articulation mode. For the Anti-roll-bar car, the stiffer front anti-roll bar tilts the vehicle to the opposite direction. Figure 7.30(a) captures the anti-roll bars effect on roll velocity, and it shows that under the same ground articulation excitation, the Anti-roll-bar car's roll velocity has the largest amplitude and is out of the phase with the other two cars. In Figure 7.30(b) the oscillation of the pitch velocity also suggests that the anti-roll-bar car's chassis is under torsion.

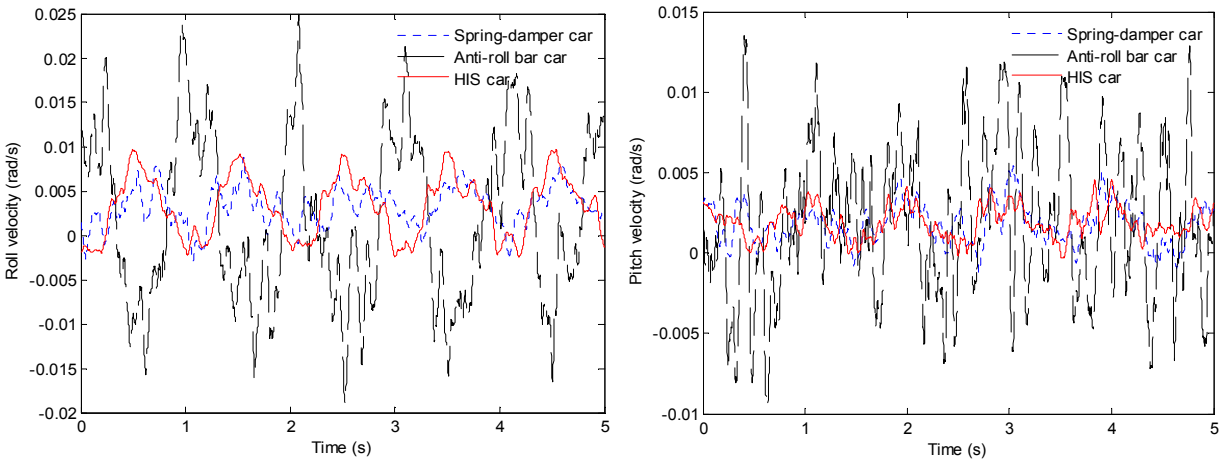

(a) (b)

Figure 7.30. Angular velocity measured at vehicle CG in: a) *roll direction*; and b) *pitch direction*.

To summarise, despite the capability of the passive HIS system in providing significant roll stiffness, it does not stiffen the vehicle's articulation mode nor does it affect the suspension deflection. Further, it does not apply extra torsional torque to the vehicle chassis. Overall the HIS car has a similar performance to the Spring-damper car in the series of articulation tests. Conversely, the anti-roll bars stiffen the articulation mode

and this is evidenced by the comparison of the suspension deflection and the roll/pitch velocity.

7.3.8.Discussion

Shifting working point

For cylinders used in the HIS system, due to the cross-sectional area difference in the top and bottom chambers, loading goods on board will increase the working (static) pressure of the passive HIS system. The added weight to sprung mass presses all coil-springs down, and compresses four cylinders installed alongside the coil-springs. Due to the merge of the piston rod, the resultant output of oil from the cylinders is forced into the accumulators, causing the pressure to increase. For example, after the loading of two testing personnel and equipment into the vehicle, the HIS pressure is observed to have risen from the pre-charged pressure of 40 bar to 47 bar. The increased working pressure benefits the loaded vehicle by providing a stiffer anti-roll system. However, if this effect is not preferred in the design, it can be eliminated by adopting double rod cylinders that have the same cross-sectional area for top and bottom chambers, or automatic pressure regulation.

Leakage

Leakage is a main issue in the implementation of the passive HIS system and it occurs once the system is beyond its lifespan or certain damage happens to the system. The function of the HIS relies on the fluid within the system, i.e., nitrogen in the accumulators; hydraulic oil in the cylinders and pipelines. The leakage of nitrogen from an accumulator will increase the accumulator-compressing rate, and reduce the lifespan of the accumulator. Generally, any leakage in the system will decrease the HIS's static pressure, shift its working point away from the designed range, and soften

the roll stiffness of the vehicle. Therefore, a drop in static pressure is the main indication of any likely leakage in the system. In particular, the hydraulic oil leakage is considered more likely to happen and hence represents major concerns. Practical methods to either better seal the system or to semi-actively compensate the pressure loss to maintain the working pressure can be investigated in future.

Limitations and future work

The site restrictions and available resources limit the presented road tests. Although the obtained test result is in good agreement with the re-constructed event and validates the effectiveness of the passive HIS system under different tests, there is still room left for the improvement of the conducted road test set up. According to the vehicle test procedures suggested by Toyota, NHTSA, or other professional communities, there are several aspects that can be made better in the future. For example, manoeuvre tests at higher vehicle speed with a smaller steering angle would be ideal for handling assessment and may show other dynamic characters. Other tests, such as the braking test, bump road test and rough road driving test, can be suggested for further investigation. Moreover, a comprehensive vehicle dynamic measurement package with higher resolution transducers will be beneficial to capture more dynamic aspects of test vehicles.

7.4 Active HIS with H∞ control

7.4.1.Introduction

Based on the understanding of the passive HIS system from the theoretical research and experimental studies conducted in the previous sessions, a novel, low-cost, active, hydraulically interconnected suspension is developed and tested. The system design and implementation please refer to the MHIS test rig in Chapter 6.

The H∞ roll control strategy is employed to control the roll motion of the vehicle body. The hydraulic suspension model used for deriving the H∞ controller is experimentally estimated from the testing data. Then, the active suspension model is combined with the half-car model through the mechanical-hydraulic interface in the cylinders. On the four-post-test rig developed in Chapter 6, the active suspension with H∞ control is validated under several road excitations.

7.4.2.Potential benefits of employing the active HIS system

Active suspensions can solve the conflicting requirements between ride and handling and have thus attracted considerable attention. However, although several active suspension systems are available in the market [111, 112], their applications are strictly limited to luxury vehicles, owing to their high manufacturing cost and excessive energy consumption. ZF Lemförder developed a novel active suspension system called active suspension via control arm (ASCA). The maximum power consumption of ASCA is claimed to be only 1.2 kW per wheel because of 'the combination of a parallel spring/actuator configuration', or a total of 4.8 kW for four wheels [113]. The active suspension developed by Bose reportedly exerts energy, with the shocks working like generators, ultimately consuming 2 horsepower (1.5 kW) of energy [114]. By contrast, the proposed active HIS system only has a motor rated 1 kW because in the design, a 2 L accumulator is employed and pre-charged with high pressure (commonly 90 bar to 100 bar) to satisfy the flow requirement, thus enabling a smaller motor. In addition, the active HIS system only responds when required to reduce energy consumption further.

The active HIS system contains four hydraulic double-directing cylinders interconnected by two circuits in the roll-plane. In this way, the two circuits can be controlled by only one servo valve, thus reducing the cost substantially compared with

conventional active suspensions that use four valves for individual cylinder control. The active HIS system, firstly, has to provide sufficient supporting force to the vehicle body during cornering, to counteract the roll moment generated by the centrifugal force. Secondly, it has to maintain the levelling of the vehicle body under uneven road excitation, by compensating on the suspension travel.

From a mechanical point of view, the first function does not require any energy consumption, because only vertical forces vary while wheel travel remains unchanged [38]. However, for the second function, energy consumption occurs because the active HIS expands/compresses actuators to achieve the desired suspension deflection. Thus, the overall energy management strategy for active suspension depends on achieving a balance between ride comfort and handling-related control objectives. Handling and safety-related objectives can be controlled with very limited energy consumption, but improving ride comfort (body levelling control) requires a certain amount of energy.

7.4.3.Control strategy

Various control approaches have recently been applied to improve the performance of the active suspensions, including root locus [115], linear and fuzzy control [116], neural networks [117], linear quadratic regulator (LQR) and linear quadratic gaussian (LQG) [118], H∞ control [119], learning automata [120], non-linear control [121], and preview control [122]. Recognised as one of the most robust and effective optimal control strategies, H∞ has long been employed in active suspension control, but the majority of the studies are based on quarter-car models [123, 124]. Several active H∞ control studies based on half-car [125] or full-car models [126, 127] showed promising results, but require four independent actuators on each wheel station. Nevertheless, these studies were predominately conducted in a computer-based simulation environment [119, 128]. The experimental H∞ control implementation at the full-car

level with a practical active suspension system is of great interest in extending the research on active suspensions into engineering practice.

The performance of the derived H∞ controller is largely determined by the accuracy of the mathematical modelling of the physical plant. Thus, an appropriate model and correct parameters of the active suspension (mainly the pressure control unit) are essential for deriving this model-based optimal controller. The derived model should be sufficiently simple for the controller design and should also capture the system dynamic characteristics. Thus an empirical approach is proposed to derive the model and estimate the necessary parameter values.

7.4.4.Model estimation

A small dimensional model is proposed based on an empirical modelling method [129]. The setup for testing is illustrated in Figure 7.31. The output ports from the pressure control unit connect to a double-acting cylinder locked in the middle position. A pressure transducer is located at the port to the upper cylinder chamber. The pressure command signal to control the servo valve is a sinusoidal signal at different frequencies, and the actual pressure measured at the cylinder port is acquired for comparison.

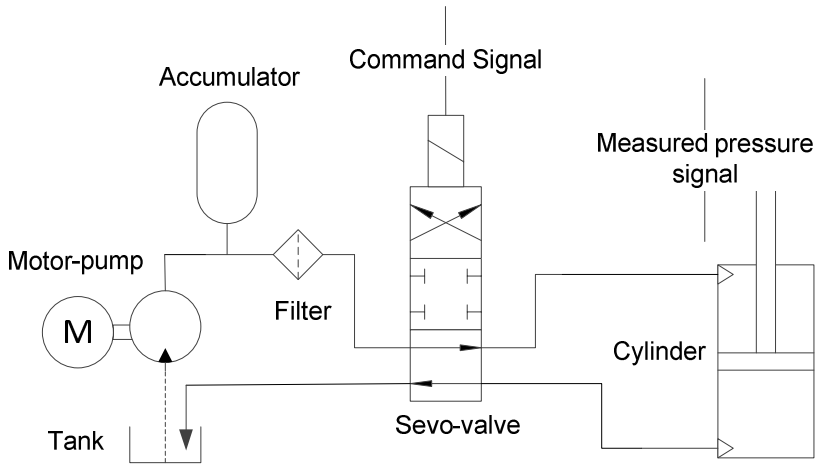

Figure 7.31. Schematic drawing of the testing setup for the model estimation of the active hydraulic suspension.

The differences among these signals in terms of magnitude and phase delay are calculated based on the obtained results and then plotted against the frequency, as shown in Figure 7.32. A second-order system is considered sufficient to cover the main dynamic characteristics of the system, as shown in Equation (7.15)

$$\frac{P(s)}{I(s)} = \frac{1}{1+(2\xi / w_n)s + s^2 / w_n^2} \tag{7.15}$$

where *P(s)* represents the measured pressure signal, and *I(s)* is the input command signal. w_n is the natural frequency, and ξ is the damping ratio. Through curve fitting, the optimised values for w_n and ξ are estimated as 68 Hz and 0.57, respectively. The estimated system frequency response is also shown by the solid line in Figure 7.32.

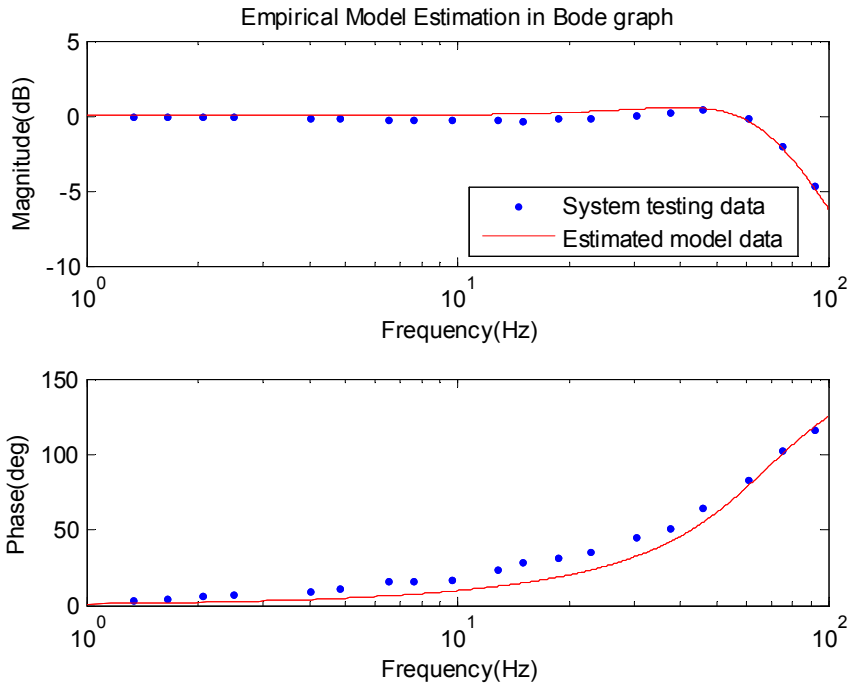

Figure 7.32. Empirical model estimation in Bode graph.

Consistent with the vehicle modelling from previous work [50], the transfer function of the hydraulic system should be converted into a state-space form. The resulting state-space equation and system matrices are presented as

$$\begin{aligned} \dot{X}_p &= A_p X_p + B_p inp \\ Y_p &= C_p X_p + D_p inp \end{aligned} \tag{7.16}$$

where $A_p = \begin{bmatrix} -487.1 & -356.5 \\ 512 & 0 \end{bmatrix}$, $B_p = \begin{bmatrix} 16 \\ 0 \end{bmatrix}$, $C_p = \begin{bmatrix} 0 & 22.28 \end{bmatrix}$, $D_p = [0]$.

The *inp* is the pressure signal command to the pressure control unit, and Y_P is the actual pressure in the actuator.

7.4.5. Model integration

A model of smaller dimension is preferable in designing advanced controllers. The obtained hydraulic model is then combined with the 4-DOF roll-plane half-car model, as shown in Figure 7.33. For the model parameters please refer to Table 4.1.

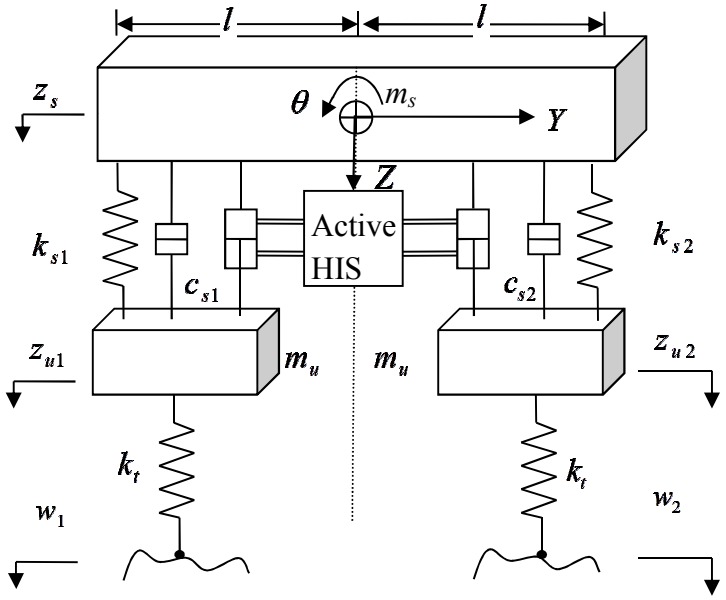

Figure 7.33. The integrated half-car model with the active HIS system.

By defining the vehicle state vector $X_c = \begin{bmatrix} \dot{\theta} & \dot{z}_s & \dot{z}_{u1} & \dot{z}_{u2} & \theta & z_s & z_{u1} & z_{u2} \end{bmatrix}^T$ and force vector $F = \begin{bmatrix} w_1 & w_2 & f_1 & f_2 \end{bmatrix}^T$, where $w_{1,\,2}$ are the road inputs, and $f_{1,2}$ are the control forces applied through the two actuators shown in the half-car model, we derive the system equations of the half-car model in the state-space form

$$\dot{X}_c = A_c X_c + B_c F \tag{7.17}$$

and the system matrices are defined as

$$A_c = \begin{bmatrix} 0 & I \\ -M^{-1}K & -M^{-1}C \end{bmatrix}_{8\times 8}, \quad B_c = \begin{bmatrix} 0 & 0 \\ B_{road} & B_{contr} \end{bmatrix}_{8x4}^T \tag{7.18}$$

where $M = \begin{bmatrix} I & 0 & 0 & 0 \\ 0 & m_s & 0 & 0 \\ 0 & 0 & m_u & 0 \\ 0 & 0 & 0 & m_u \end{bmatrix}$, $C = \begin{bmatrix} 2l^2 c_s & 0 & -lc_s & lc_s \\ 0 & 2c_s & -c_s & -c_s \\ -lc_s & -c_s & c_s & 0 \\ lc_s & -c_s & 0 & c_s \end{bmatrix}$,

$$K = \begin{bmatrix} 2l^2k_s & 0 & -lk_s & lk_s \\ 0 & 2k_s & -k_s & -k_s \\ -lk_s & -k_s & k_s + k_t & 0 \\ lk_s & -k_s & 0 & k_s + k_t \end{bmatrix}, \quad B_{road} = \begin{bmatrix} 0 & 0 \\ 0 & 0 \\ k_t / m_u & 0 \\ 0 & k_t / m_u \end{bmatrix}_{4\times 2},$$

$$B_{contr} = \begin{bmatrix} l/I & -l/I \\ 1/m & 1/m \\ -1/m_u & 0 \\ 0 & -1/m_u \end{bmatrix}_{4\times 2}.$$

We can now integrate the derived hydraulic model with this half-car model and obtain the combined system model in state-space by defining the state vector $X = \begin{bmatrix} \dot{\theta} & \dot{z}_s & \dot{z}_{u1} & \dot{z}_{u2} & \theta & z_s & z_{u1} & z_{u2} & x_{p1} & x_{p2} \end{bmatrix}^T$, and input vector $u = \begin{bmatrix} w_1 & w_2 & p \end{bmatrix}^T$ of

$$\dot{X} = AX + Bu \tag{7.19}$$

The system metrics are defined as follows:

$$A = \begin{bmatrix} -M^{-1}C & -M^{-1}K & B_{contr}\begin{bmatrix} C_p a \\ -C_p a \end{bmatrix} \\ I & 0 & 0 \\ 0 & 0 & A_p \end{bmatrix}_{10\times 10}, \quad B = \begin{bmatrix} B_{road} & 0 \\ 0 & 0 \\ 0 & B_p \end{bmatrix}_{10\times 3}$$

For C_p please refer to Equation 7.16; B_p is presented in Figure 7.17; a is the piston area with the assumption that the cylinder has equal piston areas in both chambers to simplify the system model.

7.4.6.H∞ controller design

A basic H∞ control algorithm is derived based on the combined system model which contains the dynamics of the active suspension. The sprung mass roll angle is set as the feedback signal and control target. Road excitation d is the external input to the vehicle fitted with the active suspension, body roll angle y is the feedback signal for the H∞

controller, and the pressure control command signal P_a is the output signal from the controller.

In H∞ derivation, employing weighting functions is necessary to optimise the distribution of the control resource over the excitations. W_{d1} and W_{d2} are weighting functions of the ground excitation to the left and right wheels, respectively. The low-frequency contents are more significant. In this design, a 10 Hz low-pass filter obtained and tuned from the model-based simulation in Matlab is verified in the experiments. This filter is described by Equations (7.20) and Equations (7.21).

$$W_{d1} = 0.01\left(\frac{62.83}{s+62.83}\right) \tag{7.20}$$

$$W_{d2} = 0.01\left(\frac{62.83}{s+62.83}\right) \tag{7.21}$$

$$W_d = \begin{bmatrix} W_{d1} \\ W_{d2} \end{bmatrix} \tag{7.22}$$

W_y is the measured output weighting function determined by the control strategy, which highlights the controlled frequency range of vehicle motions. Given that the active HIS targets large motions associated with the vehicle body in the low-frequency range, W_y in Equation (7.23) is applied to the roll-angle measurement.

$$W_y = 30\left(\frac{31.42}{s+31.42}\right) \tag{7.23}$$

W_{act} is the measured output weighting function, which is related to actuator response frequency. Owing to the electro-hydraulic system employed in the active suspension, the expected working frequency band is limited by the servo-valve response frequency, which is approximately 80 Hz in this case. The command signal in the higher frequency range would induce larger phase shifts and could cause oscillation or even

instability. Thus, the control forces have to be decreased in the higher frequency range. W_{act} in Equation (7.24) can reduce the effect of the control force in the high-frequency domain, and it is derived in simulation, tuned and verified in test.

$$W_{act} = \frac{0.05}{13}\left(\frac{s+50}{s+500}\right) \tag{7.24}$$

7.4.7.Experimental results

The experiments are performed on the four-post test rig which provides the ground excitation to represent the uneven road input to the vehicle. The experimental results compare the roll angle of the vehicle before and after control. Two sets of tests with different ground excitations are implemented: 0.02 m half sinusoidal and sinusoidal input. The labels 'Benchmark' and the 'Active' in the figures represent the test results with and without the active HIS system, respectively. When the right side of the vehicle body is higher than the left side, the roll angle is defined as a positive roll angle, and when it is lower, the roll angle is defined as a negative roll angle.

The ground excitation to the experimental car in the first test is a couple of oppositional half sinusoidal waves with an amplitude of 0.02 m and a frequency of 0.5 Hz, as shown in Figure 7.34. The comparison of the vehicle body roll angle from the tests with/without the active HIS control is presented in Figure 7.35. The results obtained show a 44.5% reduction in the peak roll angle from the active HIS test. However, the system takes slightly longer to return to still. The corresponding roll rate is also provided in Figure 7.36.

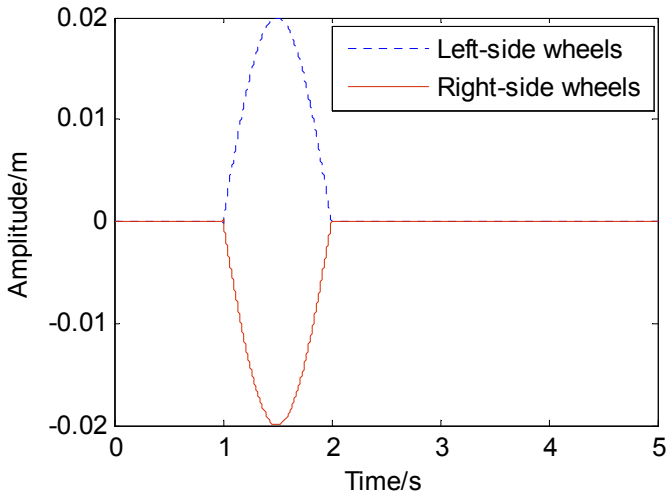

Figure 7.34. Half sinusoidal ground excitation from the test rig to the wheels of the test vehicle.

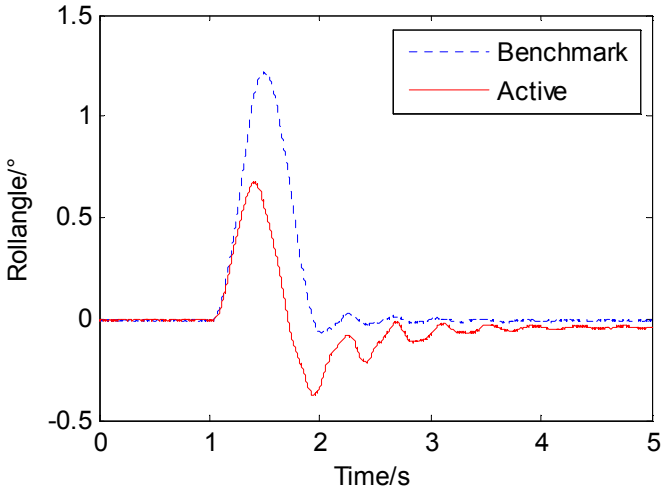

Figure 7.35. Comparison of the roll angle of vehicle body.

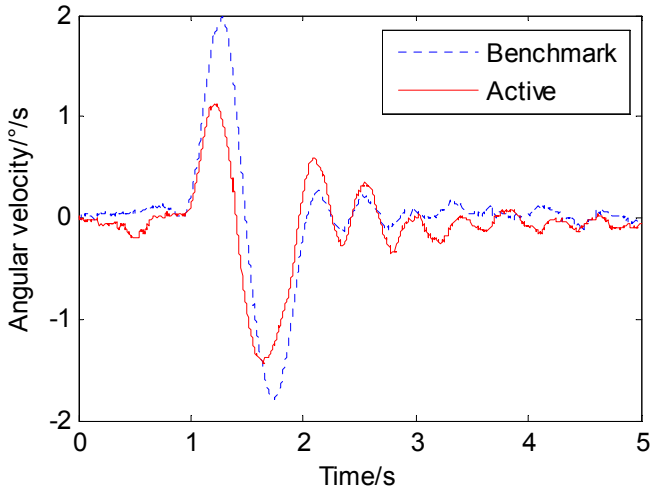

Figure 7.36. Comparison of the roll rate of vehicle body.

In the second set of tests, the ground excitations to the left and right wheels are two out-of-phase sine waves (one cycle only) at 0.5 Hz with an amplitude of 0.02 m, as shown in Figure 7.37. The roll angle and roll rate response before and after using the active HIS are compared in Figure 7.38 and Figure 7.39, respectively. The results show that the roll angle decreases by 37.2% on the positive peak and by 18.9% on the negative peak

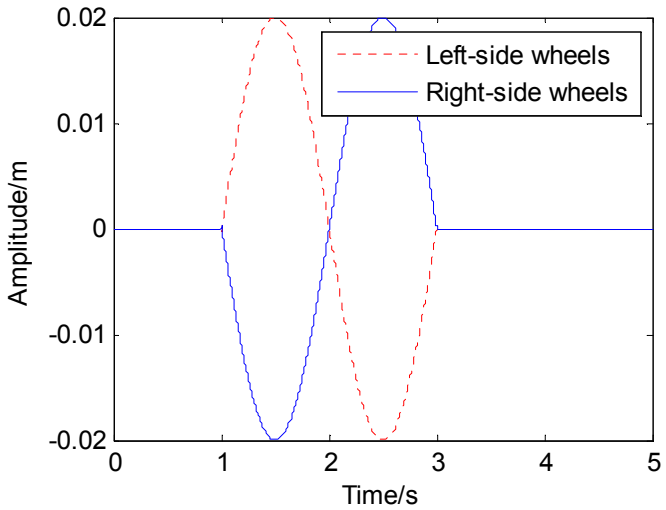

Figure 7.37. Sinusoidal ground excitation from the test rig to the wheels of the test vehicle.

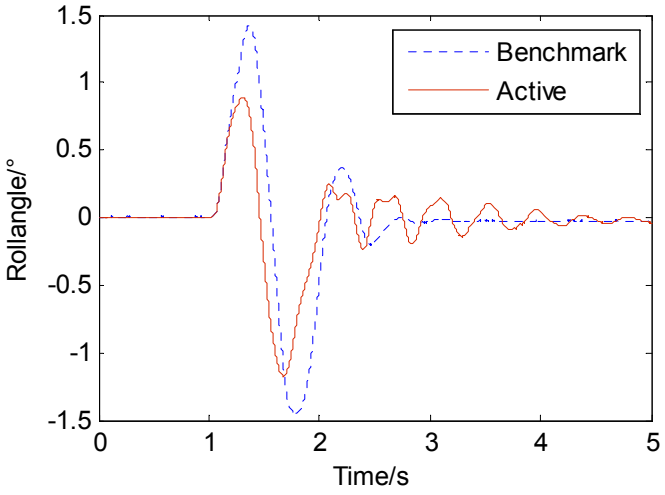

Figure 7.38. Comparison of the roll angle of vehicle body.

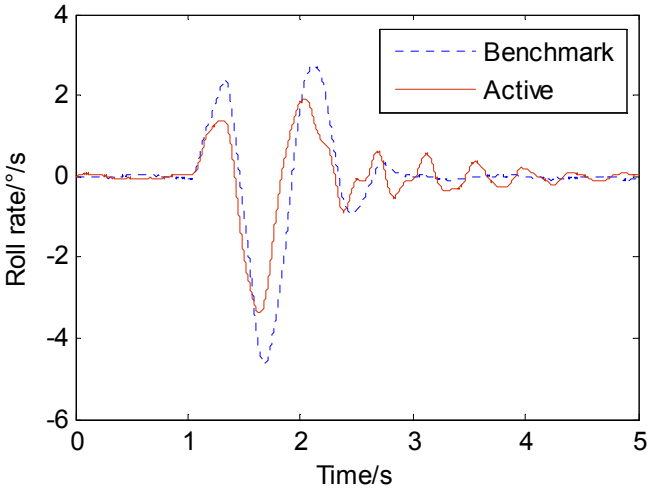

Figure 7.39. Comparison of the roll rate of vehicle body.

7.4.8.Discussion

The measured results of the suspension deflection demonstrate that at low-frequency ground excitation (e.g., 0.5 Hz), the wheels and body of the vehicle tend to roll together as a rigid body, and conventional suspensions contribute little to vehicle body position control. By contrast, the active HIS can change suspension deflection by using hydraulic actuators to minimise vehicle body roll according to its roll-angle control strategy, thereby maintaining the vehicle body at a neutral level.

The prototype could be further upgraded to respond faster; the installed sensing system and it powering unit could be made better to improve the signal quality. The current dynamic modelling is rather basic and simple, without including the flow rate. The next step of the modelling could still be linear but include the flow rate to capture the complexity of the hydraulic delay of the active HIS system. A more detailed non-linear model may be also beneficial to understand its transient dynamic under road impact or control mode switching. More advanced control strategies considering parameter variation, actuator saturation, and other nonlinear factors could also be developed, verified and compared based on the develop testing facilities.

7.5 Summary

This chapter started with a study of vehicle modelling, parameter estimation and testing with different anti-roll systems. A half-car vehicle model was derived; the testing approach of parameter estimation was explained; and test results were provided. The good agreement between the modelling and the experimental data verifies the proposed method of vehicle modelling and parameter estimation. Based on this method, the comparison of roll stiffness of the anti-roll bar and the passive anti-roll HIS in different settings was presented. Results proved that the HIS system can provide higher roll stiffness than the anti-roll bars.

Two sets of field tests were then presented to investigate and compare the passive HIS system with anti-roll bars. The theoretical model of the HIS fitted vehicle system is validated by the test results. Slalom and fishhook manoeuvre tests are conducted when cars are fitted with: (a) only spring-damper suspension, (b) anti-roll bars, and (c) the passive HIS. The experimental findings with simulations are presented and discussions are provided. Road test results demonstrate that the passive HIS system can provide improved handling and ride performance in comparison to anti-roll bars. Specifically,

in vehicle handling analysis, the comparison of test results shows that the passive HIS system effectively suppresses vehicle body roll angle thanks to the significantly increased roll stiffness, and minimises the lateral acceleration peak point oscillation. Moreover, in vertical dynamic study during cornering, the smaller RMS value of CG vertical acceleration suggests that the passive HIS system provides a better ride to passengers during cornering. The investigation of the effects of the passive HIS on the articulation mode was conducted on the four-poster test rig at low frequency. The results showed that anti-roll bars significantly stiffened the articulation mode, and in contrast, the HIS system had a negligible effect on the articulation mode and preserved the same level of articulation stiffness as the spring-damper-only suspension configuration. As a result, the HIS system minimised the torsional torque applied to vehicle body/chassis, and enhanced the vehicle's tire/ground contact ability.

Based on the knowledge of passive HIS, an active HIS system was designed, assembled to the test vehicle, and tested in laboratory with an H∞ controller. The model estimation of the pressure control unit of the active HIS system was presented. The H∞ controller was derived based on the assembled vehicle-HIS model. The weighting functions of the H∞ controller were provided, and the implementation of the controller to the test vehicle fitted with the active HIS system was presented. The performance of the controller was validated in two sets of tests under different road excitations. The preliminary experimental results on the active HIS were consistent and showed the applicability of this novel mechanism and its controller.

CHAPTER 8 CONCLUSIONS AND RECOMMENDATIONS

8.1 Summary

This thesis can be summarised as follows.

Chapter 1: the basic problem under investigation was introduced in Chapter 1 and the research objectives were established.

Chapter 2: some essential background information on the controlled suspension system and interconnected suspensions was provided in Chapter 2. It also highlighted the continuous evolution of active/semi-active interconnected suspension systems and the direction of potential development.

Chapter 3: the proposed method for real-time detecting the dominating motion-mode of a vehicle was delineated in this chapter, through the employment of a 7-DOF full-car model. The proposed motion-mode energy method (MEM) classified body-wheel relative movements of a vehicle into orthogonal motion-modes and quantified the motion-modes' contribution by their energy intensity in real time. The identified dominating motion-mode was then considered as the prioritised control objective for controllable suspensions. The verification on a 10-DOF nonlinear full-car model through numerical examples was provided. This included several realistic driving scenarios: road bump and pothole; braking and steering; and fishhook manoeuvre with road excitation. Attention was also given to the motion-mode-based control strategy which integrated the individually developed controllers in different motion-modes and the practical considerations of implementing the MEM.

Chapter 4: to address the practical consideration of MEM implementation, an alternative approach by employing neural networks (NNs) to identify vehicle primary motion-modes with acceptable accuracy was developed and tested in this chapter, including structure design, training procedure, and numerical validations. The method only required the measurement of vehicle suspension deflections. The feed-forward NNs with one hidden layer were employed and two half-car models in roll- and pitch-planes were used to generate the training data sets for these two NNs, respectively. To simplify the NNs' training process and enhance its recognition capability, a feature extraction algorithm was also proposed. The empirical analysis of the recognition error showed that the NNs can achieve an acceptable accuracy. Several simulation examples were used to verify the effectiveness of the proposed NNs on a 10-DOF nonlinear vehicle model. This included ground excitation, steering wheel input, and braking. The results confirmed that the detected mode-ratio was applicable to vehicle motion-mode-based suspension control.

Chapter 5: a conceptual MEM-based switched control architecture for vehicle integrated motion control through the employment of an active HIS system was developed in Chapter 5. The architecture provided a roadmap to derive control strategies from sketch for a system with time-variable structures or parameters, including parameter variation detection, primary mode detection, and switchable control.

It was found through numerical simulations that the MEM can provide the basis for primary mode detection and control. The results also showed that the active-HIS fitted vehicle system achieves good performance and was stable during the mode-switch.

Chapter 6: a series of test facilities for the research were developed during this project and were presented in Chapter 6. They included: (1), the six-channel vehicle dynamic

test rig, (2), the multi-functional HIS test rig, (3), the reconfigurable HIS test rig. The six-channel test rig was used to perform vehicle full-car parameter estimation, represent road arbitrary irregularity, and simulate a yaw moment or a centrifugal force that a vehicle experiences during cornering. The multi-functional anti-roll HIS test rig (MHIS), installed to the test vehicle, can be manually switched to passive HIS, semi-active HIS, or fully active HIS. The MHIS rig with the vehicle dynamic test rig was used in experimental investigation of passive and active HIS systems, and the obtained results were presented in Chapter 7. The reconfigurable hydraulically interconnected suspension test rig (RHIS) was built for the transient dynamics study during mode switching. As mentioned in Chapter 5, the dynamic stability during mode-switch was the main criterion when deriving the controller and a test rig as the one developed would be ideal to study the system's transient dynamics and to verify the derived controller.

Chapter 7: experimental investigation including vehicle parameter estimation, passive HIS equivalent roll stiffness estimation, passive HIS filed test, and active HIS with an H∞ controller were undertaken in Chapter 7. Vehicle parameters were obtained through drop-test using the State Variable Method (SVM) and inverse eigenvalue approach. The simulations provided by the estimated model agreed well with the test data. Furthermore, the estimation of the equivalent roll stiffness of the passive HIS and the anti-roll bars were conducted and the results were compared. It was found the HIS was able to provide significant roll stiffness and damping to a vehicle.

A field test of the passive HIS system was conducted under slalom and fishhook manoeuvres. It was found that the HIS system can provide improved handling and ride performance in comparison to anti-roll bars. Specifically, in vehicle handling analysis, the comparison of test results showed that the HIS system effectively suppressed vehicle body roll angle owning to the significantly increased roll stiffness, and

minimised the lateral acceleration peak point oscillation. In vertical dynamic study during cornering, the smaller RMS value of CG vertical acceleration suggested that the HIS system provided a better ride to passengers during cornering. The investigation of the HIS's effect on articulation mode conducted on the four-poster test rig at low frequency showed that anti-roll bars significantly stiffen the articulation mode, and in contrast, the HIS system had a negligible effect on the articulation mode and preserved the same level of articulation stiffness as the spring-damper-only suspension configuration. Thus, the HIS system minimised the torsional torque applied to vehicle body/chassis, and enhanced the vehicle's tire/ground contact ability.

Active HIS system verification with an H∞ controller was also conducted and some preliminary results were obtained. The model of the hydraulic pressure control unit of the active HIS was estimated from experimental tests. Based on the integrated hydraulic model and the vehicle model, an H∞ controller was derived in Matlab and tested on the MHIS test rig. The applicability of this novel active suspension mechanism and its controller was validated by the preliminary experimental results. It was found that the controller was stable and effective and the active suspension considerably reduced vehicle roll angle in the tests.

8.2 Contributions

The specific objectives and contributions of this thesis, as set out in Section 1.2, were achieved as follows.

1. To review the literature relating to the controlled suspensions and interconnected suspensions, highlighting the combination of these two features into active/semi-active hydraulic interconnected suspensions.

This was achieved by

a) presenting a thorough summary of past work relating to the controlled suspensions (Chapter 2)

b) presenting a thorough summary of past work relating to interconnected suspensions (Chapter 2)

2. To develop a methodology to detect the dominating vehicle motion-mode with real-time capability; (1), to study vehicle motions and vibrations from the modal analysis perspective and classify the relative motions between vehicle body and wheels into several body-wheel motion modes, (2), from vehicle state vector to calculate each motion-mode's energy and its contribution ratio, (3), use a trained neural network system to provide a reasonably accurate motion-mode energy contribution ratio from measured suspension travel, (4), to conceptually develop a MEM-based switched control with H∞ optimisation.

This was achieved by

a) using energy intensity to quantify the different stage from vibration to motion and further define vehicle vib-motion; for a four-wheel vehicle, using its mode shapes to describe and define its seven motion-modes (Chapter 3)

b) proposing a new method, the motion-mode energy method (MEM) to calculate the motion-mode energy through double coordination transformation (Chapter 3)

c) training a neural network system under the supervision of MEM in order to provide a motion-mode energy contribution ratio from measured suspension travel (Chapter 4)

d) proposing an architecture of MEM-based switched control which provides a roadmap of how to derive a suitable controller to address parameter uncertainly, primary mode control, and stability over mode-switching from sketch (Chapter 5).

3. To develop a series of test facilities for the research of this topic: (1), a six-channel vehicle dynamic test rig, (2), a multi-functional anti-roll HIS test rig, (3), a reconfigurable HIS test rig.

This was achieved by

a) designing and building a four-poster rig and a roll/yaw stimulator which are integrated as a six-channel vehicle dynamic test rig (Chapter 7)
b) designing and building a switchable hydraulic interconnected suspension on the test vehicle with the function of being passive, semi-active, and active (Chapter 7)
c) designing and building a separated active hydraulic interconnected suspension test rig to study the transient dynamics during control-mode-switching (Chapter 7).

4. To develop a method for vehicle and passive HIS parameter estimation through experiment.

This was achieved by

a) proposing a novel method to practically obtain vehicle parameter from its free-decay responses in different modes (Chapter 7)
b) combining parameters from different modes to construct a vehicle model (Chapter 7)
c) modelling the passive HIS system as a torsional spring attached to vehicle sprung mass and estimating its equivalent roll stiffness (Chapter 7)
d) comparing it with anti-roll bars (Chapter 7).

5. To experimentally investigate the passive HIS system in full-car level under: (1), different types of manoeuvre, (2), the articulation mode.

This was achieved by

a) driving the passive HIS fitted vehicle through a series of traffic cones to obtain the measurements for slalom test (Chapter 7)
b) repeating the test with 1), an anti-roll bar fitted vehicle; and 2), a spring-damper suspension only vehicle (Chapter 7)
c) repeating the comparison in fishhook test (Chapter 7)
d) comparing the three test vehicles under articulation excitation (Chapter 7).

6. To experimentally validate the proposed active anti-roll HIS system with an H∞ controller.

This was achieved by

a) estimating the model of the hydraulic pressure control from experimental data and integrating it with a half-car model for controller derivation (Chapter 7)
b) deriving an H∞ controller in Matlab
c) implementing the controller to the active suspension fitted test vehicle through a real-time communicating platform (within MHIS test rig developed in Chapter 6)
d) testing the controller under the excitation from the four-poster test rig (Chapter 7).

8.3 Suggestions for future work

A number of avenues exist for further research work on the MEM and active HIS system. Some of the areas that have arisen during this thesis are as follows.

1. There is a clear need to further investigate the limitations of the MEM when applied to nonlinear systems. A nonlinear system can be decomposed into several motion-modes according to MEM, but due to its nonlinear nature these motion-modes are not completely "energetically isolated", which means that the energy leakage between these motion-modes exists. This is an inherent limitation of the application of MEM in nonlinear systems, and it is necessary to track this energy leakage in future studies and further investigate its effect on primary mode selection. Moreover, a more realistic vehicle model or actual road testing data may be of some benefit to address this issue and assess the realistic functionality of MEM.

2. Based on the proposed MEM, variable control systems and different control strategies could be applied at different stage of vibrations and motions, as listed in Table 3.1, and are possibly integrated under one single stable control frame. Semi-active damping is considered most efficient and effective in absorbing high-frequency low-amplitude vehicle dynamic energy, which is mostly dominated by wheel-related motion-modes. Active system is more capable to govern low-frequency vehicle body motions with large dynamic energy. Under MEM, the combination of semi-active system and active suspension could result in an effective and also energy efficient control. Hence, the integrated semi-active and active control is recommended as a future research topic.

3. The active HIS system can directly govern a vehicle's motions in bounce, roll, pitch, and articulation, which are coupled with planar dynamics, and therefore has effect on vehicle planar dynamics, as the Crosswind Assistant System [38] mentioned in Section 3.1. Hence, how to coordinate the active HIS with other dynamic control systems affecting vehicle planar dynamics, such as Anti-Lock Brake System (ABS), Electronic Stability Control (ESC) or Electronic Stability

Program (ESP) should be investigated, and according coordination control strategy can be proposed to realize the integrated control of active HIS with ABS, ESC or ESP.

4. The neural network system trained in Chapter 4 could be further extended to cover more motion-modes, e.g., the articulation mode and other wheel-dominated modes. This may require an upgrading of the existing parallel structure of two neural networks. Providing the test rigs developed in Chapter 6, the experimental verification of the MEM trained NNs system should be able to be conducted, and the training data could also be obtained through experimental testing.

5. Key processes of the proposed architecture of MEM-based switched control have largely been worked out. These included parameter estimation, motion-mode energy method, the H∞ control for one mode (Chapter 7) and for multi-mode control (Chapter 5). To complete the proposed control architecture would require the development of real-time estimation of vehicle parameter variation. Moreover, the switched controller design could also be extended to cover more motion-modes. Providing the RHIS test rig developed in Chapter 6, investigation of the transient dynamics during cross-mode switching could be carried out as well as the verification of the proposed MEM-based control strategy.

6. The assembling of the last two channels (used for yaw and roll excitation) of the six-channel test rig in Chapter 6 needs to be carried out and completed. These two channels could be used to study vehicle lateral dynamics by simulating vehicle handling manoeuvres in the laboratory environment, e.g., verify the develop active HIS system with its controller. Since the active HIS is

mainly designed to improve road vehicle handling and enhance safety, its effectiveness and performance would best be demonstrated and studied under the lateral excitation which could be provided by these two channels. Moreover, they could also be used to excite yaw motion and to perform parameter estimation in yaw mode, such as the yaw moment of inertia and tire shear stiffness.

7. There is a need to further expand and improve the proposed vehicle parameter estimation method presented in Chapter 7. Calibrating the estimation result by adding a known mass to the vehicle could be considered and real-time estimation of parameter variation (mainly sprung mass and its moment of inertias) could be performed. It could be of great value to conduct a further series of detailed field tests to compare the HIS system with anti-roll bars on ride comfort in bounce mode as well as in pitch mode. For the articulation mode test, the measuring of the tire/ground contact force could provide solid convincing evidence that supports the results and analysis in Session 7.3.8.

8. There are several potential topics that could be continued in the development of active HIS system. A better linear hydraulic modelling of the active HIS needs to be developed to address the relation between the flow change and pressure variation. It may also be of some value to develop a detailed non-linear active HIS model, including dynamics of servo-valves and directional valves, for transient dynamics study. In addition to the H∞ controller that was developed and tested in Chapter 7, different controllers could also be studied and compared.

REFERENCE

[1] Segel, L., 1993, "The overview of developments in road-vehicle dynamics: past, present and future," *Vehicle ride and handling international conference*, Birmingham, 15-17 November.

[2] Crolla, D. A., 1996, "Vehicle Dynamics-Theory into Practice," *Proceedings of the Institution of Mechanical Engineers, Part D: Journal of Automobile Engineering,* vol. 210(2), pp. 83-94.

[3] Sharp, R. S., 1999, "Vehicle dynamics and the judgment of quality," in *Vehicle Performance*, ed: Swet&Zeitlinger, pp. 87-96.

[4] Sharp, R. S. and Peng, H., 2011, "Vehicle dynamics applications of optimal control theory," *Vehicle System Dynamics,* vol. 49(7), pp. 1073-1111.

[5] Cao, D., Song, X., and Ahmadian, M., 2011, "Editors' perspectives: road vehicle suspension design, dynamics, and control," *Vehicle System Dynamics,* vol. 49(1–2), pp. 3-28.

[6] Hrovat, D., 1997, "Survey of Advanced Suspension Developments and Related Optimal Control Applications," *Automatica,* vol. 33(10), pp. 1781-1817.

[7] Fischer, D. and Isermann, R., 2004, "Mechatronic semi-active and active vehicle suspensions," *Control Engineering Practice,* vol. 12(11), pp. 1353-1367.

[8] Crosby, M. J. and Dean, C. K., 1973, "The active damper: a new concept for shock and vibration control," *Shock and Vibration Bulletin,* vol. 43(4), pp. 119-133.

[9] Hedrick, J. K. and Wormley, D. N., 1975, "Active suspensions for ground transport vehicles - a state of the art review," *American Society of Mechanical Engineers,* vol. 15, pp. 21-39.

[10] Eckermann, E., 2001, *World history of the automobile*, Society of Automotive Engineers, Warrendale, USA.

[11] Gillespie, T. D., 1992, *Fundamentals of Vehicle Dynamics*, SAE International, Warrendale, PA.

[12] McElroy, J. J., 1924, "Air-springs and the measurement of riding quality," *SAE Tech. Paper Series, SAE 240039*, SAE International,Warrendale, PA.

[13] Warner, J. A. C., 1924, "Riding-qualities research," *SAE Tech. Paper Series, SAE 240036*, SAE International,Warrendale, PA.

[14] Dillman, O. D. and Collier, E. J., 1953, "Building stability into the modern automobile," *SAE Tech. Paper Series, SAE 530036*, SAE International, Warrendale, PA.

[15] Winkelmann, O. J., 1961, "Handling requirements," *SAE Tech. Paper Series, SAE 610035*, SAE International, Warrendale, PA.

[16] Smith, M. and Walker, G., 2005, "Interconnected vehicle suspension," *Proceedings of the Institution of Mechanical Engineers, Part D: Journal of Automobile Engineering,* vol. 219(3), pp. 295-307.

[17] Cao, D., Rakheja, S., and Su, C. Y., 2010, "Roll- and pitch-plane coupled hydro-pneumatic suspension -- Part 1: Feasibility analysis and suspension properties," *Vehicle System Dynamics,* vol. 48(3), pp. 361-386.

[18] Zapletal, E., 2000, "Balanced Suspension," *SAE paper 2000-01-3572*, PA, USA.

[19] Fontdecaba, J., 2002, "Integral suspension system for motor vehicles based on passive component," *SAE Paper 2002-01-3105*, PA, USA.

[20] Zhang, N., Smith, W. A., and Jeyakumaran, J., 2010, "Hydraulically interconnected vehicle suspension: background and modelling," *Vehicle System Dynamics,* vol. 48(1), pp. 17-40.

[21] Karnopp, D. and Crosby, M., 1974, "System for controlling the transmission of energy between spaced members," US Patent 05/290,302.

[22] Ahmadian, M., 1999, "On the Isolation Properties of Semiactive Dampers," *Journal of Vibration and Control,* vol. 5, pp. 217-232.

[23] Appleyard, M. and Wellstead, P. E., 1995, "Active suspensions: some background," *Control Theory and Applications, IEE Proceedings,* vol. 142(2), pp. 123-128.

[24] Elbeheiry, E. M., Karnopp, D. C., Elaraby, M. E., and Abdelraaouf, A. M., 1995, "Advanced Ground Vehicle Suspension Systems - a Classified Bibliography," *Vehicle System Dynamics,* vol. 24(3), pp. 231-258.

[25] Sharp, R. S. and Crolla, D. A., 1987, "Road Vehicle Suspension System Design - a review," *Vehicle System Dynamics,* vol. 16(3), pp. 167-192.

[26] Ivers, D. E. and Miller, L. R., 1991, "Semi-active Suspension Technology: An Evolutionary View," *USA: ASME Advanced Automotive Technologies, DE-40, Book No. H00719-1991,* pp. 327-346.

[27] Ahmadian, M. and Simon, D., 2004, "Can semiactive dampers with skyhook control improve roll stability of passenger vehicles? " *SAE paper 2004-01-2099*, PA, USA.

[28] Ahmadian, M. and Blanchard, E., 2010, "Non-dimensionalised closed-form parametric analysis of semi-active vehicle suspensions using a quarter-car model," *Vehicle System Dynamics,* vol. 49(1-2), pp. 219-235.

[29] Hong, K., Sohn, H., and Hedrick, J. K., 2002, "Modified Skyhook Control of Semi-Active Suspensions: A New Model, Gain Scheduling, and Hardware-in-the-Loop Tuning," *Journal of Dynamic Systems, Measurement, and Control,* vol. 124(1), pp. 158-167.

[30] Poussot, V., C., Sename, O., Dugard, L., Gáspár, P., Szabó, Z., and Bokor, J., 2008, "A new semi-active suspension control strategy through LPV technique," *Control Engineering Practice,* vol. 16(12), pp. 1519-1534.

[31] Becker, M., Jaker, K. P., Fruhauf, F., and Rutz, R., 1996, "Development of an active suspension system for a Mercedes-Benz coach (O404)," *Proceedings of the IEEE International Symposium on Computer-Aided Control System Design*, Dearborn, Michigan, USA, 15-18 September 1996, pp. 146-151.

[32] Goodall, R. and Kortum, W., 1983, "Active controls in ground transportation - a review of the state-of-the-art and future potential," *Vehicle System Dynamics,* vol. 12(4-5), pp. 225-257.

[33] Nagai, M., 1993, "Recent Researches on Active Suspensions for Ground Vehicles," *JSME international journal. Ser. C, Dynamics, control, robotics, design and manufacturing,* vol. 36(2), pp. 161-170.

[34] Lian, J. L. a. R. J., 2011, "Intelligent Control of Active Suspension Systems," *IEEE Transactions on industrial Electronics,* vol. 58(2).

[35] Jiangtao, C., Honghai, L., Ping, L., and Brown, D. J., 2008, "State of the Art in Vehicle Active Suspension Adaptive Control Systems Based on Intelligent Methodologies," *IEEE Transactions on Intelligent Transportation Systems,* vol. 9(3), pp. 392-405.

[36] Williams, R. A., 1997, "Automotive active suspensions Part 2: practical considerations," *Proceedings of the Institution of Mechanical Engineers Part D-Journal of Automobile Engineering,* vol. 211(6), pp. 427-444.

[37] Williams, R., 1997, "Automotive active suspensions Part 1: basic principles," *Proceedings of the Institution of Mechanical Engineers, Part D: Journal of Automobile Engineering,* vol. 211(6), pp. 415-426.

[38] Rauh, J. and Ammon, D., 2011, "System dynamics of electrified vehicles: some facts, thoughts, and challenges," *Vehicle System Dynamics,* vol. 49(7), pp. 1005-1020.

[39] Bose. (2013, 20 March). *Bose® suspension system*. Available: http://worldwide.bose.com/axa/en_au/web/suspension_system/page.html

[40] Prokop, G. and Sharp, R. S., 1995, "Performance Enhancement of Limited-Bandwidth Active Automotive Suspensions by Road Preview," *IEE Proceedings - Control Theory and Applications,* vol. 142(2), pp. 140-148.

[41] Pilbeam, C. and Sharp, R. S., 1996, "Performance Potential and Power Consumption of Slow-Active Suspension Systems with Preview," *Vehicle System Dynamics,* vol. 25(3), pp. 169-183.

[42] Ei-Demerdash, S. M. and Crolla, D. A., 1996, "Hydro-pneumatic Slow-active Suspension with Preview Control," *Vehicle System Dynamics,* vol. 25(5), pp. 369-386.

[43] Koch, G., Fritsch, O., and Lohmann, B., 2010, "Potential of low bandwidth active suspension control with continuously variable damper," *Control Engineering Practice,* vol. 18(11), pp. 1251-1262.

[44] Stone, E. J. and Cebon, D., 2010, "Control of semi-active anti-roll systems on heavy vehicles," *Vehicle System Dynamics,* vol. 48(10), pp. 1215-1243.

[45] Miege, A. J. P. and Cebon, D., 2005, "Optimal roll control of an articulated vehicle: theory and model validation," *Vehicle System Dynamics,* vol. 43(12), pp. 867-893.

[46] Sampson, D. J. M. and Cebon, D., 2003, "Active roll control of single unit heavy road vehicles," *Vehicle System Dynamics,* vol. 40(4), pp. 229-270.

[47] Sampson, D. J. M., McKevitt, G., and Cebon, D., 1999, "The development of an active roll control system for heavy vehicles," *Vehicle System Dynamics,* vol. 33, pp. 704-715.

[48] Lin, R. C., Cebon, D., and Cole, D. J., 1994, "An Investigation of Active Roll Control of Heavy Road Vehicles," *Vehicle System Dynamics,* vol. 23, pp. 308-321.

[49] Markus, F. (2011, 20 March). *2011 Detroit: New Tech Tries to Compensate for the Dearth of Concepts*. Available: http://wot.motortrend.com/2011-detroit-new-tech-compensate-dearth-concepts-23309.html#axzz2TEBDGTQ2

[50] Zhang, N., Wang, L., and Du, H., 2009, "Modeling of a New Active Suspension for Roll Control," *13th Asia Pacific Vibration Conference*, University of Canterbury, New Zealand, 22-25 November

[51] Wang, L., Zhang, N., and Du, H., 2009, "Design and Experimental Investigation of Demand Dependent Active Suspension for Vehicle Rollover Control," *48th IEEE Conference on Decision and Control*, Shanghai, P.R. China, 16-18 December, pp. 5158-5163.

[52] Ahmad, F. B., Hudha, K., and Jamaluddin, H., 2009, "Gain scheduling PID control with pitch moment rejection for reducing vehicle dive and squat," *International Journal of Vehicle Safety,* vol. 4(1), pp. 45-83.

[53] Liu, S. A., Yu, X. L., Yao, Y. M., and Chen, Y. L., 2010, "Vehicle optimization-intelligence integrated control active suspension system based on pitch angle optimization," *Journal of Jilin University (Engineering and Technology Edition),* vol. 40(1), pp. 17-23.

[54] Hawley, J. B., 1927, "Shock Absorber and the Like For Vehicles," US Patent.

[55] Smith, W., 2009, "An investigation into the dynamics of vehicles with hydraulically interconnected suspensions," Ph.D thesis, University of Technology, Sydney.

[56] Lovins, A. B. and Cramer, D. R., 2004, "Hypercars(R), hydrogen, and the automotive transition," *International Journal of Vehicle Design,* vol. 35(1-2), pp. 50-85.

[57] Smith, W. A., Zhang, N., and Hu, W., 2010, "Hydraulically interconnected vehicle suspension: handling performance," *Vehicle System Dynamics,* vol. 49(1-2), pp. 87-106.

[58] Smith, W. A., Zhang, N., and Jeyakumaran, J., 2010, "Hydraulically interconnected vehicle suspension: theoretical and experimental ride analysis," *Vehicle System Dynamics,* vol. 48(1), pp. 41-64.

[59] Wilde, J. R., Heydinger, G. J., Guenther, D. A., Mallin, T., and Devenish, A. M., 2005, "Experimental evaluation of fishhook maneuver performance of a kinetic suspension system," *SAE paper 2005-01-0392*, PA, USA.

[60] Cao, D., Rakheja, S., and Su, C. Y., 2010, "Roll- and pitch-plane-coupled hydro-pneumatic suspension. Part 2: dynamic response analyses," *Vehicle System Dynamics,* vol. 48(4), pp. 507-528.

[61] Cao, D., Rakheja, S., and Su, C., 2006, "A Generalized Model of a Class of Interconnected Hydro-Pneumatic Suspensions and Analysis of Pitch Properties," *Proceedings of the ASME International Mechanical Engineering Congress and Exposition*, Chicago, Illinois USA, 5-10 November, pp. 137-146.

[62] Cao, D., Rakheja, S., and Su, C. Y., 2007, "Roll plane analysis of a hydro-pneumatic suspension with twin-gas-chamber struts," *International Journal of Heavy Vehicle Systems,* vol. 14(4), pp. 355-375.

[63] Cao, D., Rakheja, S., and Su, C. Y., 2008, "Dynamic analyses of heavy vehicle with pitch-interconnected suspensions," *International Journal of Heavy Vehicle Systems,* vol. 15(2-4), pp. 272-308.

[64] Mace, N., 2004, "Analysis and synthesis of passive interconnected vehicle suspensions," Ph.D thesis, Cambridge University.

[65] Wilde, J. R., Heydinger, G. J., and Guenther, D. A., 2006, "ADAMS simulation of ride and handling performance of kinetic suspension system," *SAE Paper 2006-01-1972*, PA, USA.

[66] Docquier, N., Poncelet, A., Delannoy, M., and Fisette, P., 2010, "Multiphysics modelling of multibody systems: application to car semi-active suspensions," *Vehicle System Dynamics,* vol. 48(12), pp. 1439-1460.

[67] Newton, B. (2010, 5, April). *New Nissan Patrol bigger, more luxurious*. Available: http://smh.drive.com.au/motor-news/new-nissan-patrol-bigger-more-luxurious-20100215-nzwt.html

[68] Tenneco. (2012, 5 March). *Integrated Kinetic*. Available: http://www.tenneco.com/assets/1/7/Kinetic_Brochure.pdf

[69] Rosam, N. and Darling, J., 1997, "Development and Simulation of a Novel Roll Control System for the Interconnected Hydragas® Suspension," *Vehicle System Dynamics,* vol. 27(1), pp. 1-18.

[70] Darling, J., Dorey, R. E., and Rossmartin, T. J., 1992, "A low-cost active anti-roll suspension for passenger cars," *Journal of Dynamic Systems Measurement and Control-Transactions of the Asme,* vol. 114(4), pp. 599-605.

[71] Darling, J. and Hickson, L. R., 1998, "An experimental study of a prototype active anti-roll suspension system," *Vehicle System Dynamics,* vol. 29(5), pp. 309-329.

[72] Darling, J. and RossMartin, T. J., 1997, "A theoretical investigation of a prototype active roll control system," *Proceedings of the Institution of*

Mechanical Engineers Part D-Journal of Automobile Engineering, vol. 211(1), pp. 3-12.

[73] Audi. (2013). *Audi Glossary-Dynamic Ride Control (DRC)*. Available: http://www.audiusa.com/us/brand/en/tools/advice/glossary/dynamic_ride_control.browser.html

[74] Zhang, N., 2008, "Active Suspension," Australian Patent PCT/Au2008-000720.

[75] Mashadi, B. and Crolla, D. A., 2005, "Influence of ride motions on the handling behaviour of a passenger vehicle," *Proceedings of the Institution of Mechanical Engineers, Part D: Journal of Automobile Engineering* vol. 219(9), pp. 1047-1059.

[76] He, J. and Fu, Z. F., 2001, *Modal analysis*, Butterworth-Heinemann, Oxford.

[77] Braghin, F., Resta, F., and Sabbioni, E., 2007, "A modal control for active/semi-active suspension systems," *IEEE/ASME International Conference on Advanced Intelligent Mechatronics*, 4-7 September.

[78] Ulbrich, H. and Ginzinger, L., Eds., 2008, *Motion and Vibration Control: Selected Papers from MOVIC 2008*, Germany.

[79] Mikhlin, Y. and Mytrokhin, S., 2008, "Nonlinear vibration modes of the double tracked road vehicle," *Journal of Theoretical and Applied Mechanics,* vol. 46(3), pp. 581-596.

[80] Zhang, N., Dong, G., and Du, H., 2008, "Investigation into untripped rollover of light vehicles in the modified fishhook and the sine maneuvers. Part I: Vehicle modelling, roll and yaw instability," *Vehicle System Dynamics,* vol. 46(4), pp. 271-293.

[81] Pacejka, H. B., 2002, *Tire and vehicle dynamics*, 3 ed., Butterworth-Heinemann, Oxford, UK.

[82] Li, D. and Lu, Q., 2001, *Experimental modal analysis and its application*, Science Press, Beijing.

[83] Pesterev, A. V., Bergman, L. A., and Tan, C. A., 2004, "A novel approach to the calculation of pothole-induced contact forces in MDOF vehicle models," *Journal of sound and vibration,* vol. 275(1–2), pp. 127-149.

[84] Cole, D. J., 2001, "Fundamental Issues in Suspension Design for Heavy Road Vehicles," *Vehicle System Dynamics,* vol. 35(4-5), pp. 319-360.

[85] Valasek, M., Novak, M., SIka, Z., and Vaculin, O., 1997, "Extended Ground-Hook-New Concept of Semi-Active Control of Truck's Suspension," *Vehicle System Dynamics,* vol. 27(5-6), pp. 289-303.

[86] Wang, L., Zhang, N., and Du, H., 2012, "Real-time Identification of Vehicle Motion-Modes Using Neural Networks," *Submitted to Mechanical Systems and Signal Processing*.

[87] Morris, B. T. and Trivedi, M. M., 2008, "A Survey of Vision-Based Trajectory Learning and Analysis for Surveillance," *IEEE Transactions on Circuits and Systems for Video Technology,* vol. 18(8), pp. 1114-1127.

[88] Wang, Q., Zhao, H., Chen, W., Wang, Q., and Fan, D., 2000, "Research on the intelligence control for automotive semi-active suspensions using the multibody model," *Proceedings of the 3rd World Congress on Intelligent Control and Automation*, Hefei, P.R. China, 28 June-2 July, pp. 160-163.

[89] Guarneri, P., Rocca, G., and Gobbi, M., 2008, "A Neural-Network-Based Model for the Dynamic Simulation of the Tire/Suspension System While Traversing Road Irregularities," *IEEE Transactions on Neural Networks,* vol. 19(9), pp. 1549-1563.

[90] Wang, K., 2006, "Neural Network Approach to Vibration Feature Selection and Multiple Fault Detection for Mechanical Systems," *First International Conference on Innovative Computing, Information and Control, ICICIC '06*, August 30-September 01, pp. 431-434.

[91] Ghosh Dastidar, S., Adeli, H., and Dadmehr, N., 2008, "Principal Component Analysis-Enhanced Cosine Radial Basis Function Neural Network for Robust Epilepsy and Seizure Detection," *IEEE Transactions on Biomedical Engineering,* vol. 55(2), pp. 512-518.

[92] Mu, G., Shi, K., An, J., Li, P., and Yan, G., 2008, "Signal Energy Method Based on EMD and Its Application to Research of Low Frequency Oscillations," *Proceedings of the Chinese Society for Electrical Engineering,* vol. 28(19), pp. 36-41.

[93] Yang, Y., Yu, D., and Cheng, J., 2006, "A roller bearing fault diagnosis method based on EMD energy entropy and ANN," *Journal of Sound and Vibration,* vol. 294(1-2), pp. 269-277.

[94] Wang, L., Zhang, N., and Du, H., 2011, "Onboard Detection of Energy Distribution onto Vibration Modes of a Vehicular System," *the 14th Asia Pacific Vibration Conference*, Hong Kong, 5-8 December.

[95] Funahashi, K. I., 1989, "On the approximate realization of continuous mappings by neural networks," *Neural Networks,* vol. 2(3), pp. 183-192.

[96] Gallant, A. R. and White, H., 1988, "There exists a neural network that does not make avoidable mistakes," *IEEE International Conference on Neural Networks*, 24-27, July.

[97] Maghami, P. G. and Sparks, D. W., Jr., 2000, "Design of neural networks for fast convergence and accuracy: dynamics and control," *IEEE Transactions on Neural Networks,* vol. 11(1), pp. 113-123.

[98] Rozyn, M. and Zhang, N., 2010, "A method for estimation of vehicle inertial parameters," *Vehicle System Dynamics,* vol. 48(5), pp. 547-565.

[99] Cheng, C. and Cebon, D., 2011, "Parameter and state estimation for articulated heavy vehicle," *Vehicle System Dynamics,* vol. 49(1-2).

[100] Allen, R., Lin, K. C., and Xu, C., 2010, "Robust estimation of a maneuvering target from multiple unmanned air vehicles' measurements," *International Symposium on Collaborative Technologies and Systems,* , Chicago, IL, USA, 17-21, May, pp. 537-545.

[101] D Simon, 2006, *Optimal State Estimation: Kalman, H ∞, and Nonlinear Approaches*, John Wiley & Sons, New Jersey.

[102] Newman, M. E. J., 2005, "Power laws, Pareto distributions and Zipf's law," *Contemporary Physics,* vol. 46(5), pp. 323-351.

[103] Du, H., Zhang, N., and Wang, L., 2012, "Switched Control of Vehicle Suspension Based on Motion-Mode Detection," *submitted to Vehicle System Dynamics*.

[104] Koch, G., 2011, "Adaptive control of mechatronic vehicle suspension systems," Ph.D thesis, Technische Universitat Munchen, 38402 Crenoble Cedex, France.

[105] Bouazara, M., Richard, M. J., and Rakheja, S., 2006, "Safety and comfort analysis of a 3-D vehicle model with optimal non-linear active seat suspension," *Journal of Terramechanics,* vol. 43(2), pp. 97-118.

[106] Oung, R. and D'Andrea, R., 2011, "The Distributed Flight Array," *Mechatronics,* vol. 21(6), pp. 908-917.

[107] Zhang, N. H., Shinji, 1990, "Identification of structural system parameters from time domain data," *JSME, international journal,* vol. 33(2), pp. 168-175.

[108] Cebon, D., 1999, *Handbook of vehicle-road interaction*, Swets and Zeitlinger, Lisse, Netherlands.

[109] Cole, D. J., 2000, "Evaluation of design alternatives for roll-control of road vehicles," *AVEC*, Ann Arbor, MI, USA.

[110] Wang, L., Zhang, N., and Du, H., 2010, "Modelling, parameter estimation and testing of a vehicle with anti-roll systems," *the 6th Australasian Congress on Applied Mechanics*, Perth, Australia, 12-15 December, .

[111] Yokoya, Y., Kizu, R., Kawaguchi, H., Ohashi, K., and Ohno, H., 1990, "Integrated control system between active control suspension and four wheel steering for the 1989 Celica," *SAE Tech. Paper Series, SAE 901748*, SAE International, Warrendale, PA.

[112] Lijima, T., Akatsu, Y., Takahashi, K., and Murakami, H., 1993, "Development of a Hydraulic Active Suspension," *SAE Tech. Paper Series, SAE 931971*, PA, USA.

[113] Heiing, B. and Heißing, B., 2011, *Chassis Handbook: Fundamentals, Driving Dynamics, Components, Mechatronics, Perspectives*, Vieweg and Teubner.

[114] Trend, M. (January.2005). *The Bose Electronic Suspension, now in prototype testing, is stunning and simple*. Available: http://www.motortrend.com/features/editorial/112_0501_bosesuspension/viewall.html

[115] Thompson, A., 1970, "Design of active suspensions," *Proceedings of the Institution of Mechanical Engineers,* vol. 185(1), pp. 553-563.

[116] Yoshimura, T., Nakaminami, K., Kurimoto, M., and Hino, J., 1999, "Active suspension of passenger cars using linear and fuzzy-logic controls," *Control Engineering Practice,* vol. 7(1), pp. 41-47.

[117] Al, H., N., Lahdhiri, T., Joo, D. S., Weaver, J., and Al-Abbas, F., 2002, "Sliding mode neural network inference fuzzy logic control for active suspension systems," *IEEE Transactions on Fuzzy Systems,* vol. 10(2), pp. 234-246.

[118] Taghirad, H. D. and Esmailzadeh, E., 1998, "Automobile passenger comfort assured through LQG/LQR active suspension," *Journal of vibration and control,* vol. 4(5), pp. 603-618.

[119] Kruczek, A. and Stribrsky, A., 2004, "H∞ Control of Automotive Active Suspension with Linear Motor," *Proccedings of the 3rd IFAC Symposium on Mechatronic Systems*.

[120] Gordon, T., Marsh, C., and Wu, Q., 1993, "Stochastic optimal control of active vehicle suspensions using learning automata," *Proceedings of the Institution of Mechanical Engineers, Part I: Journal of Systems and Control Engineering,* vol. 207(3), pp. 143-152.

[121] Lin, J. S. and Kanellakopoulos, I., 1997, "Nonlinear design of active suspensions," *Control Systems, IEEE,* vol. 17(3), pp. 45-59.

[122] Hac, A., 1990, "Optimal linear preview control of active vehicle suspension," *Proceedings of the 29th IEEE Conference on Decision and Control*, Honolulu, HI, USA, 5-7 December, pp. 2779-2784.

[123] Yamashita, M., Fujimori, K., Uhlik, C., Kawatani, R., and Kimura, H., 1990, "H ∞ control of an automotive active suspension," *Proceedings of the 29th IEEE Conference on Decision and Control*, pp. 2244-2250.

[124] Lauwerys, C., Swevers, J., and Sas, P., 2005, "Robust linear control of an active suspension on a quarter car test-rig," *Control Engineering Practice,* vol. 13(5), pp. 577-586.

[125] Du, H. and Zhang, N., 2008, "Constrained H∞ control of active suspension for a half-car model with a time delay in control," *Proceedings of the Institution of Mechanical Engineers, Part D: Journal of Automobile Engineering,* vol. 222(5), pp. 665-684.

[126] Yamashita, M., Fujimori, K., Hayakawa, K., and Kimura, H., 1994, "Application of H ∞ control to active suspension systems," *Automatica,* vol. 30(11), pp. 1717-1729.

[127] Hayakawa, K., Matsumoto, K., Yamashita, M., Suzuki, Y., Fujimori, K., and Kimura, H., 1999, "Robust H ∞ output feedback control of decoupled automobile active suspension systems," *IEEE Transactions on Automatic Control,* vol. 44(2), pp. 392-396.

[128] Wang, J., Wilson, D. A., Xu, W., and Crolla, D. A., 2005, "Active Suspension Control to Improve Vehicl0e Ride and Steady-State Handling," *44th IEEE Conference on Decision and Control and European Control Conference, CDC-ECC'05*, Plaza de España Seville, Spain, 12-15 December, pp. 1982-1987.

[129] Ferreira, J. A., Almeida, F., and Quintas, M. R., 2002, "Semi-empirical model for a hydraulic servo-solenoid valve," *Proceedings of the Institution of Mechanical Engineers, Part I: Journal of Systems and Control Engineering*, vol. 216(3), pp. 237-248.